MANTLE METASOMATISM AND THE GENERATION OF ALKALINE LAMPROPHYRES IN THE SPANISH PEAKS INTRUSIVE COMPLEX, SOUTH-CENTRAL COLORADO

by

ARMINDA BROOKE HAMIL

(Under the Direction of MICHAEL F. RODEN)

ABSTRACT

The Spanish Peaks Intrusive Complex, Colorado, is composed of compositionally diverse mid-Tertiary igneous rocks. The intrusive stocks of the Spanish Peaks are surrounded by a famous radial dike system as well as subparallel dikes and sills that include lamprophyres. Some of the lamprophyres are relatively sodic ($Na_2O>K_2O$) and others are relatively potassic ($Na_2O<K_2O$). The lamprophyres are approximately the same age (20-25 Ma; Miggins, 2002), providing a unique opportunity to study the nature of the sources of two highly distinct, contemporaneous alkaline magmas. McGregor (2010) hypothesized the two groups of lamprophyres formed from sequential melting of distinct phase assemblages in the same metasomatic vein. Distinct initial Sr ratios from this study disprove this hypothesis. I hypothesize that the two types of lamprophyres were sourced from separate groups of veins that formed from the same metasomatic event but have distinct phase assemblages because they crystallized at different depths in the upper mantle.

INDEX WORDS: Spanish Peaks; alkaline rocks; lamprophyres; sodic rocks; potassic rocks; Sr analysis; metasomatism; amphibole megacrysts;

MANTLE METASOMATISM AND THE GENERATION OF ALKALINE LAMPROPHYRES IN THE SPANISH PEAKS INTRUSIVE COMPLEX, SOUTH-CENTRAL COLORADO

by

ARMINDA BROOKE HAMIL

BS, Georgia Southern University, 2009

A Thesis Submitted to the Graduate Faculty of The University of Georgia in Partial Fulfillment of the Requirements for the Degree

MASTER OF SCIENCE

ATHENS, GEORGIA

2013

MANTLE METASOMATISM AND THE GENERATION OF ALKALINE LAMPROPHYRES IN THE SPANISH PEAKS INTRUSIVE COMPLEX, SOUTH-CENTRAL COLORADO

by

ARMINDA BROOKE HAMIL

Major Professor:	Michael F. Roden
Committee:	Douglas Crowe
	Thomas Jordan

Electronic Version Approved:

Maureen Grasso
Dean of the Graduate School
The University of Georgia
May 2013

DEDICATION

This thesis is dedicated to my parents, Mark I. Hamil and Lynn G. Hamil, for always encouraging me and believing I can accomplish anything I attempt, and to my fiancé, Jonathon D. Lord, for being there for me throughout the process, keeping me motivated, and supporting me when I needed it.

ACKNOWLEDGEMENTS

First I would like to thank my advisor, Mike Roden, for helping me every step of the way. I thank the Geology department of The University of Georgia and all the faculty and staff for providing the equipment and knowledge to pursue this research. Thank you to Chris Fleisher for guidance with the electron microprobe, Doug Dvoracek for help with X-ray fluorescence analysis, and Vincent Salters and the staff at the National High Magnetic Field Laboratory at Florida State University for guidance and the use of equipment and laboratories; Sharon McMullen, Jon Primm, and Jonathon Lord for help with field work and sampling; Cliff and Roe Manuel for letting us stay on their property, and Mr. Goemmer for access Goemmer's Butte.

TABLE OF CONTENTS

Page

LIST OF TABLES

Page

LIST OF FIGURES

Page

CHAPTER 1

INTRODUCTION AND PREVIOUS WORK

The Spanish Peaks Intrusive Complex is composed of a compositionally diverse suite of igneous rocks that intruded the continental crust of south-central Colorado during the mid-Tertiary, and consists of dikes, sills, laccoliths, plugs, and stocks that range in composition from alkaline lamprophyres to granites. This complex lies within the Raton basin, a broad structural basin that includes a portion of northern New Mexico (Fig. 1.1) on the eastern flank of the Rio Grande Rift. The Raton Basin is the easternmost basin formed due to compression related to the Laramide orogeny during the late-Cretaceous and early-Tertiary (Lindsey, 1996). Locally, the Spanish Peaks Intrusive Complex lies within the La Veta syncline, an asymmetric structural trough that makes up the northern portion of the Raton basin, and which lies between the Sangre de Cristo Mountains to the west and the high plains to the east (Fig. 1.2). To the west of the Sangre de Cristo Mountains is the San Luis Valley, which is the expression of the Rio Grande Rift in southern Colorado (Fig. 1.2). The Rio Grande Rift trends north-south through New Mexico and Colorado; rifting of the continental crust was initiated between 30 and 25 Ma (Lipman and Mehnert, 1975). Magmas of the Spanish Peaks Intrusive Complex intruded between 33-25 Ma and are associated with the inception of the Rio Grande Rift (Miggins, 2002). The most striking features in this area are the stocks of East and West Spanish Peaks, which are surrounded by prominent radial and subparallel dike systems (Fig. 1.3).

Previous workers have disagreed on the classification and on the timing of emplacement of the lamprophyric dikes in the area. The earliest worker in the area (Hills, 1889) divided the lamprophyres into two groups, one that intruded before the emplacement of the Spanish Peaks and one that occurred after. Knopf (1936) was the first worker to describe the chemistry and petrography of the igneous rocks in the area in detail and he noted that there was no chemical or petrographic distinction between Hill's early and late lamprophyres. Johnson (1968) conducted extensive fieldwork in the area between the years of 1948-1962 for the USGS, and created a detailed map of the igneous features in the area (Fig. 1.4). He divided the dikes into three groups: radial dikes, subparallel dikes, and independent dikes. He then classified the rocks into seven groups based on their mineralogy in thin section. Lamprophyres were included in five of the seven groups. Smith (1975) studied the dikes in order to determine their relationship to the central stocks of East and West Spanish Peak and was the first to obtain absolute ages. He found that the Spanish Peaks Igneous Complex was not contemporaneous with the Laramide orogeny as previously believed, but was associated with the Rio Grande Rift. Jahn et al. (1979) evaluated trace element and strontium isotopic analyses for rocks of the Spanish Peaks Igneous Complex including several lamprophyric dikes. They suggested that crystal fractionation and magma mixing could not account for the variations among the rocks, and that at least two sources must be involved. They also concluded that the lamprophyres were generated from partial melting of the upper mantle. Penn and Lindsey (1996) divided the group of dikes into two sets geographically, chemically, and temporally (through high precision Ar/Ar dating) and argued that the dikes north of the Spanish Peaks were minettes, and that they intruded after the

emplacement of the stocks. The dikes south of the stocks were camptonites, and intruded before the emplacement of the stocks. It's notable that Penn and Lindsey only dated one sample of each of these two separate 'sets' of dikes. Miggins (2002) also used Ar/Ar dating methods and claimed that all the lamprophyres were emplaced after the intrusions of the stocks, regardless of composition (27 to 21 Ma). McGregor (2010) chose to divide the lamprophyres into 'relatively sodic' and 'relatively potassic' lamprophyres rather than use specific rock names, and did not distinguish between the sets north and south of the peaks. He analyzed major element oxides and trace element contents of whole rocks (by X-ray fluorescence) and individual minerals (with the electron microprobe) to determine the relationship between the two types. He found that the groups are not related by fractional crystallization from the same parent magma and they are different enough to suggest that they formed by melting of distinct phase assemblages. Based on the ideas of Foley (1992), McGregor proposed a model to explain these two types of lamprophyres which includes sequential melting of metasomatized veins in the upper mantle. First, a fluid metasomatizes the mantle, producing hydrous phases such as amphibole and phlogopite. When heat is introduced due to a later tectonic event, the amphibole and phlogopite within the metasomatized vein sequentially melt. Foley (1992) proposed that metasomatic veins melt before the wall rocks due to the concentration of hydrous phases and incompatible elements. Experiments have shown that a high ratio of F/OH in minerals such as amphiboles and micas allows them to be stable at higher temperatures (Foley, 1991). Because phlogopite has a higher concentration of fluorine than amphibole, McGregor (2010) hypothesized that amphibole melts initially generating a melt that is relatively rich in sodium. Once the amphibole is exhausted, phlogopite melts causing the

melt to have a relatively potassic composition. In this case, the source for each type of lamprophyre has a distinct phase assemblage, but they came sequentially from the same physical space and have not been separated for a significant amount of time. Because the ages of the two lamprophyre groups, sodic and potassic, overlap, and assuming isotopic equilibrium due to high temperatures in the source region, the isotopic compositions for both groups should be the same if McGregor (2010) is correct. As part of this study, I determined initial Sr isotope ratios with the aim of supporting or disproving McGregor's hypothesis.

High precision trace elemental analysis was completed at the National High Magnetic Field Laboratory at Florida State University. If the mantle was metasomatized by fluids from a subducted plate, trace element signatures may provide evidence. For example, potassic alkaline rocks from the Navajo volcanics show a negative Nb-Ta anomaly that is considered a signature of fluids from the subducting Farallon plate (Gibson et al., 1993; Carlson and Nowell, 2001). If the potassic lamprophyres in the Spanish Peaks Intrusive Complex also show this signature, that would indicate that subduction-related fluids from the Farallon plate were involved in the petrogenesis of the potassic lamprophyres and would support the metasomatized vein hypothesis of McGregor (2010).

Goemmer's Butte is an igneous feature located near the Spanish Peaks that contains megacrysts of amphibole and xenoliths of amphibole and apatite. This feature may be rare evidence of explosive volcanic activity in the Spanish Peaks area. This feature was thoroughly canvassed to determine what rock types were present, and what evidence of volcanic activity was present. Amphibole megacrysts and xenoliths were

collected for microprobe analysis, and high precision trace element and Sr isotopic analysis was conducted on both the host rock and an amphibole megacryst from this location to determine whether the megacryst was in equilibrium with the host magma.

North Lake Sill Complex is exposed in a road cut on CO-12 between Cuchara and Stonewall, Colorado. This location contains multiple lamprophyric sills, both relatively sodic and potassic, and at least one of the lamprophyres contains amphibole megacrysts. Tres Valles dike is a dike near Mt. Mestas, Colorado which has been dated by Miggins (2002) to be older than the other igneous rocks from this study, but was noted to contain large amphibole megacrysts. Goemmer's Butte, North Lake Sill Complex, Big Dike, and Tres Valles Ranch dike are all examples of igneous features containing amphibole megacrysts in the Spanish Peaks area. Megacrysts were sampled from each locality and subjected to microprobe analysis to characterize similarities and differences and stable isotope analysis was performed to determine whether meteoric water was involved in their formation. Tres Valles was investigated to determine whether it was related to the Spanish Peaks magmatism that formed the lamprophyres and/or whether the amphibole megacrysts it contains are similar to those related to Spanish Peaks.

Alkaline lamprophyres in the Spanish Peaks area were chosen to be sampled based on previously sampled and dated dikes from Miggins (2002) and Penn and Lindsey (1996), but which were not sampled by McGregor (2010). Thus, samples from this study were selected to complement the dataset of McGregor (2010) and those results were combined with this study to draw the conclusions from this research.

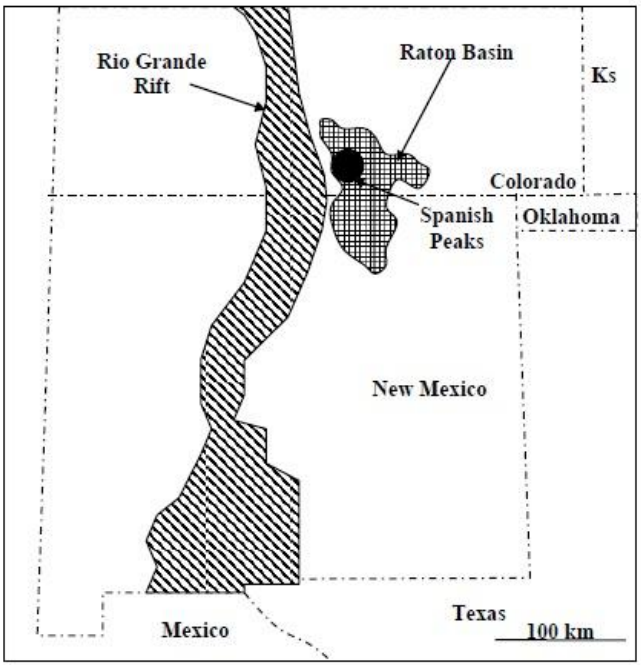

Figure 1.1: Map showing the location of the Raton Basin and the Spanish Peaks, in relation to the Rio Grande Rift (McGregor, 2010).

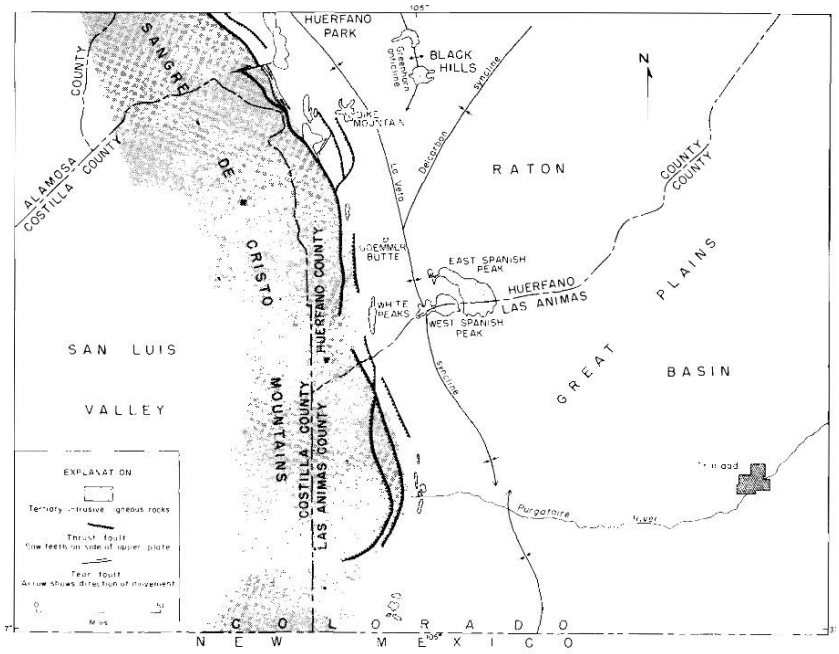

Figure 1.2: Map showing the locations of the Spanish Peaks, in relation to the Sangre de Cristo Mountains and the San Luis Valley (Johnson, 1968).

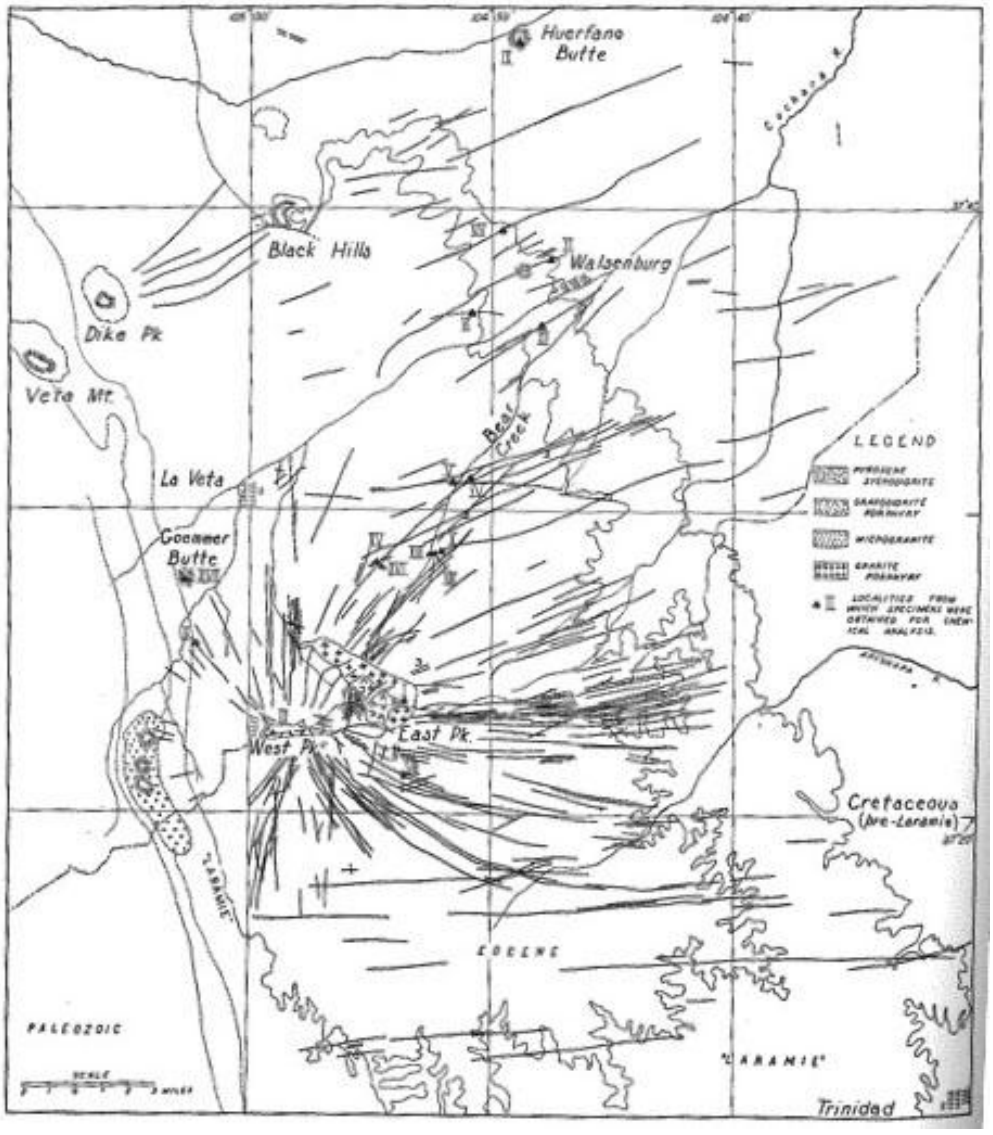

Figure 1.3: Map of stocks and dikes of the Spanish Peaks (Knopf, 1936).

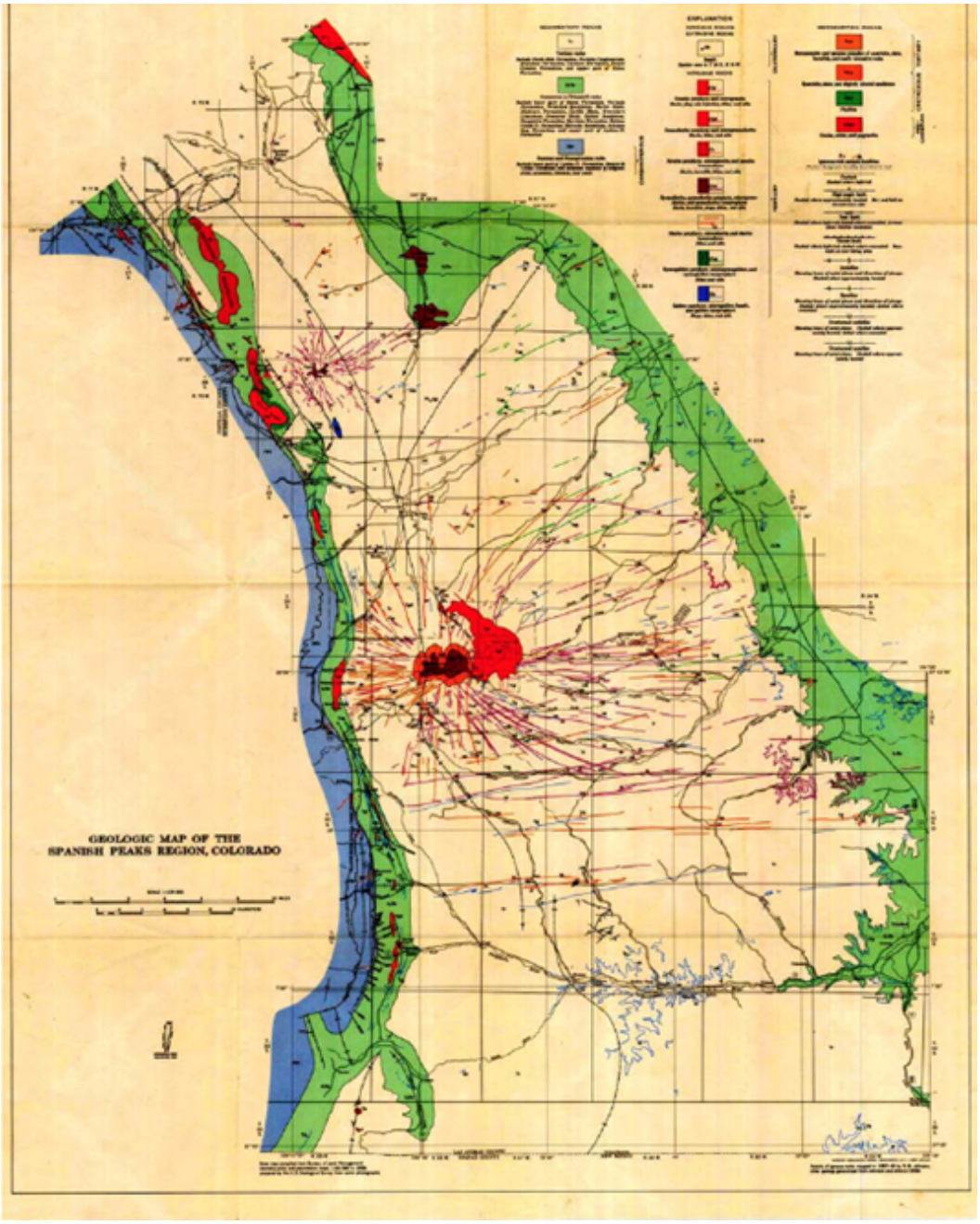

Figure 1.4: Map of the Spanish Peaks area from Johnson (1968).

CHAPTER 2

EXPERIMENTAL METHODS

In this chapter I describe the field and laboratory methods used in this study of the Spanish Peaks region, south-central Colorado.

FIELD SAMPLING METHODS

The Spanish Peaks area is unusual because several different types of magma intruded a relatively small area during a relatively short time period. Stocks, dikes, sills, and volcanic features are just a few of the large variety of igneous features in the area. Many of the subparallel dikes in this region are alkaline and range from relatively potassic ($K_2O/Na_2O \geq 1$) to relatively sodic ($K_2O/Na_2O < 1$) lamprophyres. Several of the dikes have been dated (Miggins, 2002; Penn, 1994), and many of these dated dikes were sampled by Heath McGregor (former UGA Master's student). Samples from this study were chosen to complement the samples of McGregor (2010) in order to ensure a representative range of compositions was included from across the sampling area. The Spanish Peaks location provides an unusual opportunity to explore the petrogenesis of a range of alkaline magma types knowing that their age and location are similar. Descriptions, photographs, GPS coordinates, and sketches were taken at each sample location (see "RESULTS: Field and Thin Section Descriptions). Weathered surface rock was removed and fist sized samples were taken from the center of the dikes, away from chilled margins.

Goemmer's Butte is one of the few features in the area that shows evidence of volcanic activity; it also contains large amphibole megacrysts, which are found in several other locations in the Spanish Peaks area. While Goemmer's Butte has been sampled and described before, it has not been thoroughly explored and described in detail. Goemmer's Butte was sampled for megacrysts and canvassed in order to determine the range of rock types and their locations. Many sketches, photos, samples, and notes were taken from this feature (see "RESULTS: Field and Thin Section Descriptions").

LABORATORY METHODS

Thin section blanks were prepared using a diamond-tipped water-cooled saw and sent to Quality Thin Sections (Tucson, AZ) for thin section preparation. Thin section descriptions (see "RESULTS: Field and Thin Section Descriptions) were completed with a standard petrographic microscope.

Electron Microprobe Methods

Thin sections were polished and carbon coated, and all electron microprobe analyses were performed using a JEOL 8600 electron microprobe located at the University of Georgia Department of Geology in Athens, Georgia. X-ray analysis was performed with a wavelength dispersive spectrometer (WDS) and typical conditions were an electron beam current of 15 nA, 1μm electron beam diameter, and an accelerating voltage of 15 kV. Apatite concentrations were measured using a lower beam current of 5 nA and a flared beam diameter of 5-10 μm. Analyses were processed with dQUANT automation software and back scattered electron images (BSE) were taken with Dpict software.

Powdering Samples

Seven samples were chosen for bulk rock x-ray fluorescence analysis to complement the data set of McGregor (2010). Samples were trimmed using a diamond tipped 20 cm water lubricated saw to remove any writing or weathered surfaces, then rinsed with tap and deionized water. Samples were placed in an oven (~120° F) to dry overnight.

Samples were crushed using a Braun Chipmunk Crusher which was cleaned with soap and water and dried with an air gun before and in between each sample. Crushed rock was then placed in a stainless steel Spex shatterbox and powdered to the consistency of flour. All parts of the shatterbox were cleaned with acetone and kimwipes before and in between samples.

X-Ray Fluorescence Methods

Fusion disks for x-ray fluorescence analysis were prepared by weighing 10.000 ± 0.005 g of flux (Lithium Borates/Lithium Bromide Fusion Flux, Spex Certiprep) into an aluminum boat with 2.500 ± 0.005 g powdered sample and placing the boat into an oven (~120° F) to prevent moisture contamination. Each sample and flux was transferred to a 50 mL 95/5 Pt/Au crucible and mixed with an electric shaker. Six drops of $LiNO_3$ and six drops of NH_4I were added and the mixture was placed in an oven at ~1085°. After 7.5 minutes the sample was removed and swirled for 30 seconds over a Bunsen burner, then placed back into the oven for 7.5 more minutes. Samples were removed, swirled again over a Bunsen flame for 30 seconds, then poured into a platinum crucible. Cooled disks were labeled and placed into a dessicator until analysis with a Philips Panalytical Wavelength Dispersive Sequential Spectrometer.

Loss on Ignition

8.50 ± 0.01 g of powdered sample was weighed into a 30 mL ceramic crucible with lid, which were prebaked at ~925º C for 1 hour prior to adding sample. Each sample was baked at ~925º C for 45 minutes, placed in a dessicator, and reweighed once cooled. The baked sample weight was subtracted from the prebaked sample weight, divided by 8.5 g and multiplied by 100 to obtain the loss on ignition percentage.

Stable Isotope Analysis

All stable isotope samples were amphibole megacrysts from the Spanish Peaks area and were prepared in the stable isotope lab in the Department of Geology at the University of Georgia, Athens, Georgia. For oxygen isotopic analysis, small pieces (~2 mg) of amphibole were picked from the megacrysts, either from the core or the rim of the crystal, and placed in a sample chamber for laser fluorination analysis. Sample chamber was exposed to BrF_5 and pumped down on the laser fluorination line overnight. During analysis, the sample is exposed to BrF_5 and a laser, which ablates the sample and releases all gas. The gas is purified and converted to CO_2 on the laser ablation line, then isotope ratios are measured with a duel inlet MAT 252 mass spectrometer.

Trace Element Analysis by ICP-MS

All trace element preparation for the inductively coupled plasma mass spectrometer (ICP-MS) and the analyses were performed at the National High Magnetic Field Laboratory at Florida State University in Tallahassee, Florida. Powdered sample was dissolved in 3:1 HF:HNO_3 and dissolved on a hot plate (~125ºC) for 48 hours, then evaporated until dry at ~100ºC. Sample was re-dissolved in 2 ml of 7N HNO_3 and placed in an ultrasonic bath for ~40 minutes. Sample was removed to a clean beaker and diluted

with quartz distilled water to 0.1% total dissolved solids. This solution was further diluted to ~0.05% TDS once initial analysis showed high concentrations of many elements. Solutions were analyzed with a Thermofisher Element 2XR high resolution ICP-MS.

Radiogenic Isotopes

Sr, Nd, Hf, and Pb were analyzed at the National High Magnetic Field Laboratory, and a four column separation was employed to extract elements for analysis. Sr analyses are discussed here, and Nd, Hf, and Pb results are in the appendix and will be discussed in a later publication. Techniques for separation chemistry are described in detail in Tschegg et al. (2011). Analyses for Sr isotopes were completed on a Finnigan MAT 262 TIMS (thermal ionization mass spectrometer) and analyses for Nd, Hf, and Pb isotopes were on a ThermoFinnigan Neptune MC-ICP-MS (multi-collector inductively coupled plasma mass spectrometer).

CHAPTER 3

RESULTS

This chapter presents the results from the relatively sodic and relatively potassic lamprophyres, Goemmer's Butte, and Tres Valles dike.

FIELD AND THIN SECTION DESCRIPTIONS

This section describes the sample localities of relatively potassic and sodic dikes that were sampled in this study, along with descriptions of thin sections produced from these outcrops.

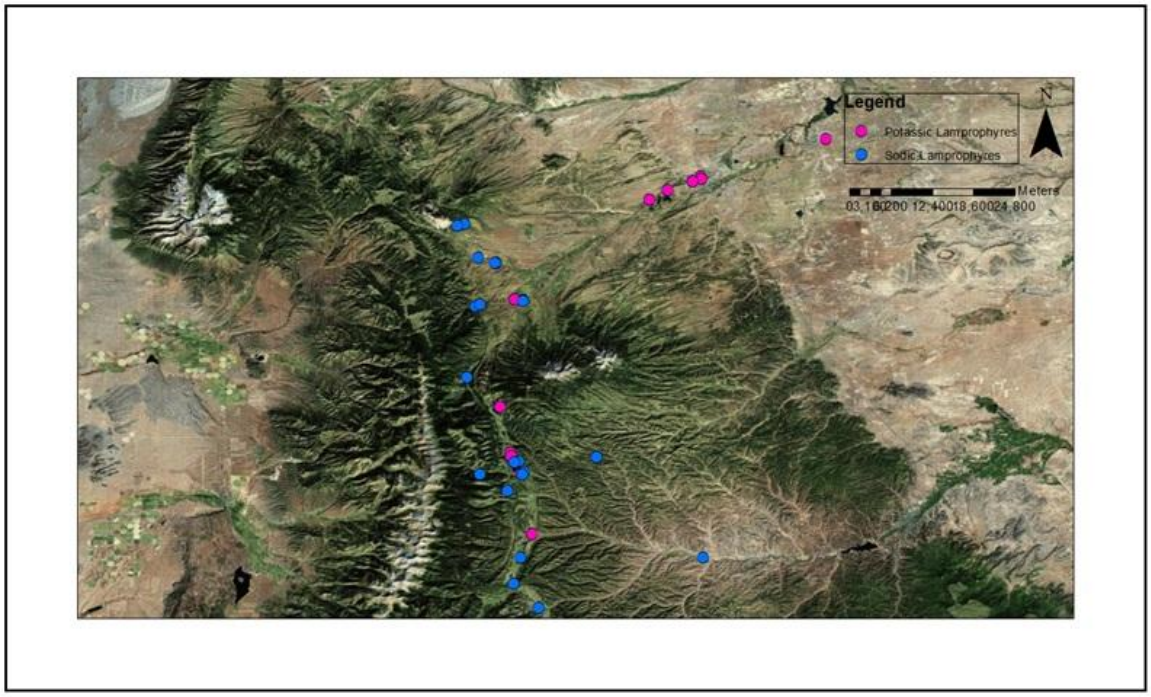

Figure 3.1: Map of study area including locations of samples from this study and those from McGregor (2010). Map produced using ArcMap 10.0 software.

BH-SW

This relatively sodic sill near Stonewall, CO is about 0.5 m wide and is poorly exposed off of County Rd. 13 (Fig. 3.2). This sill intrudes Pierre Shale and is highly weathered at the surface. Weathered surfaces were removed and the sample collected from the interior of the sill (BH-SW). This sample is fine-grained and dark grey in color. In thin section, BH-SW has a fine- to medium-grained porphyritic texture (Fig. 3.3). The major phenocrysts include amphibole, biotite/phlogopite, highly altered clinopyroxene, and completely replaced olivine. The groundmass consists of smaller grains of amphibole, biotite/phlogopite, clinopyroxene, plagioclase feldspar, calcite (~5%), apatite (<1%), and abundant opaque minerals (>1%). Additionally, there are some areas where feldspar, calcite, and euhedral quartz crystals are filling voids or have replaced minerals.

Figure 3.2: View looking northeast at the sill near Stonewall, CO where BH-SW was sampled. The Spanish Peaks can be seen in the background. Image adapted from Miggins (2002).

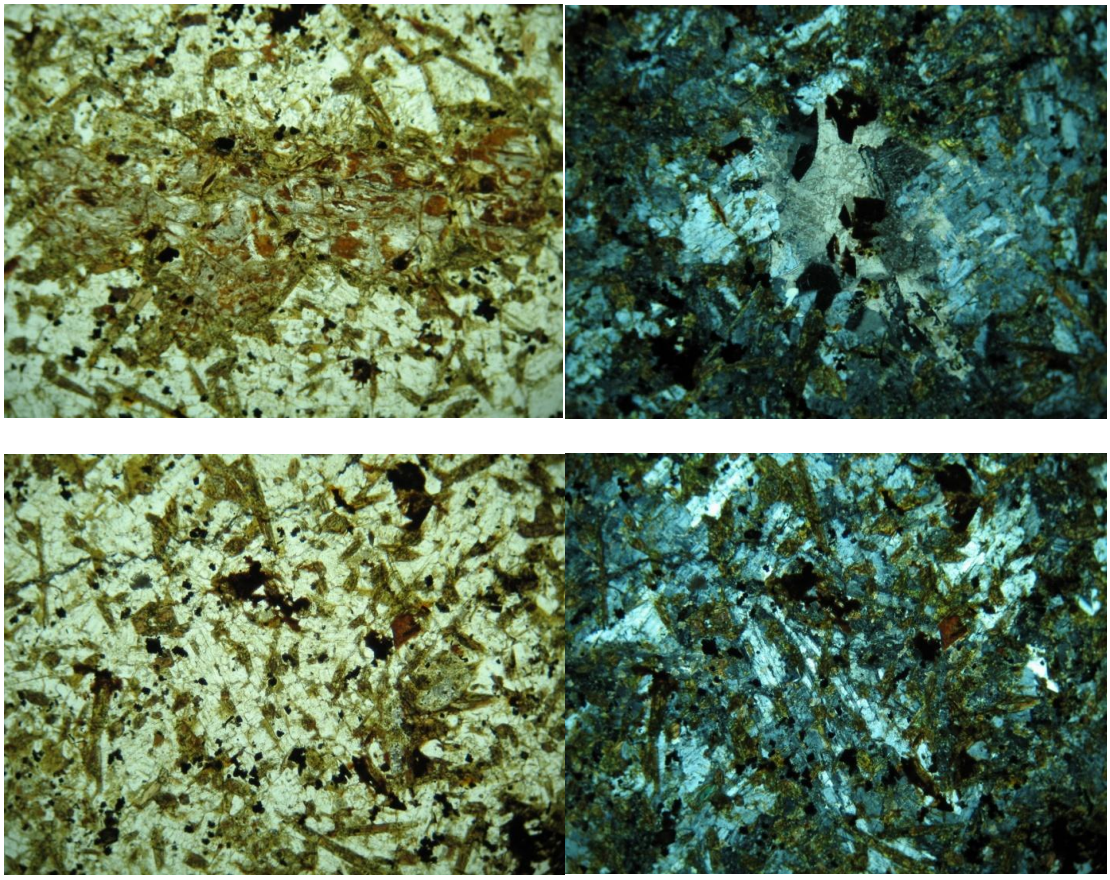

Figure 3.3: Multiple views of BH-SW. Top left panel shows a relict olivine completely replaced by calcite, iron oxides, and clays (PPL). Top right panel shows a void filled with calcite and euhedral quartz crystals (XPL). Bottom left and right panels show the same image in PPL and XPL, illustrating the groundmass and phenocrysts. All views are 3 mm across.

Dike 1 (BH-D1)

This relatively sodic dike is northwest of the town of La Veta, CO off of County Rd 440 (Fig. 3.4). This dike is ~1 m wide and dark grey and porphyritic aphanitic with elongate vesicles (up to 1 cm) throughout, paralleling the margins of the dike (Fig. 3.5). Surfaces of the dike were weathered to red-brown with some very dark patches. Weathered surfaces were removed and sample BH-D1 was taken from the center of the dike. In thin section, this sample is fine grained and is highly altered (Fig. 3.6). All Fe-Mg silicates have been altered to calcite, quartz, clays, hematite and other oxides. The only remaining igneous phenocrysts are subhedral plagioclase laths and glomeroporphyritic clusters, some of which are up to ~6 mm in length. Large calcite grains occur throughout. The groundmass consists of feldspar, apatite, calcite, quartz, clays, hematite and other oxides.

Figure 3.4: Dike 1 near La Veta, CO and sample location of BH-D1. Sharon McMullen for scale.

Figure 3.5: Photograph of Dike 1 near La Veta, CO illustrating elongate vesicles and fine-grained, dark gray surface.

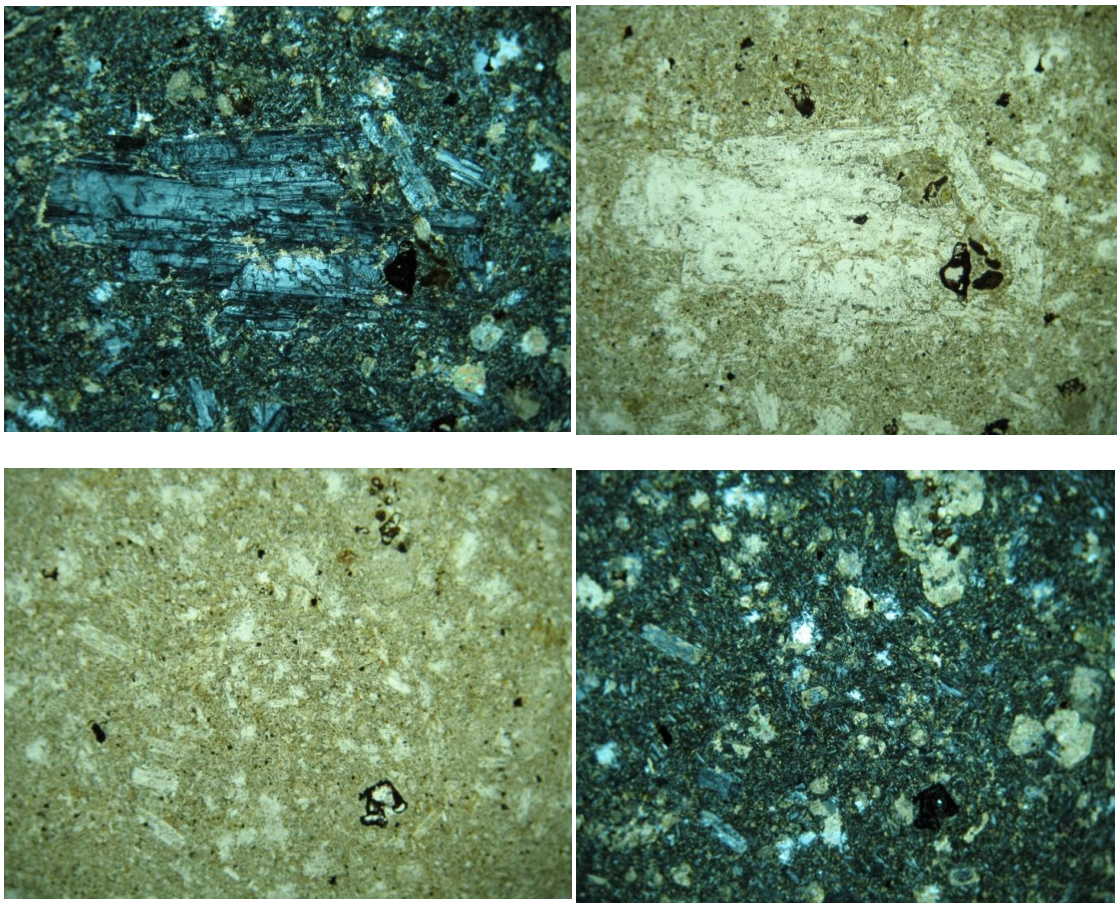

Figure 3.6: Multiple views of BH-D1. Top left and right panels are the same view in XPL and PPL, respectively, of a glomeroporphyritic feldspar cluster that has been partially replaced by calcite, hematite, and clays. Bottom left and right panels are typical views of the fine-grained texture of BH-D1, in PPL and XPL, respectively. Calcite has replaced all Fe-Mg minerals and the only phenocrysts remaining are feldspar. Hematite is the dark mineral shown in the bottom right of these two panels. All views are 3 mm across.

Dike 2 (BH-D2)

Dike 2 is relatively sodic and was sampled where it outcrops on County Rd 421 northwest of La Veta, CO. This ~1.5 m wide dike is porphyritic aphanitic and dark grey with red to tan weathering surfaces. Weathered surfaces were removed and BH-D2 was sampled from the center of the dike (Fig. 3.7). In thin section, this sample is medium- to coarse-grained porphyritic with phenocrysts of clinopyroxene that have been partially replaced by calcite and olivine that has been completely replaced by a green/light brown mixture of calcite, clays, micas and oxides (Fig. 3.8). Some large calcite grains occur. The groundmass consists of randomly oriented feldspar laths, biotite and chlorite, abundant oxides, calcite, and apatite.

Figure 3.7: View of Dike 2 and sample location of BH-D2.

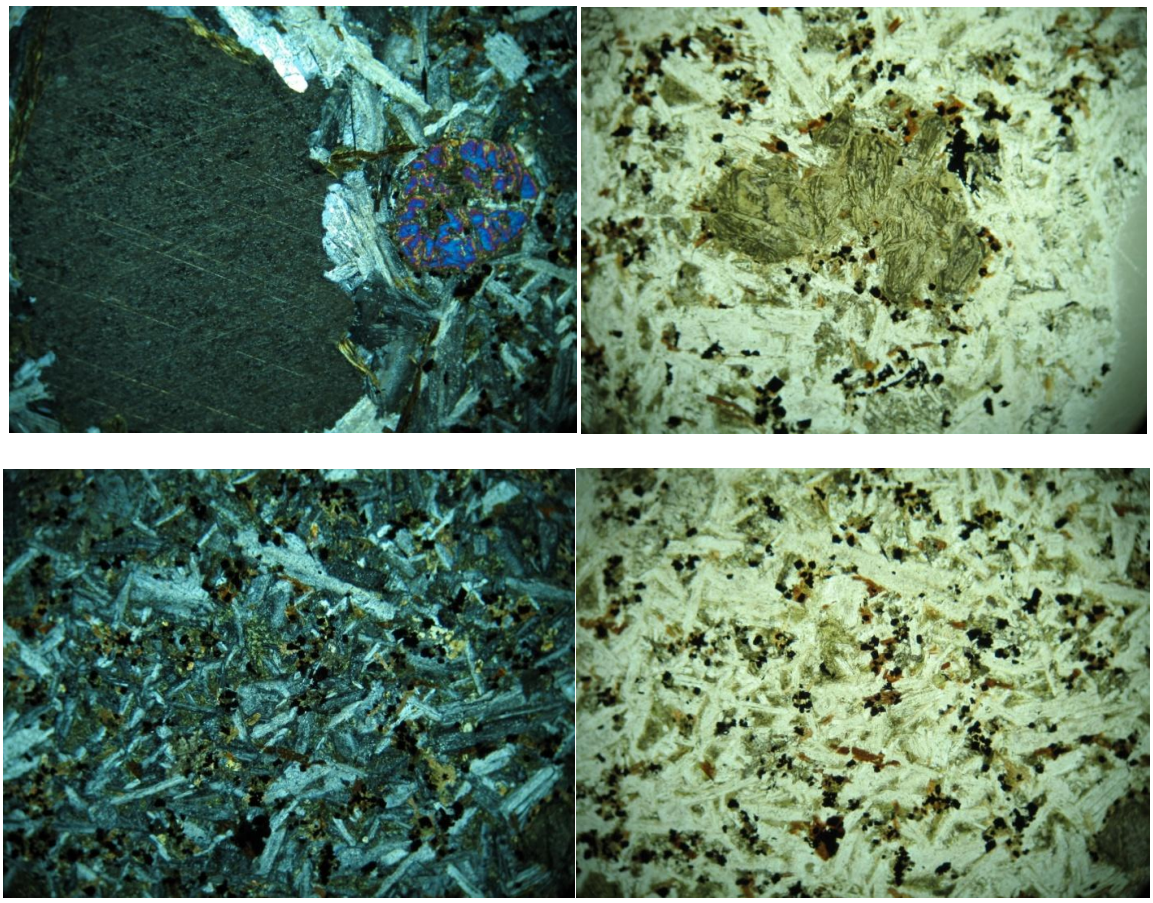

Figure 3.8: Multiple views of BH-D2 from Dike 2 northwest of La Veta, CO. The top left panel shows a large calcite grain adjacent to a smaller pyroxene that has been partially replaced by calcite (XPL). The top right panel shows an olivine phenocryst that has been completely replaced by calcite, oxides, and clays (PPL). The bottom left and right panel show a typical view of BH-D2 in XPL and PPL, respectively, with feldspar laths, biotite, clinopyroxene, calcite, and oxides. All photomicrographs are 4 mm across.

BH-31

This relatively sodic dike is ~6 m wide and located off of CO-12 near Monument Lake south of the North Lake Sill Complex (Fig. 3.9). This sill is dark grey, porphyritic apanitic, and highly weathered, especially near the contacts with baked shale. Weathered surfaces were removed and BH-31 was sampled from the center of this sill. In thin section, this sample has a glomeroporphyritic texture with clusters of phenocrysts of clinopyroxene up to ~3 mm that have many oscillatory zones, and olivine that has been completely replaced by calcite and clays (Fig. 3.10). The groundmass of this sample consists of plagioclase, biotite, abundant oxides, apatite, and secondary calcite.

Figure 3.9: Image of dike near Monument Lake off of CO-12. Sample BH-31 is from the center of this sill.

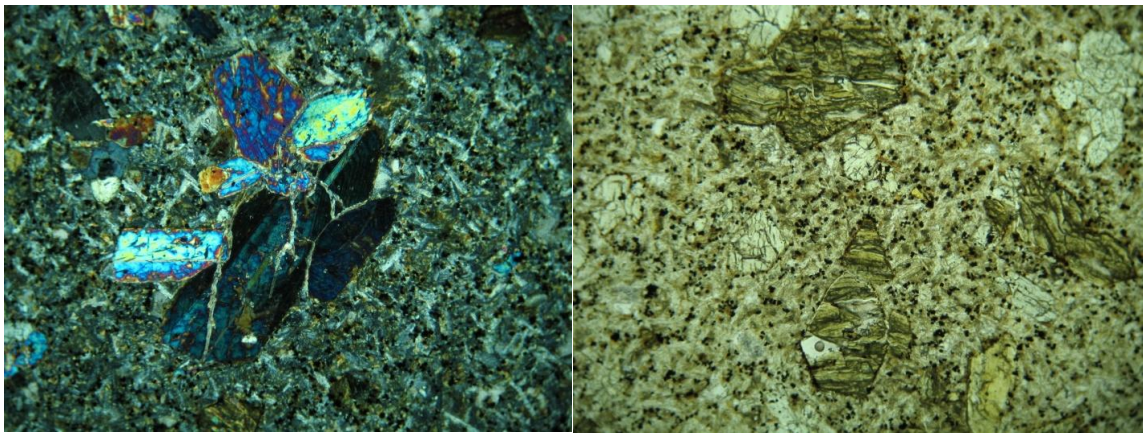

Figure 3.10: Views of BH-31. Left photomicrograph depicts a glomeroporphyritic cluster of clinopyroxene showing oscillatory zoning (XPL). Right panel depicts remnant olivine grains that have been completely altered to calcite and clays (PPL). Both views are 3 mm across.

BH-CO10

This dike relatively potassic and is the northernmost sample taken from the Raton Basin, and crops out on CO-10, northeast of Walsenburg, CO. The exposure here is poor and sampling was limited to a small exposure on the south side of the road. This dike is ~1.5 m wide and very weathered on the surface, and in some places caliche is evident. Weathered surfaces were removed and BH-CO10 was sampled from the center of the outcrop. This sample is grey-green and coarse-grained with numerous grains of biotite. In thin section, biotite is by far the most common and largest phenocryst, up to 3 mm in length. Biotites are zoned in color (Fig. 3.11) and sometimes have oxide and apatite inclusions. Other phenocrysts include clinopyroxene, which are zoned with distinct cores and rims in crossed polars. The groundmass of this sample contains plagioclase, pyroxene, biotite, abundant oxides (> 5%), and abundant apatite (> 1%), sometimes occurring as large euhedral crystals.

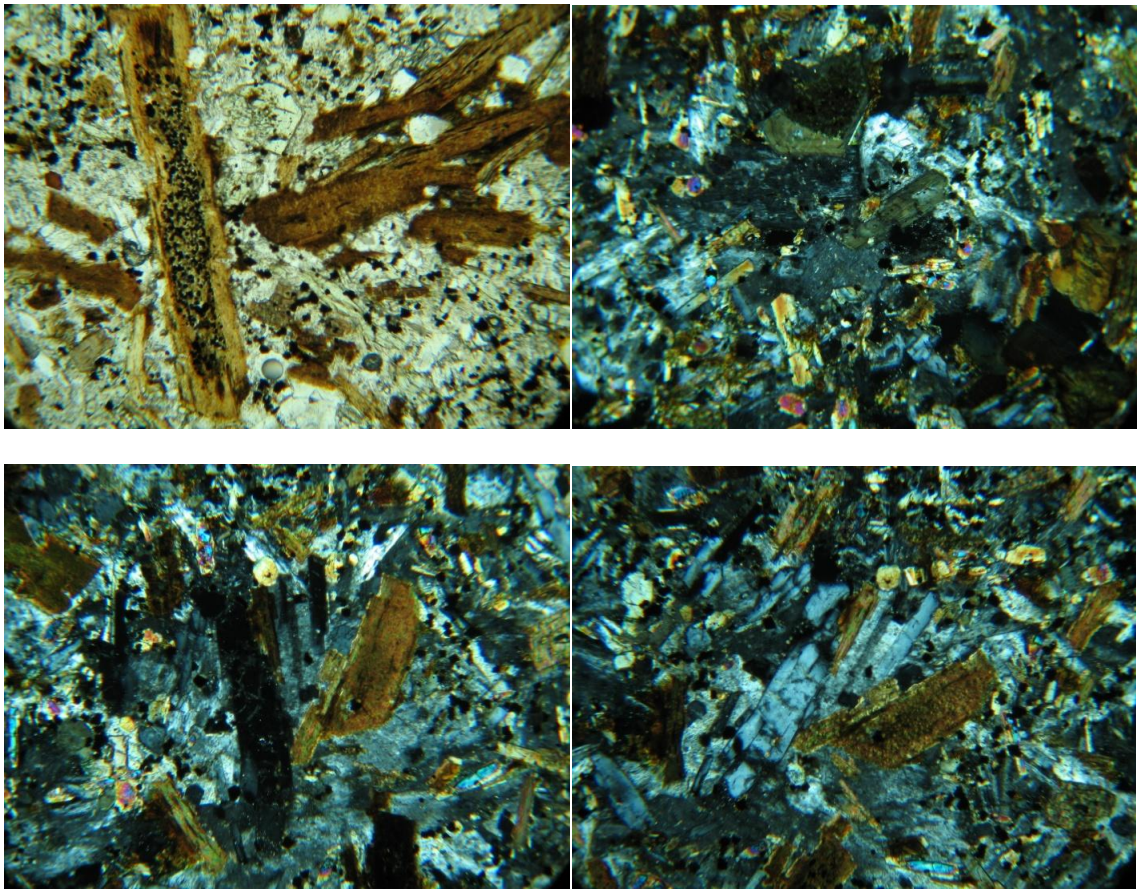

Figure 3.11: Multiple views of BH-CO10. Top left panel illustrates large zoned biotite phenocrysts and one that contains abundant oxide inclusions. Top right panel contains a zoned pyroxene phenocryst in the center (XPL). Top two panels are 5 mm across. Bottom left and right panels are the same view, turned slightly to illustrate the parallel extinction of large apatite crystals in the center of the photomicrograph (both XPL, 2.5 mm across).

Sill on Tercio Ranch (BH-TR)

This 7 m wide, relatively potassic sill is located off of County Rd. 13 south of Stonewall, CO (Fig. 3.12). This sill is fine-grained, dark grey in color and weathers to tan/light brown. Weathered surfaces were removed and BH-TR was sampled from the center of the dike. In thin section, this sample contains amphibole and psuedomorphs of calcite + clay in place of olivine (Fig. 3.13) as phenocrysts. Feldspar, pyroxene, amphibole, oxides, and sulfides make up the groundmass.

Figure 3.12: Photo of ~7 m wide sill at Tercio Ranch. Jon Primm in the foreground for scale.

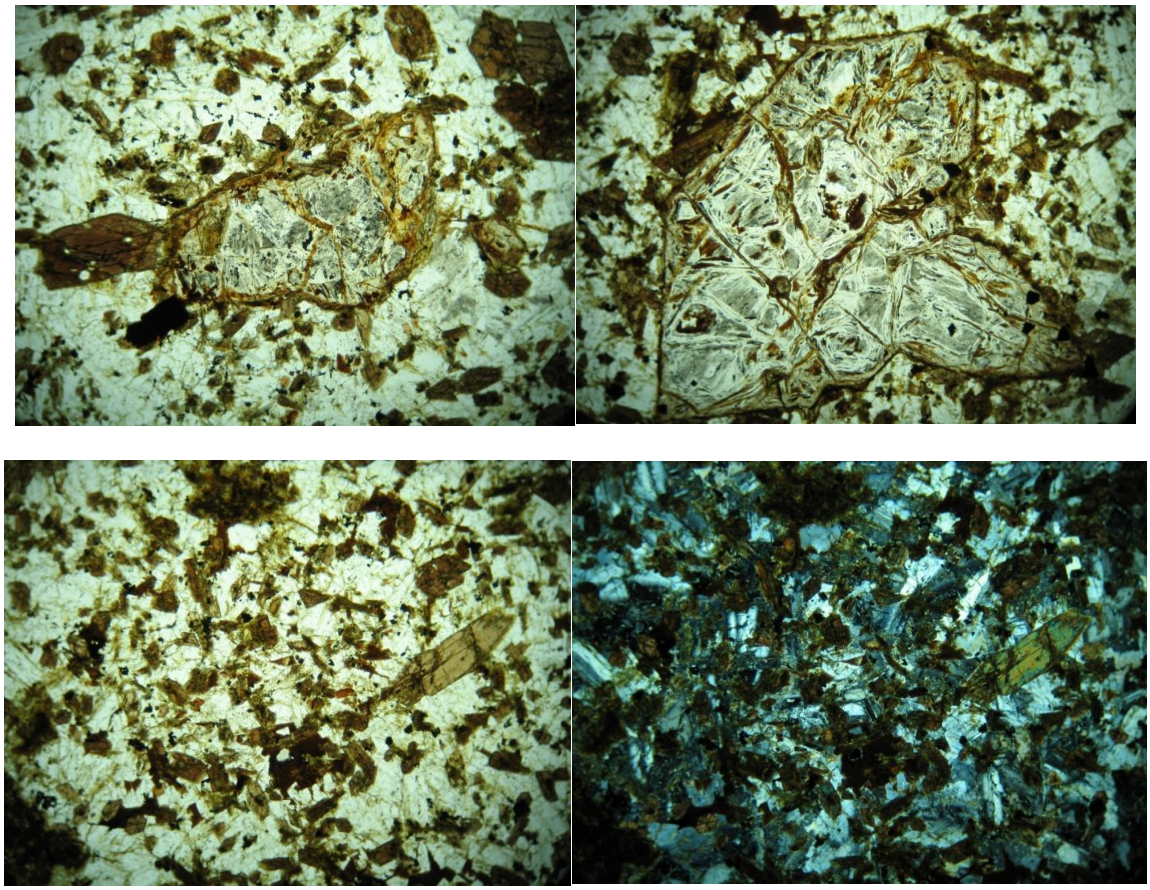

Figure 3.13: Multiple views of BH-TR in thin section. Top left and right panels are olivine that has been completely replaced (PPL). Bottom left and right panels show the same view of typical groundmass of BH-TR in PPL and XPL, respectively. All views are 3 mm.

Cuchara

This relatively sodic dike outcrops south of the town of Cuchara, CO on the west side of CO-12. It is roughly 2 meters in width and is highly altered on the surface. The exposed weathered surface of the dike was removed in the center, and a fist sized sample was collected. In thin section, this sample is porphyritic aphanitic with phenocrysts of clinopyroxene and secondary calcite that has completely replaced any other Fe-Mg phenocrysts that were originally present (Fig. 3.14). The groundmass consists of randomly oriented feldspar laths, clinopyroxene, abundant oxides and sulfides, calcite, and apatite.

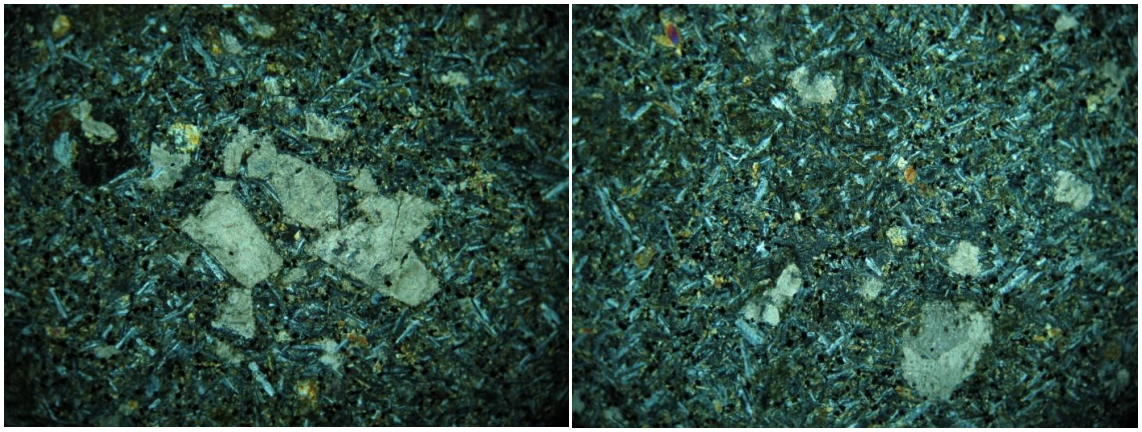

Figure 3.14: Photomicrographs of dike south of Cuchara, CO (BH-CUCH). The left panel shows calcite completely replacing phenocrysts; the right panel shows voids being filled with large calcite crystals as well as the ground mass consisting of feldspar, calcite, abundant oxides, and apatite. Both views are 3 mm by 5 mm, XPL.

North Lake Sill Complex

The North Lake Sill Complex outcrops off of CO-12 between the towns of Cuchara and Stonewall, Colorado, in a roadcut near North Lake (Fig 3.15). This is a large outcrop with multiple relatively sodic and relatively potassic lamprophyric sills exposed, ranging from 0.5 to ~5 meters thick. One relatively sodic sill was chosen from the outcrop for detailed analysis because it is large (2.5 meters thick) and contains amphibole megacrysts up to 3 cm in diameter (Fig. 3.16).

This sill is fine grained at the contacts with country rock grading into coarse grained in the center, with a maximum phenocryst size of 3 mm. The most abundant phenocryst is phlogopite (30%), with lesser amounts of oscillatory zoned clinopyroxene. The groundmass consists of smaller grains of phlogopite, clinopyroxene, abundant oxides, and apatite in a feldspar matrix. Chlorite alteration and secondary infilling calcite is also present in the groundmass. Amphibole occurs only as a megacryst, ranging from 0.5 to 3 cm in diameter, has red-brown to yellow-brown pleochroism, and is not zoned. The megacrysts of amphibole are concentrated in a one meter band in the center of the sill.

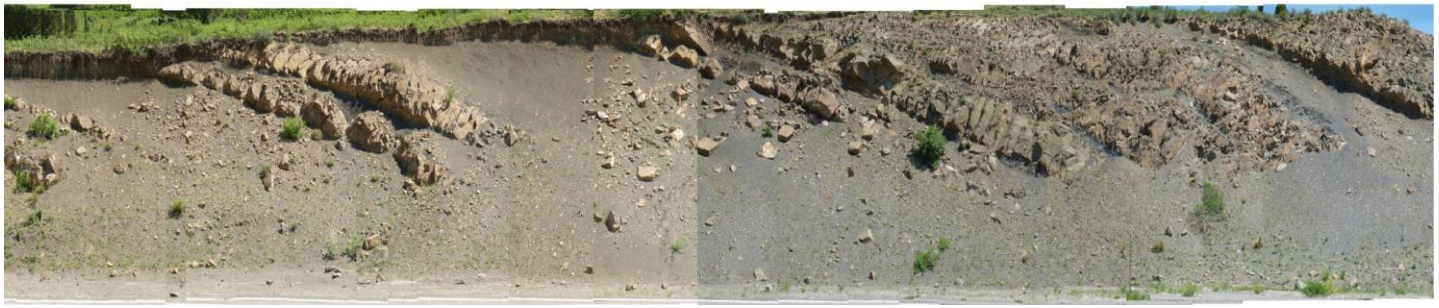

Figure 3.15: Panoramic photo compilation of the North Lake Sill Complex on Co. 12. Sills consist of both relatively sodic and potassic lamprophyres.

Figure 3.16: Sill from North Lake Sill Complex that contains amphibole megacrysts. Amphibole is concentrated in the center one meter of the sill.

Goemmer's Butte

Goemmer's Butte is located NW of West Spanish Peak, and is possibly a vent facies that primarily consists of gray trachyandesite (Fig. 3.17) and volcanic breccia that may have been an extrusive feature. The butte is located at an elevation of 8043 feet and West Spanish Peak, a volcano from the same time period is located at an elevation of 13,626 feet. West Spanish Peak has been eroded to its stock, and the fact that volcanic vent deposits are located ~5500 ft below the top of West Spanish Peak is an interesting puzzle, and these deposits may represent subvolcanic breccia. Goemmer's Butte is located in the Cuchara formation (Eocene; Lindsey, 1995), which consists of stratified alluvial fan deposits of sand to boulder sized clasts. The majority of the butte consists of very fine-grained gray trachyandesite, with no phenocrysts except for sparse, large (up to 10 cm), amphibole megacrysts and rare amphibole/pyroxene/apatite xenoliths. A tan igneous rock (trachydacite) was found in one location on the north side of the butte (Fig. 3.23). This rock was in contact with both gray trachyandesite and breccia, and commonly occurred between the two rock types. Evidence of explosive volcanic activity is present in the form of breccia surrounding and adhered to the surface of the butte (Fig. 3.18) and the sides of radial dikes (Fig. 3.25). The breccia is tan in color and contains clasts from sand up to boulder in size with quartz sand in the matrix. Several large gray trachyandesite dikes radiate from the north side of the butte, and several knobs of gray trachyandesite surround the butte. Each of these dikes and knobs are surrounded by breccia. In several places, large clasts of Cuchara formation that retain stratification have been tilted and incorporated into the breccias (Fig. 3.22). The north side of the butte

consists entirely of gray trachyandesite, with no adhering breccia or obvious radiating dikes (Fig. 3.20).

Figure 3.17: View of the north side of Goemmer's Butte. Photo taken about 300 meters from the base. The gray trachyandesite is visible at the top of the butte and in the center of radiating dikes (see Fig. 3.19). Tan breccias are visible adhering to the base of the butte and on the sides of the radiating dikes.

Figure 3.18: Same view of the north side of Goemmer's Butte. Red outlined area is breccia adhering to the sides of the butte and radiating dikes.

Figure 3.19: Same view of the north side of Goemmer's Butte as figure 3.17. Blue outlined area is gray trachyandesite making up the butte and radiating dikes. Pink outlined area is the location of tan trachydacite.

Figure 3.20: View of the south side of Goemmer's Butte. All exposed surfaces on this side of the butte are gray trachyandesite. No adhering breccia or obvious radiating dikes are found on this side of the butte. Photo was taken about 200 meters from the base of the butte.

Figure 3.21: View of breccia adhering to the west side of a dike of gray trachyandesite from Goemmer's Butte. Clasts in the breccia range from sand to boulder size with quartz sand in the matrix.

Figure 3.22: Photo of large block of Cuchara formation that retains sedimentary structures. It has been tilted and emplaced with the breccia.

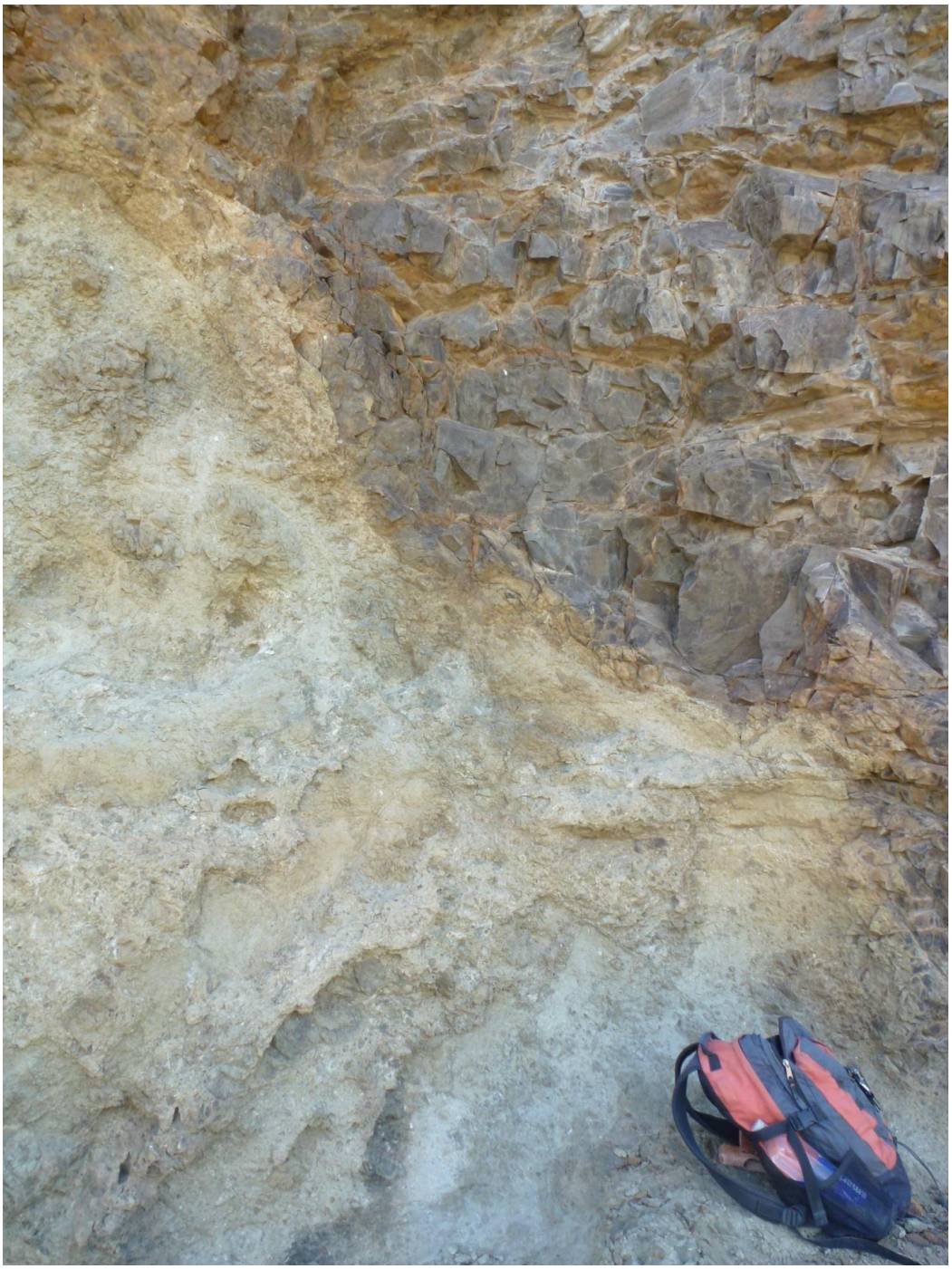

Figure 3.23: Photo of contact between dike of gray trachyandesite and breccia.

Figure 3.24: Image of contact between gray trachyandesite and breccia. Small gray spherical bodies that may be trachyandesite magma are incorporated into the breccia nearby this contact.

Figure 3.25: Image of breccia adhering to the side of a large gray trachyandesite dike.

BULK ROCK MAJOR ELEMENT COMPOSITIONS

X-ray fluorescence (XRF) data for samples from this study are tabulated in table 3.1. In this study, alkaline lamprophyres from the Spanish Peaks area range from very potassic to very sodic, and for discussion purposes are placed in one of two groups (Fig. 3.26): relatively potassic ($K_2O/Na_2O > 1$) and relatively sodic ($K_2O/Na_2O < 1$). Seven new analyses were obtained for rocks from the Spanish Peaks area, and these are combined with those from McGregor (2010) in figure 3.26. Rocks from Goemmer's Butte and Tres Valles dike are also plotted for comparison. Two rocks from Goemmer's Butte were analyzed, one from the gray trachyandesite that composes the majority of the butte, and one from a newly described tan trachydacite from this locality. Tres Valles dike and two Goemmer's Butte analyses are relatively sodic, but the tan rock from Goemmer's Butte is very potassic.

The IUGS TAS (total alkali vs. silica) diagram (Fig. 3.27) is used for nomenclature of extrusive volcanic rocks. All rocks in this study are probably hypabyssal intrusive rocks but their fine grain size prohibits the use of the IUGS classification system for plutonic rocks. Consequently, the rocks are classified using the TAS diagram. All the rocks in this study (except for one Goemmer's Butte sample) plot above the alkaline/subalkaline dividing line (dashed line in figure 3.26). The relatively potassic lamprophyres plot primarily in the tephrite basanite field, with one analysis each in the trachybasalt and basaltic trachyandesite fields. The relatively sodic lamprophyres plot primarily in the trachybasalt and basaltic trachyandesite fields, with a couple of analyses in the tephrite basanite field and one in the foidite field. Goemmer's Butte samples are the most silicic samples, with two analyses in the trachyandesite field (one above and one

below the alkaline/subalkaline dividing line) and one (tan sample) in the trachydacite field. The Tres Valles dike sample plots on the dividing line between the trachybasalt and basaltic trachyandesite fields.

Major oxides are plotted vs. Mg # for rocks from the Spanish Peaks in figure 3.28 to determine trends for the different groups. While there is overlap between the relatively potassic and sodic lamprophyres in each figure, as a group the relatively potassic lamprophyres have higher concentrations of TiO_2, K_2O, CaO, and P_2O_5, lower SiO_2, Na_2O, Al_2O_3, and higher Mg # than the relatively sodic lamprophyres. Goemmer's Butte samples have higher SiO_2 and Al_2O_3 than any of the lamprophyres, and much lower Mg #. They have lower concentrations of TiO_2, total Fe, CaO, and P_2O_5 than any of the lamprophyres. Tres Valles dike has a TiO_2 concentration and Mg # intermediate between the Goemmer's Butte and lamprophyre samples, but has similar concentrations of other oxides as the lamprophyres (particularly the relatively sodic lamprophyres).

Table 3.1: XRF data for rocks from the Spanish Peaks region.							
Sample:	**Dike 2**	**Co-10**	**Cuchara**	**grey Goemmer's Butte**	**tan Goemmer's Butte**	**Tres Valles**	**BH-SW**
SiO_2	49.91	44.43	43.08	56.73	59.50	49.86	49.10
TiO_2	1.95	2.87	2.01	0.95	0.77	1.25	1.95
Al_2O_3	15.33	11.23	14.78	16.57	16.12	15.29	13.80
FeO*	6.13	4.63	7.34	4.82	3.60	7.95	5.01
Fe_2O_3*	3.45	4.37	3.51	2.45	2.27	2.75	3.45
MnO	0.14	0.12	0.17	0.13	0.07	0.19	0.12
MgO	5.84	4.89	7.77	2.20	1.26	5.33	5.62
CaO	5.86	8.81	11.50	4.29	2.04	7.60	7.30
Na_2O	4.87	2.80	3.53	4.62	3.22	3.93	3.03
K_2O	1.91	4.88	0.32	3.64	6.86	2.44	2.57
P_2O_5	0.59	2.53	0.71	0.62	0.49	0.69	0.98
LOI**	3.54	1.07	7.51	2.13	2.85	1.39	6.43
Total:	99.51	92.63	102.23	99.15	99.04	98.66	99.36
Mg#***	49	51	51	31	26	40	53

* iron recalculated according to Irvine and Baragar (1971);
** loss on ignition; *** 100*(MgO/(MgO+FeO))

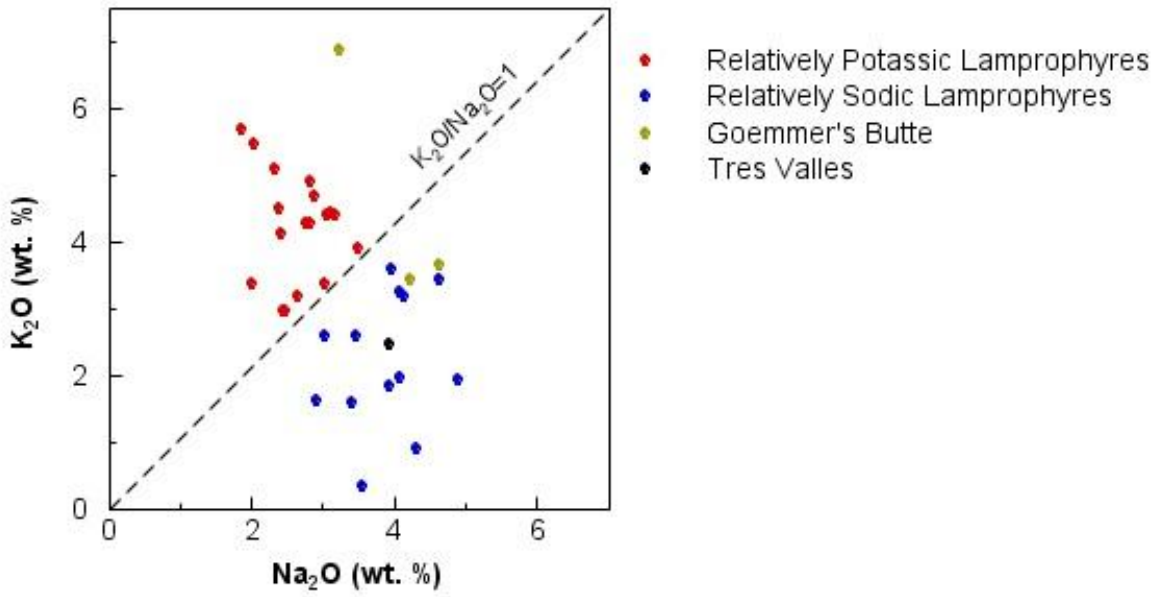

Figure 3.26: The dashed line represents the ratio of $K_2O/Na_2O = 1$. In this study, lamprophyres with $K_2O/Na_2O > 1$ are "relatively potassic" and plot above the dashed line, and lamprophyres with $K_2O/Na_2O < 1$ are "relatively sodic" and plot below the dashed line. Goemmer's Butte and Tres Valles dike are also plotted for comparison. Data from this study are combined with those from McGregor (2010) for this figure.

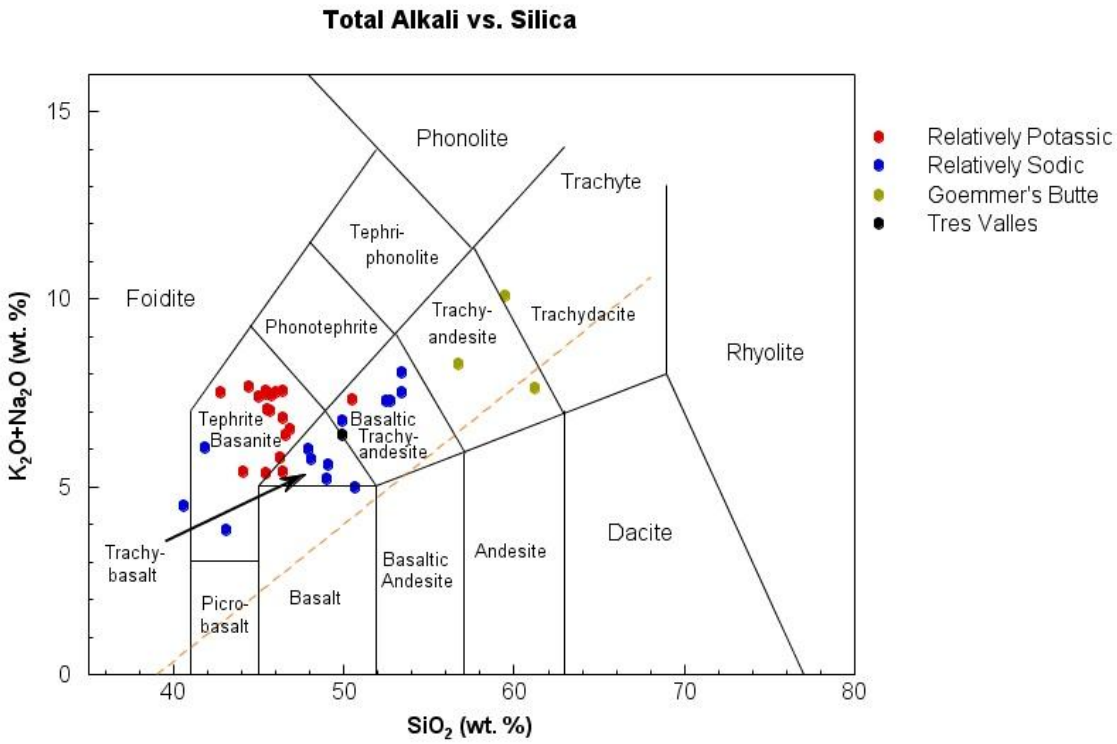

Figure 3.27: IUGS TAS classification diagram after LeBas et al. (1986) showing the positions of rocks from this study and those from McGregor (2010). Dashed orange line is the alkaline/subalkaline dividing line.

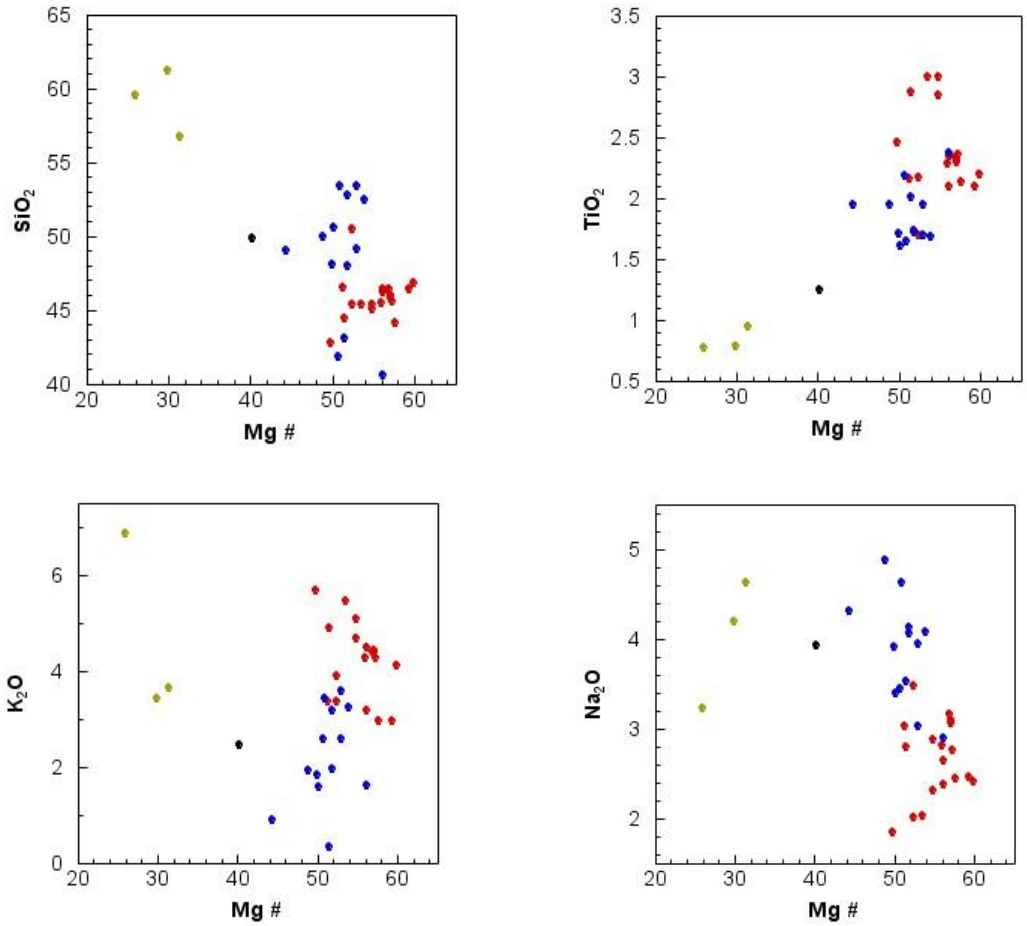

Figure 3.28

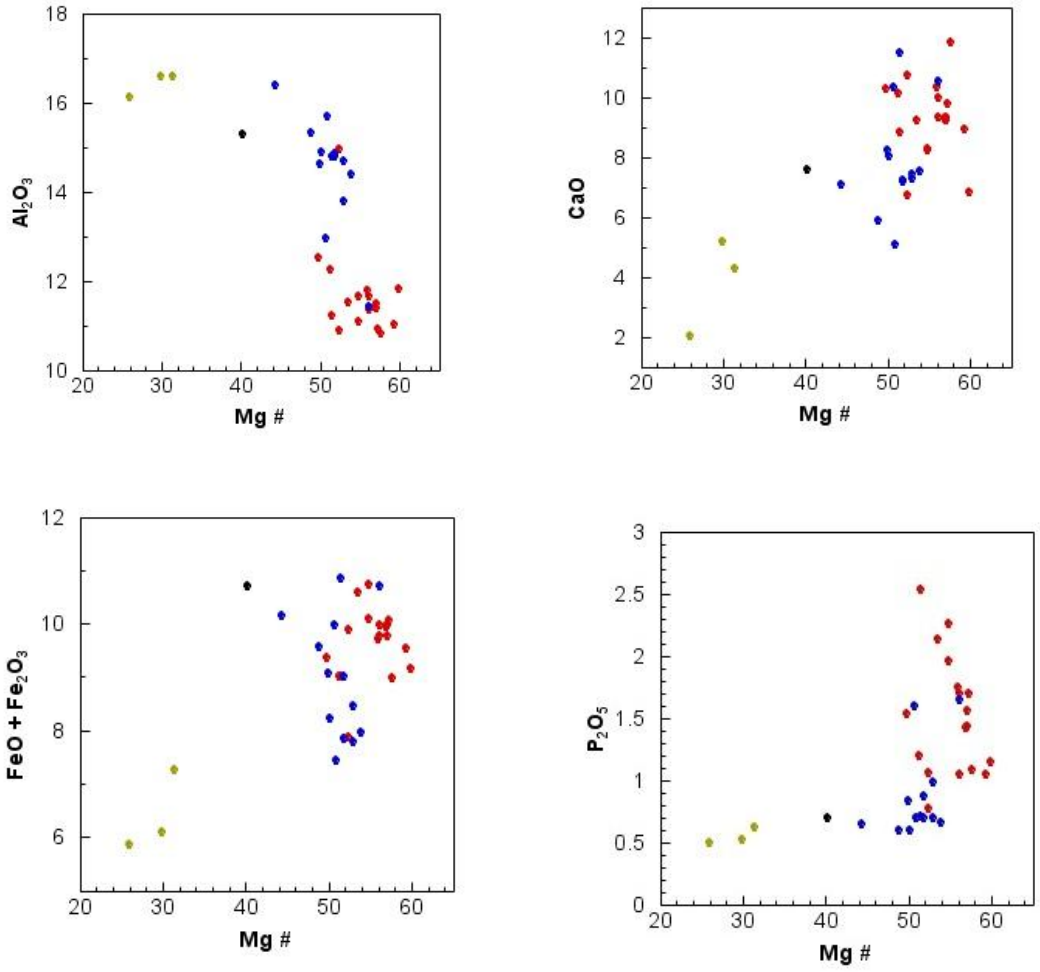

Figure 3.28: Major oxides of rocks from the Spanish Peaks area plotted vs. Mg #. Red circles are relatively potassic lamprophyres, blue circles are relatively sodic lamprophyres, yellow circles are Goemmer's Butte analyses, and the black circle is the Tres Valles dike analysis. Data from this study are combined with those of McGregor (2010) for this figure.

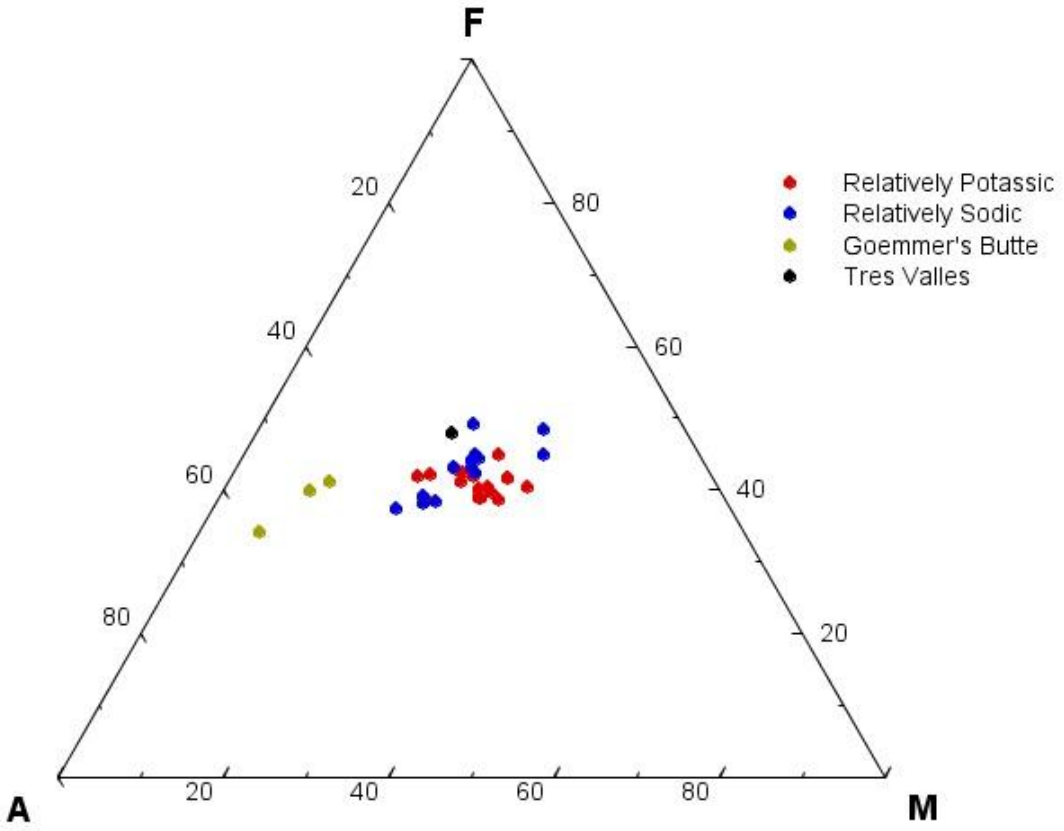

Figure 3.29: AFM diagram for rocks from the Spanish Peaks area. Corner A is total alkalis ($Na_2O + K_2O$), corner M is MgO, and F is ($FeO + Fe_2O_3$). Data from McGregor (2010) was combined with those from this study to produce this figure.

BULK ROCK TRACE ELEMENT ABUNDANCES

Samples analyzed at the Center for Applied Isotope Studies for major elements were also analyzed for trace elements (Table 3.2).

Trace elements were also measured by ICP-MS at the National High Magnetic Field Laboratory (NHMFL) at Florida State University. Seven samples were chosen from this study and three samples from McGregor (2010) were measured as well. One sample from this study, GB-M2, is an amphibole megacryst from Goemmer's Butte. ICP-MS data are shown in table 3.3. In table 3.4 the data from XRF and ICP-MS are tabulated in order to compare. For almost all elements there is good agreement between the two methods (Fig. 3.30).

Because of higher precision, the ICP-MS data are used in the plots that follow. In figure 3.31, samples are normalized to primitive mantle values from Lyubetskaya and Korenaga (2007). All samples show a similar pattern enriched in Ba and depleted in Ni and Cr. One sodic sample shows a different pattern with depletions in Cs, Rb, and K compared to other sodic lamprophyres. Tres Valles dike is very similar to both the sodic and potassic lamprophyres. Goemmer's Butte trachyandesite also has a similar pattern to the lamprophyres, but is slightly more depleted in Ni, Cr, and Cu. The amphibole megacryst from Goemmer's Butte has a different pattern than the host and other samples.

Figure 3.32 is normalized to NMORB values from Lehnert (2000). Overall the patterns of both the sodic and potassic lamprophyres are similar, but one sodic lamprophyre shows depletions in Cs, Rb, and K as in the primitive mantle normalized multi-element diagram. Most of the potassic lamprophyres are more enriched in Cs than the sodic lamprophyres. Goemmer's Butte and Tres Valles dike are more depleted in Ni

and Cr than the lamprophyres, and the amphibole megacryst from Goemmer's Butte again shows a different pattern than its host.

In chondrite-normalized REE diagram figure 3.33, all samples show depletions in the heavy rare earths and enrichment in light rare earths except the amphibole megacryst from Goemmer's Butte. Relatively potassic lamprophyres have a slightly higher enrichment in the light rare earths than relatively sodic lamprophyres. Goemmer's Butte trachyandesite has a very similar pattern to the relatively sodic lamprophyres. Tres Valles Ranch dike has a very similar pattern to Goemmer's Butte trachyandesite and the relatively sodic lamprophyres, but is slightly more enriched in the heavy rare earths than other samples. The amphibole megacryst from Goemmer's Butte is depleted in light rare earths compared to the other samples.

Table 3.2: Trace element concentrations from XRF							
Element	Tres Valles	Goemmer's Butte gray	Goemmer's Butte tan	sodic Dike 2	sodic Cuchara	sodic BH-SW	potassic BH-CO10
V*	279	90.5	89.3	235	267	170	113
Cr	54.9	15.1	17.6	145	222	176	122
Co	19.0	< 2.0	< 2.0	49.0	56.6	23.7	< 2.0
Ni	28.3	6.80	3.40	74.7	153	86.3	77.0
Cu	76.8	10.3	9.70	44.7	60.2	45.1	66.7
Zn	83.2	106	86.3	81.2	90.6	76.3	141
Ga	21.9	24.8	17.9	25.0	21.6	23.1	24.9
Rb	39.8	59.5	156	45.7	3.00	32.0	60.9
Sr	913	836	402	984	717	1116	1237
Y	27.0	26.9	24.3	22.8	24.1	21.3	23.8
Zr	118	206	196	205	159	280	339
Nb	15.6	19.6	18.8	40.9	33.2	44.6	80.3
Ba	931	2056	2659	1971	569	2935	3086
La	30.8	46.5	53.4	39.4	36.6	65.3	120
Ce	53.9	64.6	66.5	58.7	71.2	93.9	219
Nd	40.1	59.7	58.2	49.1	31.8	75.3	151
Hf	4.00	8.80	8.60	8.10	5.10	5.70	9.50
Pb	6.70	12.8	9.50	9.20	9.90	8.40	15.8
Th	3.30	3.50	3.50	6.10	3.40	4.30	5.30
*all concentrations in ppm							

Table 3.3: Trace element abundances from ICP-MS					
Element	Tres Valles	Goemmer's Butte	Goemmer's Amphibole megacryst	sodic Dike 2	sodic Cuchara
Rb*	40.00	59.94	7.22	46.20	3.181
Sr	916.0	829.5	327.6	980.5	721.9
Y	26.63	24.03	19.65	21.81	23.28
Zr	109.6	205.2	30.25	223.3	167.5
Nb	16.16	20.45	4.667	49.39	38.21
Cs	0.496	0.259	0.280	0.477	0.036
Ba	977.1	2015	286.5	2020	581.9
La	32.80	42.26	2.870	44.31	38.86
Ce	65.74	90.07	11.25	84.51	77.23
Pr	8.594	11.12	2.320	9.715	9.442
Nd	35.91	44.07	13.96	36.80	37.47
Sm	7.193	8.512	4.608	6.874	7.148
Eu	2.231	2.468	1.504	2.260	2.239
Gd	6.970	8.069	5.051	6.878	7.074
Tb	0.921	1.016	0.795	0.860	0.914
Dy	4.995	4.967	4.384	4.332	4.683
Ho	0.953	0.832	0.743	0.785	0.840
Er	2.656	2.003	1.683	2.036	2.196
Tm	0.369	0.249	0.193	0.269	0.288
Yb	2.377	1.482	1.029	1.695	1.813
Lu	0.338	0.200	0.128	0.233	0.247
Hf	3.063	5.059	1.179	5.211	3.944
Ta	0.797	1.144	0.201	2.914	1.984
Pb	5.863	11.64	3.213	10.32	8.071
Th	3.460	4.260	0.089	9.636	4.910
U	0.813	1.257	0.026	2.708	1.145
Li	9.829	23.04	2.818	36.95	20.56
Sc	27.15	8.286	29.04	15.13	24.36
Ti	7696	6026	15255	11231	13491
V	270.2	108.7	524.1	193.3	259.2
Cr	49.27	10.37	17.21	119.1	272.8
Co	30.07	15.31	67.13	32.67	48.30
Ni	27.18	6.608	103.4	74.46	176.8
Cu	67.96	10.07	16.61	45.50	64.20
Zn	126.1	125.1	111.4	105.8	120.3
*all values in ppm					

Table 3.3 cont.					
Element	sodic BH-SW	potassic HM-28	potassic HM-18	potassic HM-4	potassic BH-CO10
Rb*	32.37	53.99	51.97	95.11	50.05
Sr	1173	1295	893	1680	1056
Y	20.23	23.85	22.51	23.37	17.67
Zr	298.0	322.8	296.0	379.1	295.3
Nb	53.01	61.54	55.30	84.08	80.62
Cs	0.307	1.535	1.901	3.013	0.378
Ba	3209	3202	3071	3612	2615
La	57.17	57.90	50.98	114.1	91.22
Ce	120.2	130.3	115.7	240.2	212.8
Pr	14.23	16.03	14.63	28.99	26.79
Nd	54.61	63.91	58.69	112.9	105.9
Sm	8.999	10.94	10.26	17.29	15.72
Eu	2.625	3.258	3.076	4.726	4.145
Gd	8.302	10.08	9.397	14.69	12.71
Tb	0.919	1.130	1.057	1.401	1.178
Dy	4.207	5.101	4.793	5.337	4.178
Ho	0.737	0.885	0.819	0.836	0.634
Er	1.906	2.220	2.077	1.994	1.455
Tm	0.250	0.286	0.268	0.241	0.179
Yb	1.572	1.766	1.618	1.492	1.080
Lu	0.216	0.241	0.221	0.198	0.142
Hf	6.966	7.999	7.408	9.347	7.062
Ta	3.105	3.772	3.476	4.986	3.932
Pb	8.228	12.33	9.915	11.77	11.63
Th	7.281	7.207	6.084	6.708	5.784
U	2.236	2.032	1.745	2.249	2.646
Li	59.46	23.35	38.88	17.03	13.78
Sc	14.77	17.97	22.45	17.27	10.41
Ti	10821	11128	12425	16702	13641
V	160.5	169.6	195.6	206.0	125.9
Cr	161.4	263.6	454.0	180.8	89.33
Co	30.35	30.42	45.35	38.19	26.09
Ni	83.81	116.9	250.6	111.7	60.43
Cu	42.42	52.01	68.02	60.71	46.20
Zn	75.22	100.8	111.4	150.0	128.7
*all values in ppm					

	Table 3.4: Comparison of trace element abundances between ICP-MS and XRF.							
	BH-TV		**GB-gray**		**BH-D2**		**BH-CUCH**	
	ICP-MS	XRF	ICP-MS	XRF	ICP-MS	XRF	ICP-MS	XRF
Rb*	39.43	39.80	64.07	59.50	50.34	45.70	3.198	3.000
Sr	969.6	913.0	911.1	836.0	1051	984.4	802.5	717.1
Y	27.14	27.00	24.78	26.90	22.97	22.80	24.64	24.10
Zr	114.0	118.0	213.2	205.9	238.4	205.0	177.8	159.2
Nb	16.82	15.60	21.55	19.60	52.46	40.90	40.74	33.20
Ba	1017	930.6	2101	2056	2092	1971	603.4	568.9
La	36.36	30.80	47.24	46.50	50.15	39.40	43.51	36.60
Ce	72.78	53.90	98.11	64.60	93.91	58.70	85.69	71.20
Nd	38.76	40.10	47.08	59.70	39.16	49.10	38.67	31.80
Hf	3.328	4.000	5.272	8.800	5.283	8.100	3.982	5.100
Pb	5.914	6.700	11.11	12.80	9.496	9.200	7.316	9.900
Th	3.762	3.300	4.595	3.500	10.19	6.100	5.189	3.400
Ti	7357	7494	5182	5689	11360	11678	12697	12062
V	252.4	279.3	94.46	90.50	202.4	234.9	253.6	267.2
Cr	45.82	54.80	8.451	15.10	117.7	144.6	253.1	222.2
Co	27.64	19.00	13.33	nd	32.49	49.00	45.01	56.60
Ni	25.21	28.30	6.130	6.800	71.81	74.70	159.4	153.1
Cu	64.31	76.80	8.624	10.30	42.69	44.70	58.55	60.20
Zn	122.4	83.20	106.56	106.1	98.36	81.20	109.7	90.60
* all concentrations in ppm								

Table 3.4 cont.								
	BH-SW		**HM-28**		**HM-18**		**HM-4**	
	ICP-MS	XRF	ICP-MS	XRF	ICP-MS	XRF	ICP-MS	XRF
Rb*	32.70	32.00	57.66	60.00	54.59	59.00	102.6	94.00
Sr	1197	1116	1349	1260	935.9	896.0	1734	1495
Y	18.62	21.30	22.07	25.00	20.51	23.00	21.65	21.00
Zr	268.8	279.7	300.5	316.0	268.6	293.0	351.7	333.0
Nb	49.50	44.60	57.21	63.00	51.73	58.00	78.44	82.00
Ba	3200	2935	3235	3080	3136	3200	3686	3360
La	52.43	65.30	53.64	63.00	46.98	60.00	101.1	100.0
Ce	105.7	93.90	115.7	nd**	102.8	nd	220.0	nd
Nd	50.35	75.30	58.42	nd	54.66	nd	103.9	nd
Hf	6.269	5.700	7.374	nd	6.690	nd	8.392	nd
Pb	7.868	8.400	11.95	10.00	9.409	8.000	11.20	10.00
Th	6.355	4.300	6.348	6.000	5.242	6.000	5.864	10.00
Ti	12946	11684	11607	12949	13294	12769	21557	17925
V	197.5	169.7	179.4	223.0	211.2	237.0	267.4	250.0
Cr	202.6	175.8	286.4	264.0	502.0	423.0	238.9	174.0
Co	37.25	23.70	32.34	nd	49.61	nd	49.26	nd
Ni	105.0	86.30	126.9	138.0	277.6	217.0	149.8	121.0
Cu	54.27	45.10	59.26	62.00	78.30	70.00	82.72	62.00
Zn	101.6	76.30	117.1	118.0	134.2	126.0	207.2	134.0

* all concentrations in ppm; ** no data; Ce, Nd, and Hf were not measured by XRF in McGregor (2010)

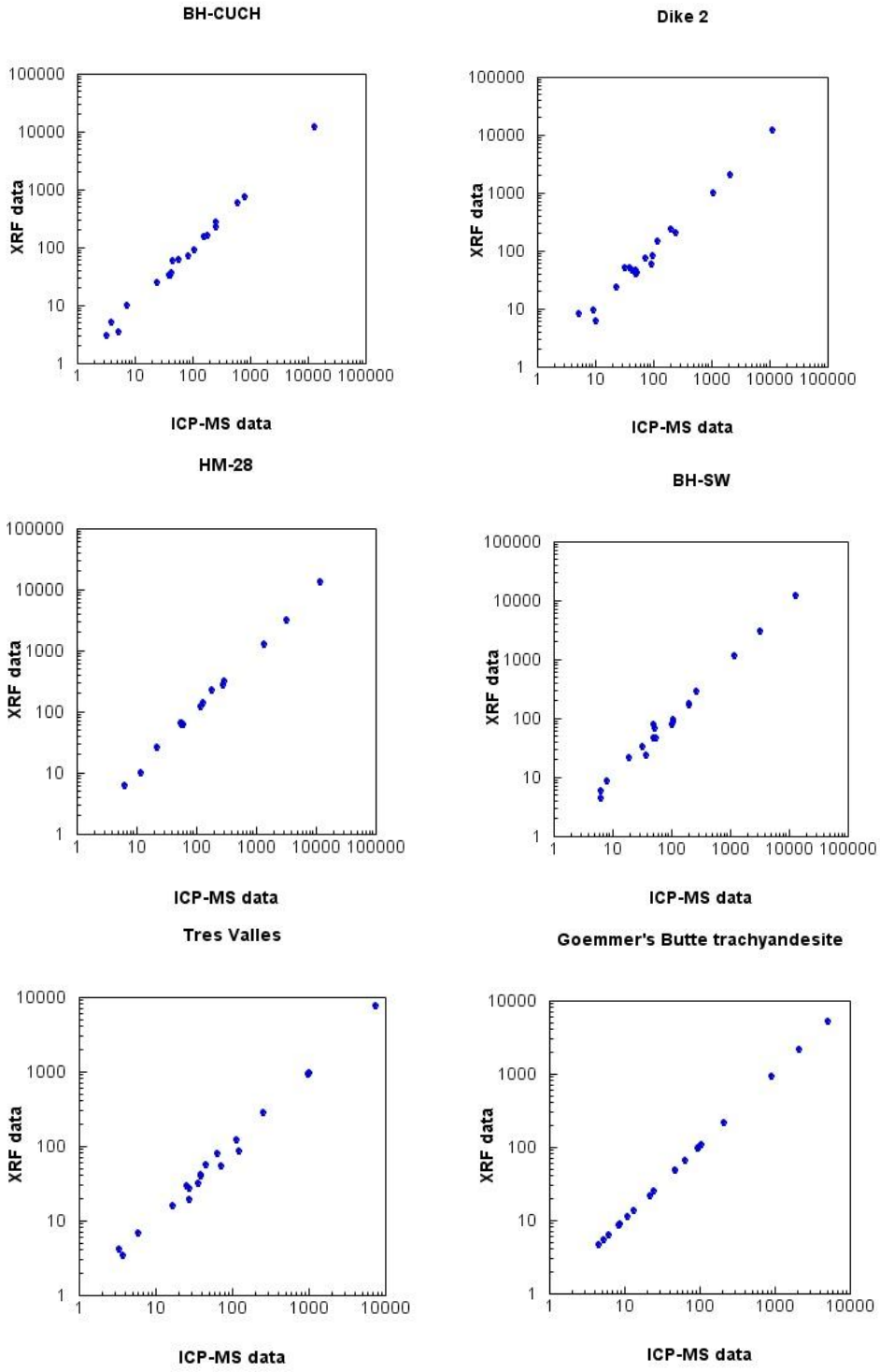

Figure 3.30: Comparison between XRF and ICP-MS data for trace element abundances from selected samples. A one to one ratio, or straight line with a slope of 1, indicates good agreement between the methods. All samples show good agreement. X and Y scales are log base 10.

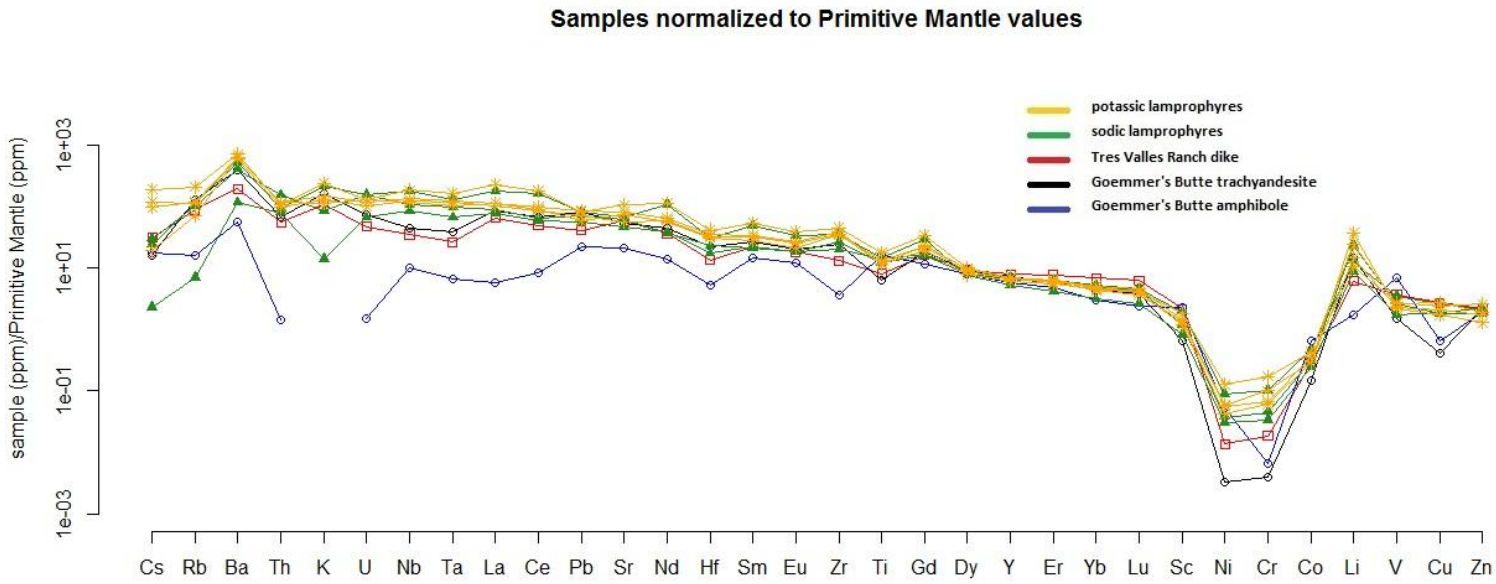

Figure 3.31: Multi-element diagram for samples from this study and McGregor (2010) normalized to primitive mantle composition (Iyubetskaya, 2007). Elements are ordered from least compatible on the left to compatible on the right.

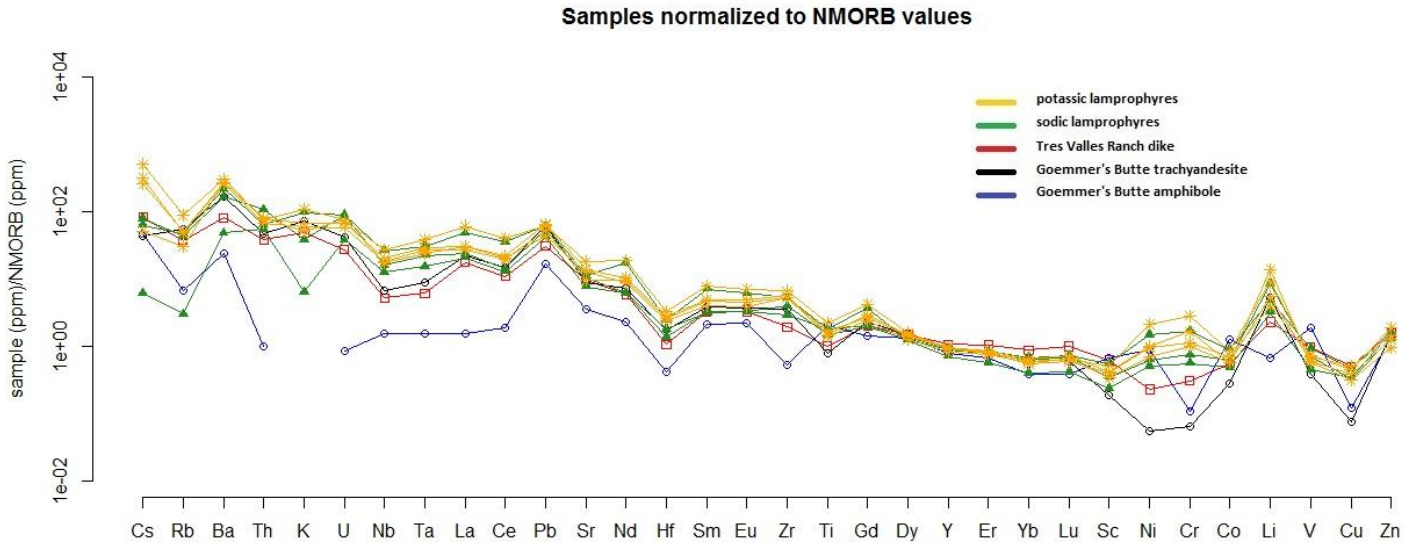

Figure 3.32: Multi-element diagram for samples from this study and McGregor (2010) normalized to NMORB composition (Lehnert, 2000). Elements are ordered from least compatible on the left to compatible on the right.

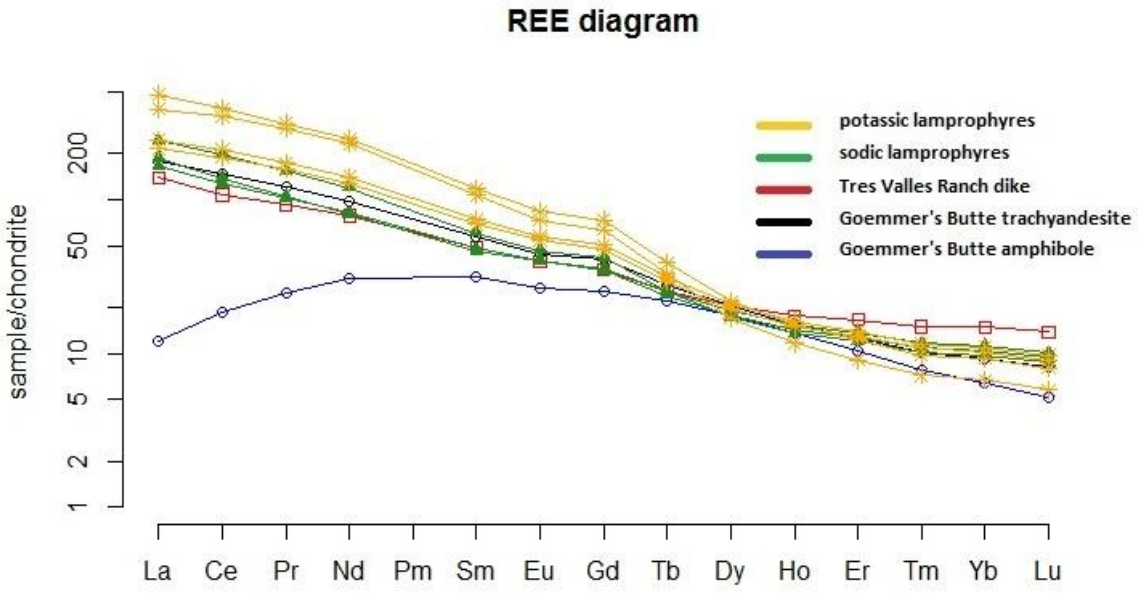

Figure 3.33: Chondrite-normalized rare earth element diagram for samples from this study and McGregor (2010).

MINERAL COMPOSITIONS

Electron microprobe analysis was performed on minerals in rocks from the Spanish Peaks area. These rocks were broken out into four groups: relatively sodic lamprophyres (K_2O/Na_2O wt. % < 1), relatively potassic lamprophyres (K_2O/Na_2O wt. % > 1), Goemmer Butte, and a xenolith/megacryst-bearing dike from Tres Valles Ranch near Mount Mestas approximately 16 miles north of Spanish Peaks. Minerals (primarily Fe-Mg silicates) were probed in order to use zoning and mineral compositions to constrain magmatic processes.

Pyroxene

Table 3.5 presents a representative suite of analyses taken from over 90 point analyses performed on samples from the study area. All analyzed pyroxenes are calcic clinopyroxenes and plot in the diopside and augite fields in the pyroxene quadrilateral (Fig. 3.34). Pyroxenes from Goemmer Butte and from Tres Valles dike are similar in composition to the other pyroxenes.

The pyroxenes from the relatively sodic dikes have Ti contents that range from less than 0.70 to more than 3.30 percent (Table 3.5 and Fig. 3.36), whereas the Ti content of the pyroxenes from the relatively potassic dikes is more restricted (<0.70 to ~1.10 percent). The ranges of Mg # of pyroxenes from the sodic dikes (54-90) and potassic dikes (42-90) overlap; however, the Mg #'s of two core analyses from pyroxenes of relatively potassic dikes are below 50. Pyroxenes from Goemmer Butte and Tres Valles are similar and have restricted ranges of Ti and Mg #, and overlap with pyroxenes from both the relatively sodic and potassic dikes. Oscillatory zoning is present in many pyroxenes, and often many oscillations are present. Typically oscillations in color

represent zones of different levels of Ti, Al, and Mg #. Figure 3.35 shows back-scatter electron (BSE) images of zoned pyroxenes where the oscillations are readily apparent. The darker oscillations generally have a higher Mg # than the lighter zones. The pyroxenes from the relatively sodic dikes commonly exhibit dark cores with dark and light oscillations. The pyroxenes from the relatively potassic dike often have light cores and darker outer zones. Pyroxenes from the sodic dikes have a strong negative correlation between Ti and Mg #, and a wide range in Mg # (Fig. 3.36). The core and rim analyses from pyroxenes of sodic dikes overlap, but the rim analyses have a larger range of Ti. The core and rim analyses from pyroxenes from relatively potassic dikes overlap, but the rim analyses tend to plot at the higher range of Mg #'s. The rims of pyroxenes from Tres Valles have lower Mg #'s than the cores.

In Figure 3.37, there is a positive correlation between Al and Ti in pyroxenes from all locations, indicating coupled substitution of Al^{3+} for Si^{4+}, and Ti^{4+} for Fe^{3+}. The rims of pyroxenes from sodic dikes tend to have higher Al than the cores. The core and rim analyses of pyroxenes from the potassic dikes overlap; however, the range of analyses from the potassic dikes is smaller and as a group they have lower concentrations of Si and Al. Analyses of pyroxenes from Goemmer Butte and Tres Valles are similar to each other and fall within the ranges of pyroxene analyses from both the sodic and potassic dikes.

Table 3.5: Representative Pyroxene Analyses							
Type:	sodic	sodic	sodic	sodic	sodic	sodic	
Location:	Cuchara	Cuchara	Tercio Ranch	Tercio Ranch	North Lake	North Lake	MDL:*
XL position:	C**	R	C	Ranch	C	R	
SiO_2***	51.00	46.59	46.80	49.09	52.09	52.77	0.04
TiO_2	0.69	2.32	2.27	1.59	0.98	0.90	0.06
Al_2O_3	4.69	7.13	7.47	4.24	2.09	1.60	0.04
MgO	16.68	12.33	12.76	14.51	16.63	17.15	0.04
FeO	5.85	8.42	7.41	7.93	6.89	6.13	0.16
CaO	19.72	21.83	21.69	21.04	20.72	21.27	0.04
MnO	n.d.****	0.14	n.d.	n.d.	0.20	0.18	0.14
Na_2O	0.65	0.43	0.42	0.30	0.41	0.41	0.06
Cr_2O_3	0.89	n.d.	0.30	n.d.	n.d.	0.19	0.17
Total:	100.18	99.20	99.12	98.70	100.01	100.60	
	cations normalized to 6 oxygens						
Si	1.867	1.762	1.761	1.851	1.921	1.931	
Ti	0.019	0.066	0.064	0.045	0.027	0.025	
Al	0.202	0.318	0.331	0.188	0.091	0.069	
Mg	0.910	0.695	0.716	0.815	0.914	0.935	
Fe^{2+}	0.179	0.266	0.233	0.250	0.213	0.188	
Ca	0.773	0.885	0.875	0.850	0.819	0.834	
Mn	n.d.	0.005	n.d.	n.d.	0.006	0.006	
Na	0.046	0.031	0.031	0.022	0.030	0.029	
Cr	0.026	n.d.	0.009	n.d.	n.d.	0.005	
Total:	4.023	4.029	4.020	4.021	4.021	4.022	
Mg#=	74	59	63	65	71	74	
Wo=	0.42	0.48	0.48	0.44	0.42	0.43	
Fs=	0.10	0.14	0.13	0.13	0.11	0.10	
En=	0.49	0.38	0.39	0.43	0.47	0.48	

* minimum detection limit; ** C=core, R=rim; *** oxides in wt. %;

**** not detected (below detection limit)

Table 3.5 cont.							
Type:	sodic	sodic	sodic	sodic	potassic	potassic	
Location:	BH-31	BH-31	Dike 2	Dike 2	CO-10	CO-10	MDL:
Xl position:	C	C	C	R	C	R	
SiO_2	50.02	50.84	51.24	51.48	51.68	51.31	0.04
TiO_2	1.21	0.67	0.74	0.78	1.00	1.08	0.06
Al_2O_3	3.81	3.90	4.19	2.37	2.06	2.40	0.04
MgO	14.86	15.71	16.29	14.47	14.92	14.69	0.04
FeO	7.57	4.86	5.21	11.47	8.45	8.39	0.16
CaO	21.15	21.31	21.56	19.06	20.90	21.32	0.04
MnO	0.17	0.14	0.18	0.46	n.d.****	0.19	0.14
Na_2O	0.36	0.50	0.50	0.64	0.77	0.89	0.06
Cr_2O_3	n.d.	1.18	0.89	n.d.	n.d.	n.d.	0.17
Total:	99.14	99.11	100.80	100.72	99.78	100.28	
	cations normalized to 6 oxygens						
Si	1.873	1.884	1.870	1.920	1.927	1.909	
Ti	0.034	0.019	0.020	0.022	0.028	0.030	
Al	0.168	0.170	0.180	0.104	0.090	0.105	
Mg	0.830	0.868	0.886	0.804	0.829	0.815	
Fe^{2+}	0.237	0.151	0.159	0.358	0.263	0.261	
Ca	0.849	0.846	0.843	0.761	0.835	0.850	
Mn	0.005	0.004	0.006	0.014	n.d.	0.006	
Na	0.026	0.036	0.036	0.046	0.056	0.064	
Cr	n.d.	0.034	0.026	n.d.	n.d.	n.d.	
Total:	4.022	4.013	4.025	4.030	4.028	4.040	
Mg#=	66	76	76	56	64	64	
Wo=	0.44	0.45	0.45	0.40	0.43	0.44	
Fs=	0.12	0.08	0.08	0.19	0.14	0.14	
En=	0.43	0.47	0.47	0.42	0.43	0.42	

* minimum detection limit; ** C=core, R=rim; *** oxides in wt. %;

**** not detected (below detection limit)

Table 3.5 cont.					
Location:	Goemmer's Butte	Goemmer's Butte	Tres Valles	Tres Valles	MDL:
Xl position:	C	C	C	R	
SiO_2	49.91	48.61	51.61	50.52	0.04
TiO_2	0.99	1.09	0.40	0.48	0.06
Al_2O_3	5.45	5.05	2.02	2.86	0.04
MgO	13.47	13.19	13.60	14.41	0.04
FeO	8.59	9.72	7.94	8.87	0.16
CaO	22.12	21.40	23.03	22.07	0.04
MnO	0.31	0.20	0.23	0.48	0.14
Na_2O	0.47	0.26	0.72	0.35	0.06
Cr_2O_3	n.d.	n.d.	n.d.	n.d.	0.17
Total:	101.31	99.52	99.55	100.05	
	cations normalized to 6 oxygens				
Si	1.841	1.835	1.937	1.893	
Ti	0.027	0.031	0.011	0.014	
Al	0.237	0.225	0.089	0.126	
Mg	0.741	0.742	0.761	0.805	
Fe^{2+}	0.265	0.307	0.249	0.278	
Ca	0.874	0.866	0.926	0.886	
Mn	0.010	0.006	0.007	0.015	
Na	0.033	0.019	0.053	0.026	
Cr	n.d.	n.d.	n.d.	n.d.	
Total:	4.029	4.031	4.033	4.043	
Mg#=	61	58	63	62	
Wo=	0.47	0.45	0.48	0.45	
Fs=	0.14	0.16	0.13	0.14	
En=	0.39	0.39	0.39	0.41	

* minimum detection limit; ** C=core, R=rim; *** oxides in wt. %;

**** not detected (below detection limit)

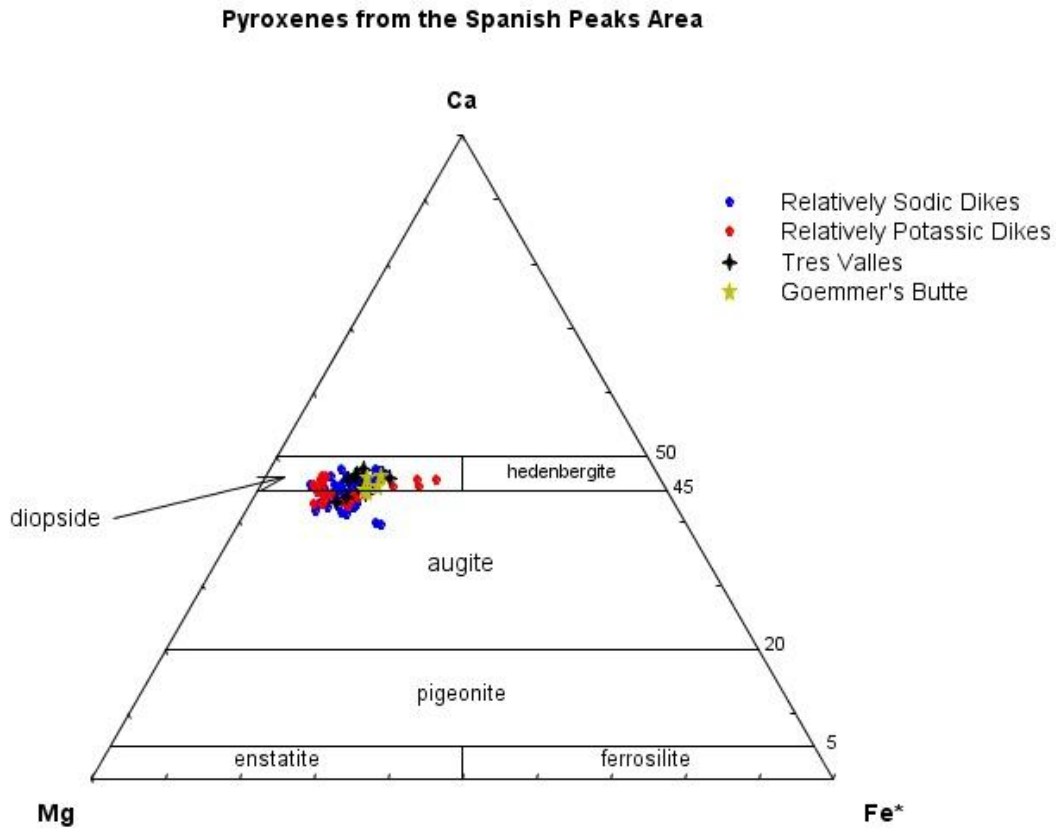

Figure 3.34: Pyroxene analyses from rocks of the Spanish Peaks area are plotted on the pyroxene quadrilateral (modified from Morimoto, 1989) displaying relative atomic proportions of Fe, Mg, and Ca. Data from this study were combined with those from McGregor (2010).

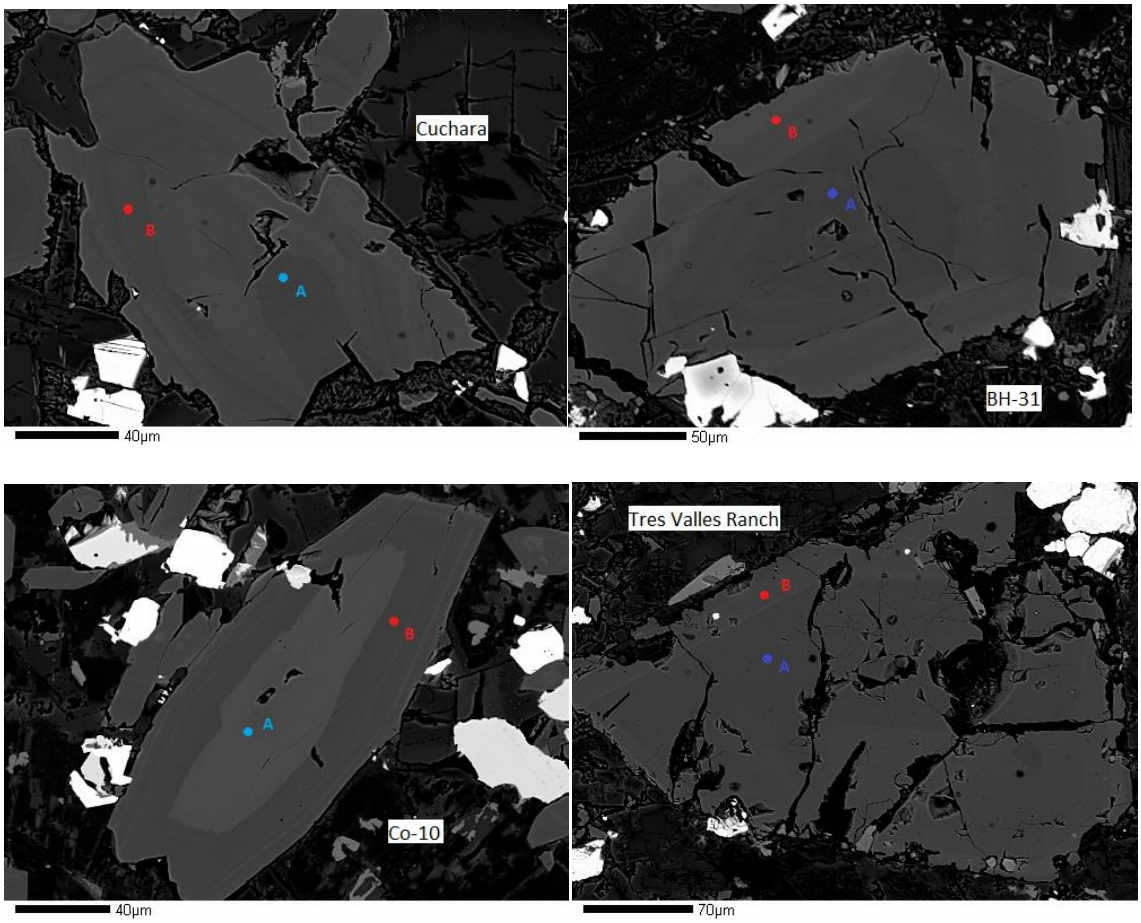

Figure 3.35: BSE (back-scatter electron) images of pyroxenes from the Spanish Peaks area. Blue circles (A) are core analyses. Red circles (B) are rim analyses. Cuchara and BH-31 are relatively sodic dikes, and Co-10 is a relatively potassic dike that has an Fe-rich core and more Mg-rich rim (note lighter color of core).

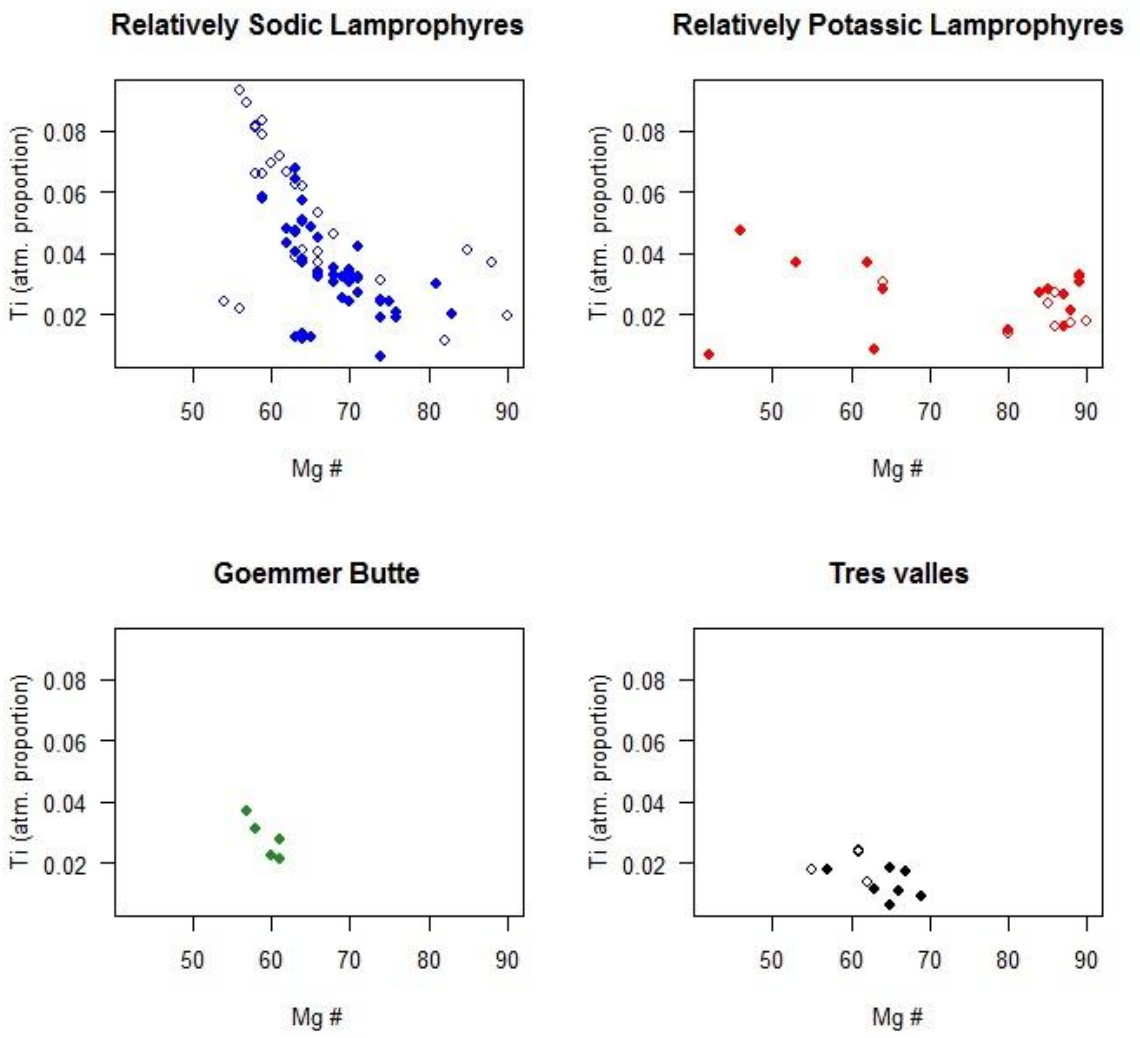

Figure 3.36: Atomic proportion of Ti is plotted versus Mg # for pyroxenes from the relatively sodic and potassic dikes, Goemmer Butte, and Tres Valles dike. Closed symbols represent analyses from the cores of grains; open symbols are rim analyses. Data from this study were combined with those of McGregor (2010) to produce this figure.

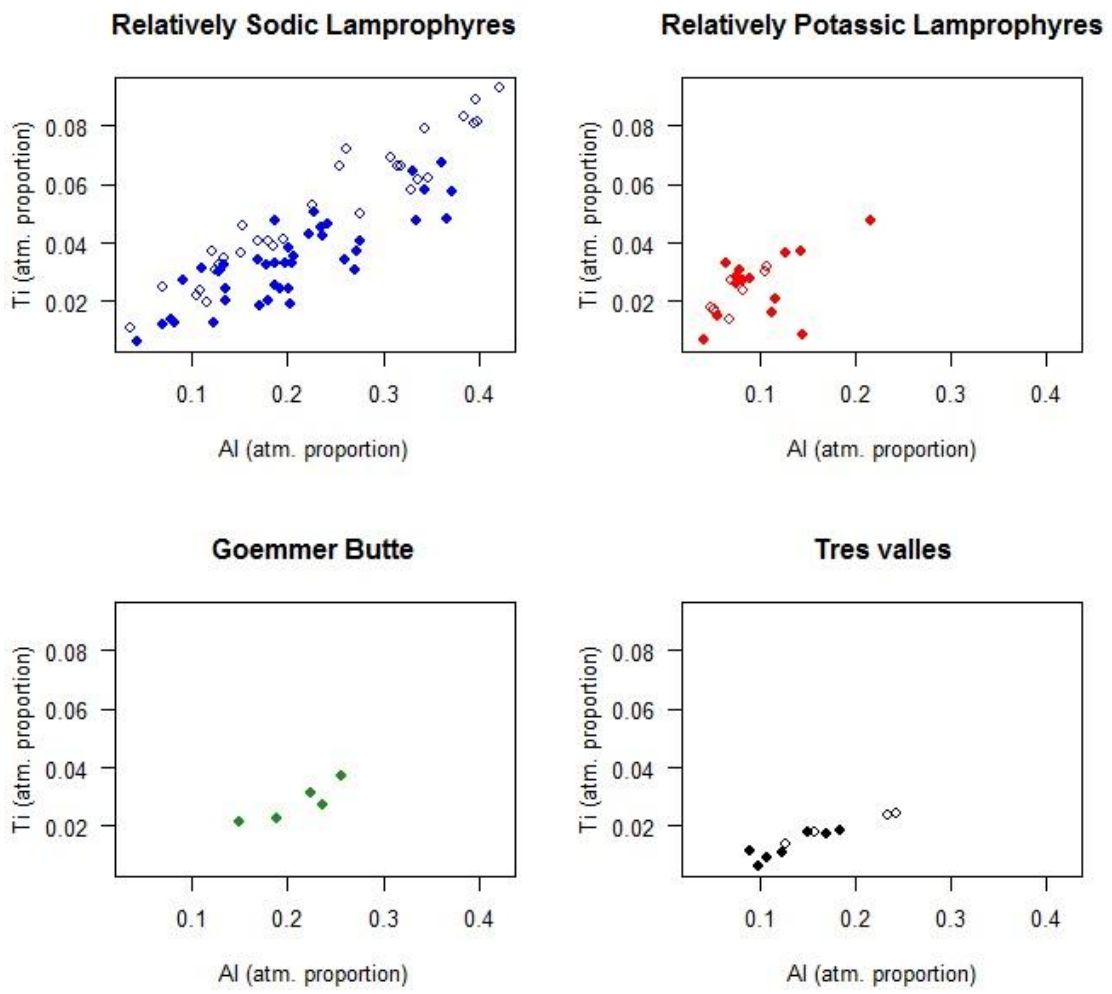

Figure 3.37: Atomic proportion of Ti and Al are plotted for pyroxenes from the relatively sodic and potassic dikes, Goemmer Butte, and Tres Valles dike. Closed symbols represent analyses from the cores of grains; open symbols are rim analyses. Data from this study were combined with those of McGregor (2010) to produce this figure.

Amphibole

Over 60 point analyses were preformed on amphiboles from relatively sodic dikes, relatively potassic dikes, and megacrysts from Goemmer's Butte, Tres Valles Ranch, and the North Lake Sill Complex. No amphibole was found in the relatively potassic lamprophyres sampled in this study; however, McGregor (2010) reported amphibole in several relatively potassic lamprophyres and these data were used in conjunction with those from this study to produce the figures in this chapter. In this study, amphibole megacrysts are defined as crystals that are 1 cm or longer in the longest dimension, and at least 2 times larger than any other phenocryst in the sample. Megacrysts were found at Goemmer's Butte, the dike at Tres Valles Ranch, and a relatively sodic lamprophyre from the North Lake Sill Complex. Table 3.6 lists analyses of representative amphibole phenocrysts from the Spanish Peaks area, and table 3.7 lists analyses of representative amphibole megacrysts from the Spanish Peaks area. Goemmer's Butte also contained xenolith amphibole.

Leake et al. (1997) divided amphiboles into four major groups based on structural formulas. All amphiboles in this study fall into the calcic group, and are plotted in figure 3.38. Data from McGregor (2010) and data from this study are consistent. Amphibole phenocrysts from the relatively sodic dikes have a range of Ti contents and thus plot in both the pargasite and magnesiohastingsite field and the kaerstutite field. Most of the relatively potassic dikes contain mica as a phenocryst rather than amphibole, but McGregor (2010) documented amphibole in some of the relatively potassic lamprophyres, and they plot in the kaerstutite field. Tres Valles amphiboles are similar to amphibole from the sodic lamprophyres. Most amphiboles were not compositionally

zoned; however, several small amphiboles from Tres Valles (phenocrysts) exhibited zoning of Mg#s (see BSE images, Fig. 3.39, table 3.6) with higher Mg #s in the rims than the cores. Normal magmatic zoning would produce a lower Mg# in rims as the magma evolves. Higher Mg# in the rim than the core reflects some other process than normal magmatic zoning such as magma mixing.

In figure 3.40, the megacrysts and xenolith amphibole from Goemmer's Butte form a separate compositional group from the lamprophyres. Tres Valles megacrysts are compositionally similar to phenocrysts from Tres Valles. The North Lake megacrysts are contained in a relatively sodic lamprophyre, and are compositionally similar to the phenocrysts from the other relatively sodic lamprophyres, as well as those from Tres Valles.

Amphiboles from the sodic and potassic lamprophyres and North Lake megacrysts have similar Mg #'s, aluminum, and titanium contents. All of the analyses of amphiboles from the Spanish Peaks area have a similar level of alkalis (Na + K) but amphiboles from Goemmer's Butte are separated from the others because they have much lower Mg #'s (Fig. 3.40). Goemmer's Butte amphiboles also are more aluminous than amphiboles from other locations. Tres Valles amphiboles are similar in Mg# to amphiboles from the lamprophyres; however, they have a lower Ti content similar to that of Goemmer's Butte amphiboles, especially those contained within xenoliths.

Table 3.6: Electron microprobe analyses of representative amphibole phenocrysts							
Type	sodic	sodic	sodic	sodic			
Location	Tercio Ranch	Tercio Ranch	BH-SW	BH-SW	Tres Valles	Tres Valles	MDL:*
Xl position	C**	R	C	C	C	R	
SiO_2***	39.56	41.15	40.80	40.51	40.71	41.24	0.05
TiO_2	4.29	3.92	4.68	5.14	2.34	2.21	0.06
Al_2O_3	13.98	12.54	12.24	12.43	14.29	13.47	0.04
MgO	14.76	14.14	14.05	14.50	12.03	14.58	0.04
FeO	10.75	10.89	10.74	10.87	14.61	11.62	0.16
CaO	11.84	11.29	11.70	11.59	11.30	11.94	0.04
MnO	n.d.****	n.d.	n.d.	0.16	0.40	0.00	0.14
K_2O	0.84	0.96	1.18	1.23	1.01	1.30	0.03
Na_2O	2.45	2.46	2.50	2.13	2.14	2.28	0.06
Cl	0.05	0.04	0.03	n.d.	0.06	0.02	0.02
BaO	n.d.	0.16	0.18	0.19	0.00	0.00	0.13
	98.52	97.55	98.11	98.75	98.67	98.44	
$^{-}$O=F,Cl	n.d.	0.04	0.04	0.04	0.01	0.01	
Total	98.52	97.51	98.06	98.71	98.87	98.66	
cations normalized to 23 oxygens							
Si	5.798	6.077	6.015	5.938	6.021	6.045	
Ti	0.473	0.436	0.519	0.567	0.260	0.244	
Al	2.415	2.183	2.127	2.147	2.491	2.327	
Mg	3.225	3.113	3.088	3.168	2.652	3.186	
Fe^{2+}	1.318	1.345	1.324	1.332	1.807	1.424	
Ca	1.859	1.786	1.848	1.820	1.791	1.875	
Mn	n.d.	n.d.	n.d.	0.020	0.049	0.000	
K	0.158	0.182	0.223	0.230	0.190	0.244	
Na	0.697	0.704	0.715	0.605	0.615	0.649	
Ba	n.d.	0.009	0.011	0.011	0.000	0.000	
Total	15.943	15.834	15.869	15.839	15.876	15.994	
Mg#	71	70	70	70	59	69	
*minimum detection limit, **C=core, R=rim, ***oxides in wt. % ****not detected (or below MDL)							

Table 3.7: Electron microprobe analyses of representative amphibole megacrysts							
Type					sodic	sodic	
Location	Goemmer's Butte	Goemmer's Butte	Tres Valles	Tres Valles	North Lake	North Lake	MDL:*
Xl position	C**	R	C	R	C	R	
SiO_2***	38.92	38.94	41.80	41.24	40.10	41.45	0.05
TiO_2	2.67	2.64	2.16	2.21	5.53	3.97	0.06
Al_2O_3	15.32	15.25	12.92	13.47	13.43	12.54	0.04
MgO	10.89	10.59	14.77	14.58	13.07	14.15	0.04
FeO	15.80	15.69	11.59	11.62	11.74	11.99	0.16
CaO	10.75	10.50	11.52	11.94	11.29	10.88	0.04
MnO	n.d****	0.15	n.d.	n.d.	n.d.	0.24	0.14
K_2O	1.61	1.62	1.19	1.30	1.01	0.91	0.03
Na_2O	2.27	2.25	2.22	2.28	2.70	2.66	0.06
Cl	0.04	0.00	0.05	0.02	n.d.	0.05	0.02
BaO	0.15	0.00	n.d.	n.d.	0.15	0.18	0.13
	98.42	97.63	98.21	98.67	99.02	99.02	
$^{-}$O=F,Cl	0.03	n.d.	n.d.	n.d.	0.03	0.04	
Total	98.39	97.63	98.21	98.67	98.99	98.98	
cations normalized to 23 oxygens							
Si	5.842	5.880	6.136	6.044	5.875	6.061	
Ti	0.301	0.300	0.238	0.244	0.610	0.437	
Al	2.710	2.714	2.235	2.327	2.319	2.161	
Mg	2.437	2.384	3.232	3.186	2.855	3.084	
Fe^{2+}	1.983	1.982	1.423	1.424	1.439	1.466	
Ca	1.729	1.699	1.812	1.875	1.772	1.705	
Mn	n.d.	0.019	n.d.	n.d.	n.d.	0.030	
K	0.309	0.312	0.223	0.244	0.189	0.169	
Na	0.661	0.658	0.631	0.648	0.767	0.754	
Ba	0.009	0.000	n.d.	n.d.	0.009	0.010	
Total	15.981	15.948	15.929	15.992	15.834	15.877	
Mg #	55	55	69	69	66	68	
*minimum detection limit, **C=core, R=rim, ***oxides in wt. % ****not detected (or below MDL)							

Amphiboles from the Spanish Peaks area

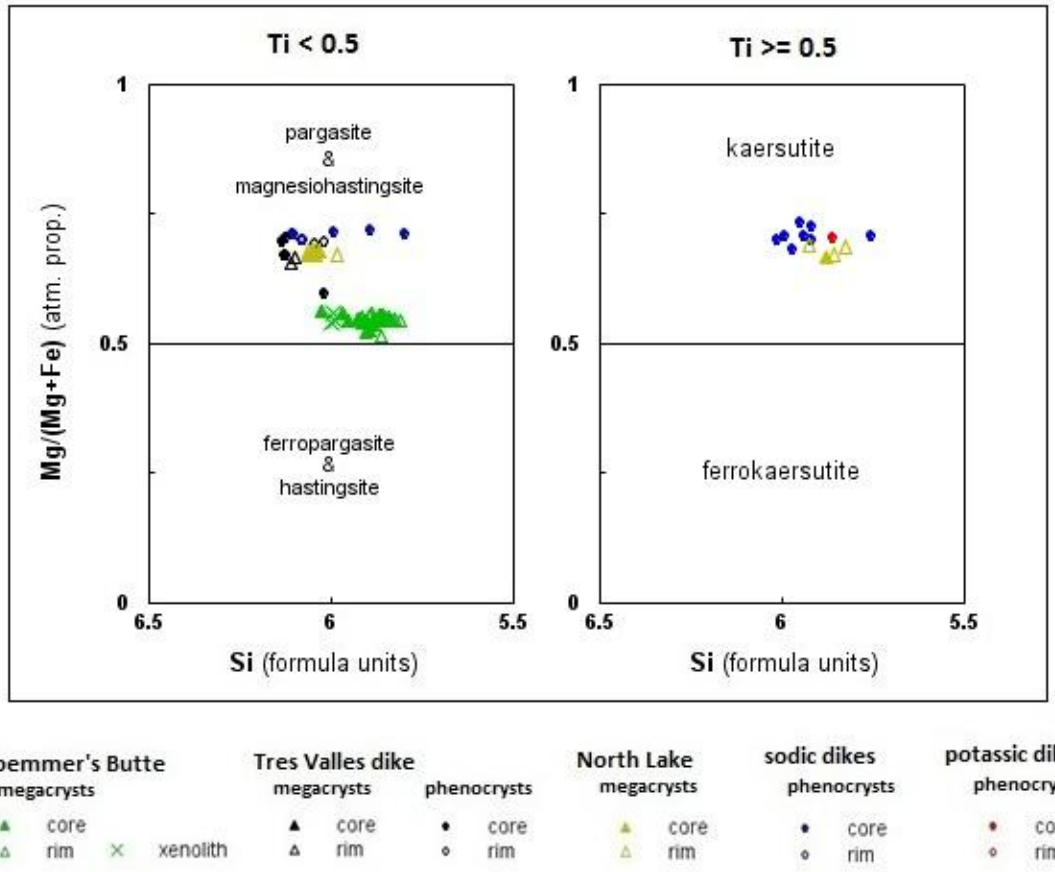

Figure 3.38: Figure modified from Leake (1997) for the calcic amphiboles. Data from McGregor (2010) were combined with those from this study to produce this figure. All Fe is assumed to be Fe^{2+}.

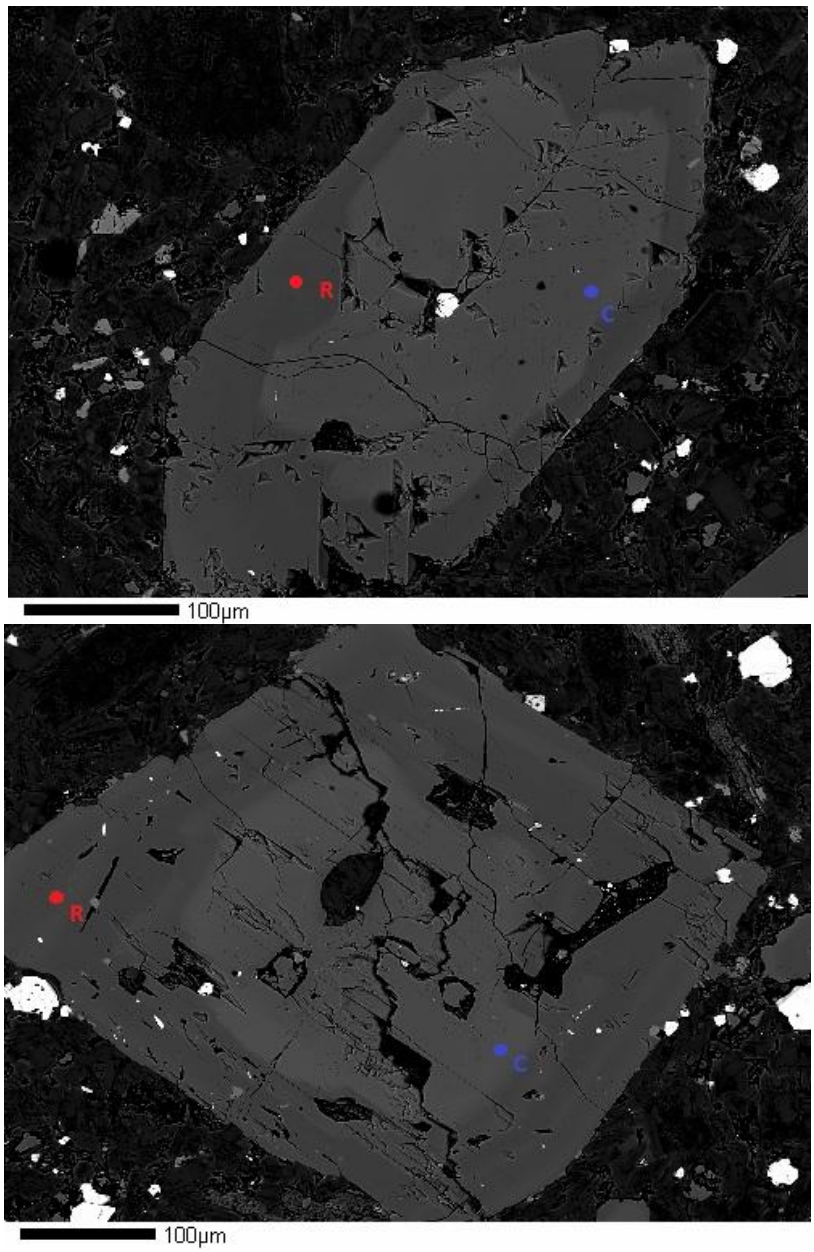

Figure 3.39: BSE (back-scatter electron) images of amphiboles from Tres Valles Ranch dike showing core-rim zoning. Blue circles (C) are core analyses and red circles (R) are rim analyses. In this case, the light grey cores are more Fe-rich than the rims.

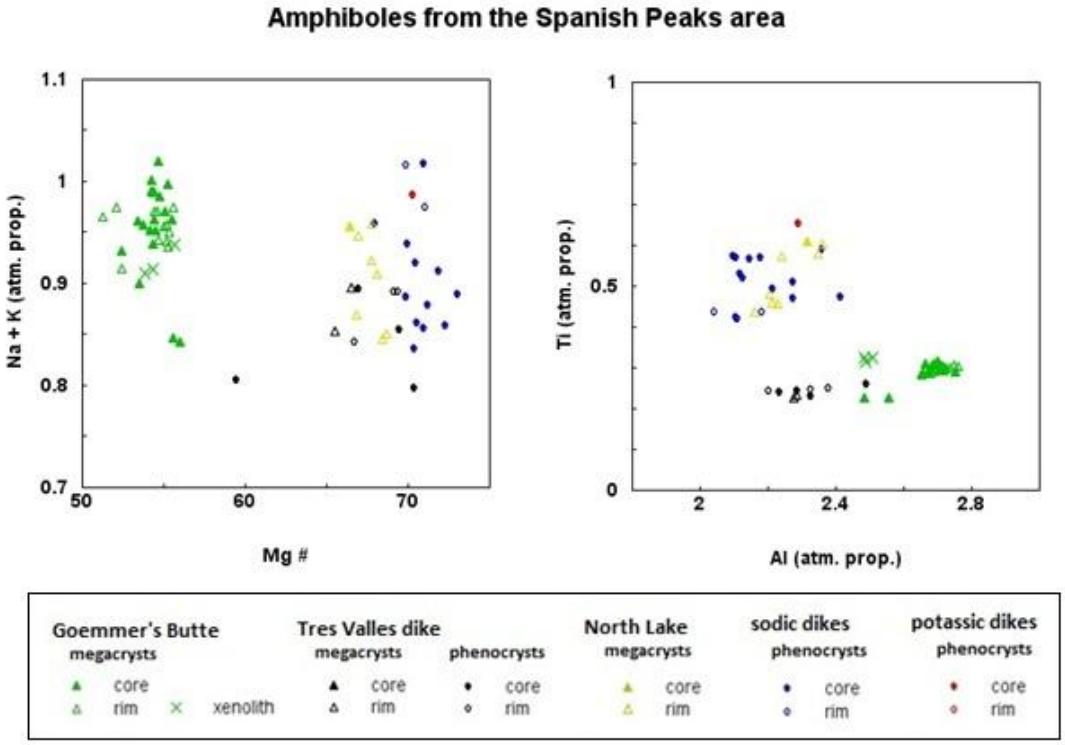

Figure 3.40: Relative atomic proportions of (Na + K) and Mg#, and Ti and Al are plotted for amphiboles from the Spanish Peaks area. Data from this study are combined with those of McGregor (2010) to produce this figure.

Mica

Over 40 point analyses were preformed on micas from relatively sodic dikes, relatively potassic dikes, and Goemmer's Butte. Table 3.8 lists analyses of representative micas from the Spanish Peaks area. Micas from both the sodic and potassic dikes have relatively high Ti contents (4.5-7.5 wt. %). The micas have a wide range in Mg # (Fig. 3.44) and straddle the phlogopite/biotite boundary in figure 3.41. The micas from Goemmer's Butte are contained within an amphibole/mica/apatite xenolith and are members of the chlorite group.

Most of the micas are not zoned; however, those from potassic dike Co-10 exhibit dark cores and light rims with a sharp boundary between core and rim in back scattered electron imagery (Fig. 3.42). The cores of these micas have higher Mg and F contents than the rims, which have higher Fe contents (Table 3.8). The rims also have higher Ti contents than the cores. McGregor (2010) noted normal zoning in the micas of both relatively sodic and relatively potassic lamprophyres.

Micas from the sodic dikes are compositionally similar and plot in the biotite and phlogopite fields of figure 3.41. The cores of micas from potassic dikes plot in the phlogopite field while the rims plot in the biotite field. All of the micas from potassic lamprophyres contain measurable fluorine (Fig. 3.43), and commonly contain more F than micas from the sodic dikes. Ti contents for micas from both the sodic and potassic dikes are high and the ranges overlap.

The ranges of Mg #'s for micas from the sodic and potassic dikes overlap, but the cores and rims of micas from the potassic dikes are distinct because the rims have lower

Mg #'s and higher sodium contents than the cores. The range of sodium contents of micas from sodic and potassic dikes are similar.

Table 3.8: Electron microprobe analyses of representative micas							
Type			potassic	potassic	potassic	potassic	
Location	Goemmer's Butte	Goemmer's Butte	Co-10	Co-10	Co-10	Co-10	MDL:*
Xl position	C1**	C2	C1	R1	C2	R2	
SiO_2***	31.95	31.74	37.83	35.22	37.91	34.49	0.05
TiO_2	1.02	0.91	5.51	7.36	5.99	7.22	0.06
Al_2O_3	17.32	16.77	13.37	13.97	12.80	13.97	0.03
MgO	23.70	23.38	16.76	14.68	17.14	13.92	0.03
FeO	13.49	12.88	11.36	14.09	11.69	14.58	0.16
CaO	0.77	0.60	0.19	0.06	0.37	n.d.****	0.04
MnO	0.33	0.30	n.d.	0.13	n.d.	0.17	0.13
K_2O	0.07	0.08	8.86	8.07	8.84	7.93	0.03
Na_2O	n.d.	n.d.	0.48	0.72	0.45	0.56	0.05
F	n.d.	n.d.	1.44	0.76	1.23	0.60	0.09
Cl	n.d.	0.04	n.d.	n.d.	n.d.	n.d.	0.02
BaO	n.d.	0.00	0.69	2.27	0.64	2.36	0.13
	88.65	86.69	96.49	97.33	97.05	95.80	
$^{-}$O=F,Cl	n.d.	0.01	0.61	0.32	0.52	0.25	
Total	88.65	86.68	95.88	97.01	96.54	95.54	
cations normalized to 11 oxygens							
Si	2.444	2.474	2.757	2.618	2.753	2.615	
Ti	0.059	0.054	0.302	0.412	0.327	0.412	
Al	1.561	1.541	1.148	1.224	1.096	1.248	
Mg	2.702	2.717	1.821	1.627	1.856	1.573	
Fe^{2+}	0.863	0.840	0.692	0.876	0.710	0.924	
Ca	0.063	0.050	0.015	0.005	0.029	n.d.	
Mn	0.021	0.019	n.d.	0.008	n.d.	0.011	
K	0.007	0.008	0.824	0.765	0.819	0.767	
Na	n.d.	n.d.	0.068	0.104	0.063	0.082	
F	n.d.	n.d.	0.333	0.179	0.283	0.145	
Cl	0.000	0.005	n.d.	n.d.	n.d.	n.d.	
Ba	0.000	0.000	0.020	0.066	0.018	0.070	
Total	7.720	7.708	7.979	7.883	7.954	7.846	
Mg #	76	76	72	65	72	63	

*minimum detection limit, **C=core, R=rim, ***oxides in wt. %
****not detected (or below MDL)

Table 3.8: Mica analyses cont.					
Type	sodic	sodic	sodic	sodic	
Location	BH-SW	BH-SW	North Lake	North Lake	MDL:*
Xl position	C1**	C2	C1	C2	
SiO_2***	34.84	34.30	35.98	35.81	0.05
TiO_2	5.74	5.83	7.16	7.41	0.06
Al_2O_3	15.70	14.24	15.22	15.54	0.03
MgO	14.19	13.37	14.21	17.29	0.03
FeO	14.92	16.64	13.95	10.95	0.16
CaO	0.09	0.12	0.04	0.11	0.04
MnO	0.22	0.27	0.24	n.d.****	0.13
K_2O	7.38	6.83	7.85	8.15	0.03
Na_2O	0.62	0.39	0.79	0.68	0.05
F	0.59	0.27	0.39	0.37	0.09
Cl	n.d.	0.04	n.d.	n.d.	0.02
BaO	2.06	1.29	1.53	1.99	0.13
	96.34	93.59	97.36	98.30	
$^{-}$O=F,Cl	0.25	0.12	0.16	0.16	
Total	96.09	93.46	97.20	98.14	
cations normalized to 11 oxygens					
Si	2.607	2.649	2.643	2.583	
Ti	0.323	0.339	0.396	0.402	
Al	1.384	1.296	1.318	1.321	
Mg	1.583	1.539	1.556	1.859	
Fe^{2+}	0.934	1.075	0.857	0.661	
Ca	0.007	0.010	0.003	0.008	
Mn	0.014	0.018	0.015	n.d.	
K	0.704	0.673	0.736	0.750	
Na	0.089	0.058	0.112	0.095	
F	0.139	0.066	0.091	0.084	
Cl	n.d.	0.005	n.d.	n.d.	
Ba	0.060	0.039	0.044	0.056	
Total	7.844	7.766	7.772	7.819	
Mg #	63	59	64	74	
minimum detection limit, **C=core, R=rim, ***oxides in wt. % ****not detected (or below MDL)					

Table 3.8: Mica analyses cont.					
Type	sodic	sodic	sodic	sodic	
Location	BH-31	BH-31	Dike 2	Dike2	MDL:*
Xl position:	C1**	C2	C1	C2	
SiO_2***	30.29	31.67	36.07	35.67	0.05
TiO_2	6.70	4.57	6.19	7.19	0.06
Al_2O_3	15.98	16.10	13.94	13.22	0.03
MgO	19.25	19.58	15.49	14.01	0.03
FeO	12.81	14.56	12.53	13.46	0.16
CaO	3.18	0.46	n.d.****	n.d.	0.04
MnO	0.37	0.41	n.d.	0.14	0.13
K_2O	1.80	2.34	7.47	7.89	0.03
Na_2O	0.17	0.15	0.74	0.68	0.05
F	n.d.	n.d.	0.27	n.d.	0.09
Cl	n.d.	0.02	0.03	0.03	0.02
BaO	0.27	0.29	1.61	1.15	0.13
	90.83	90.15	94.34	93.45	
$^{-}$O=F,Cl	n.d.	0.01	0.12	0.01	
Total	90.83	90.15	94.22	93.44	
cations normalized to 11 oxygens					
Si	2.322	2.442	2.713	2.725	
Ti	0.386	0.265	0.350	0.413	
Al	1.444	1.463	1.236	1.190	
Mg	2.200	2.251	1.737	1.596	
Fe^{2+}	0.821	0.939	0.788	0.860	
Ca	0.261	0.038	n.d.	n.d.	
Mn	0.024	0.027	n.d.	0.009	
K	0.176	0.230	0.717	0.769	
Na	0.025	0.022	0.108	0.101	
F	n.d.	n.d.	0.065	n.d.	
Cl	n.d.	0.003	0.003	0.004	
Ba	0.008	0.009	0.048	0.035	
Total	7.670	7.689	7.765	7.703	
Mg #	73	71	69	65	
minimum detection limit, **C=core, R=rim, ***oxides in wt. % ****not detected (or below MDL)					

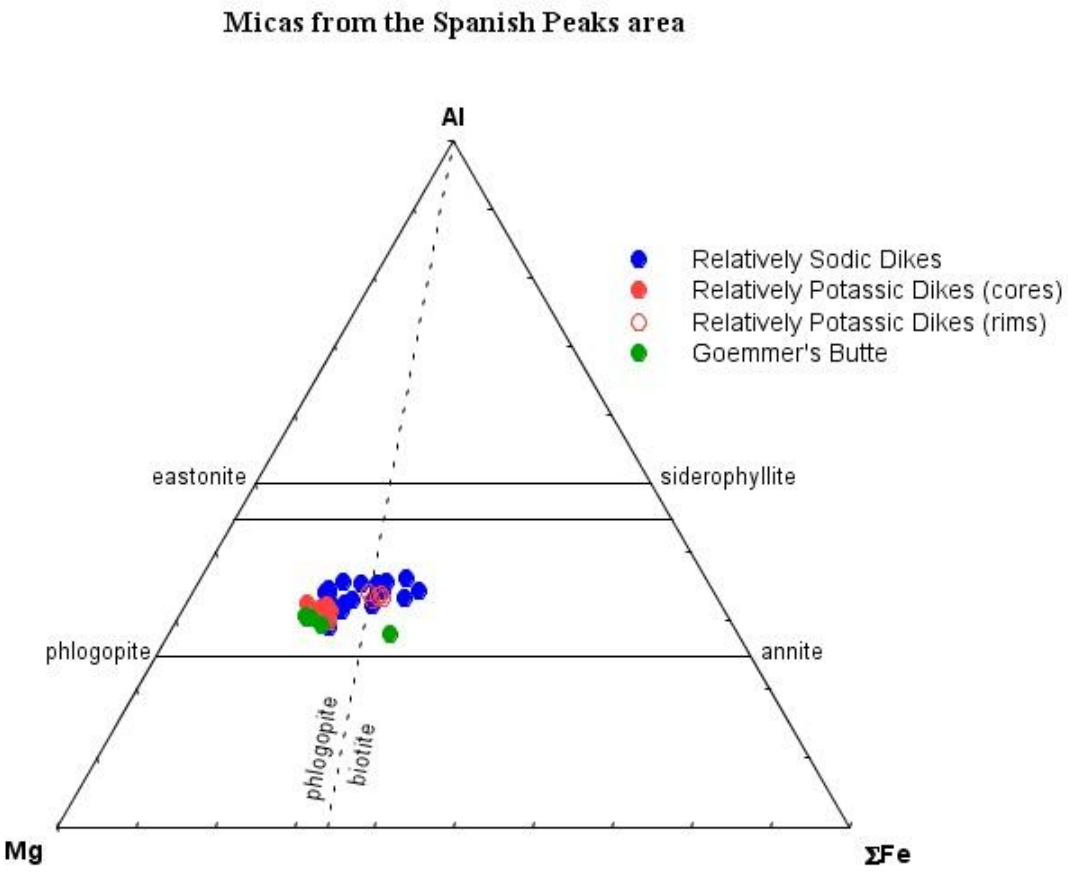

Figure 3.41: Mica analyses from rocks of the Spanish Peaks area (figure modified from Shaw et al. (1996)) showing relative atomic proportions of Al, Mg, and total Fe. Data from this study were combined with those from McGregor (2010) to produce this figure.

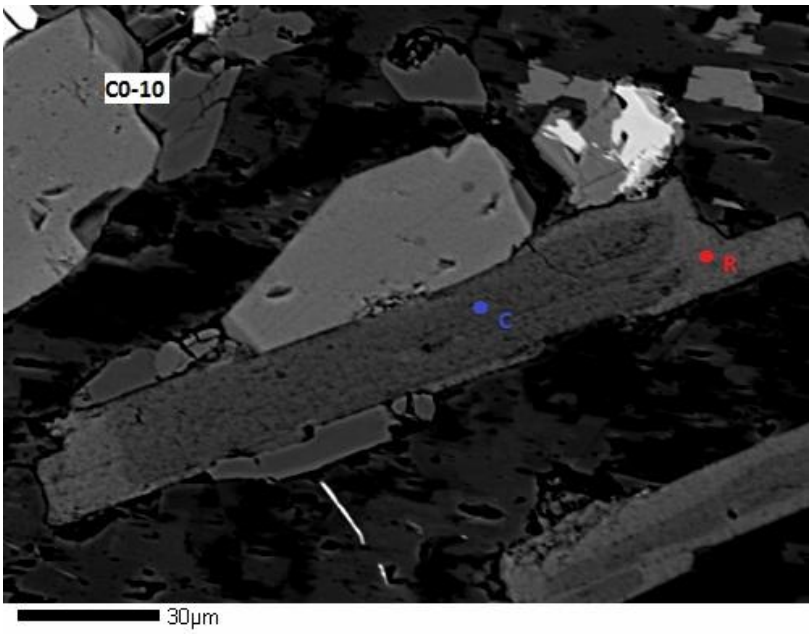

Figure 3.42: BSE (back-scatter electron) image of mica from Co-10 (relatively potassic lamprophyre) showing core-rim zoning. Blue circle (C) represents the location of a core analysis. Red circle (R) is the location of a rim analysis. The darker core is richer in Mg than the light rim.

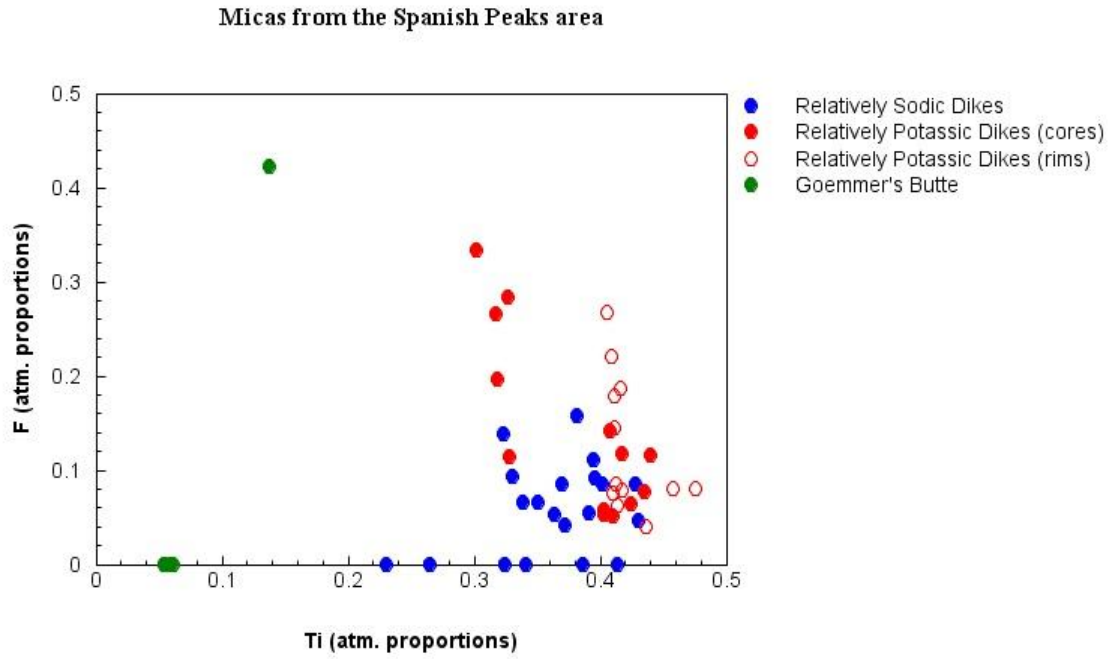

Figure 3.43: Relative atomic proportions of F and Ti are plotted for micas from the Spanish Peaks area. Solid circles are core analyses and open circles are rim analyses. Data from this study were combined with those from McGregor (2010) to produce this figure.

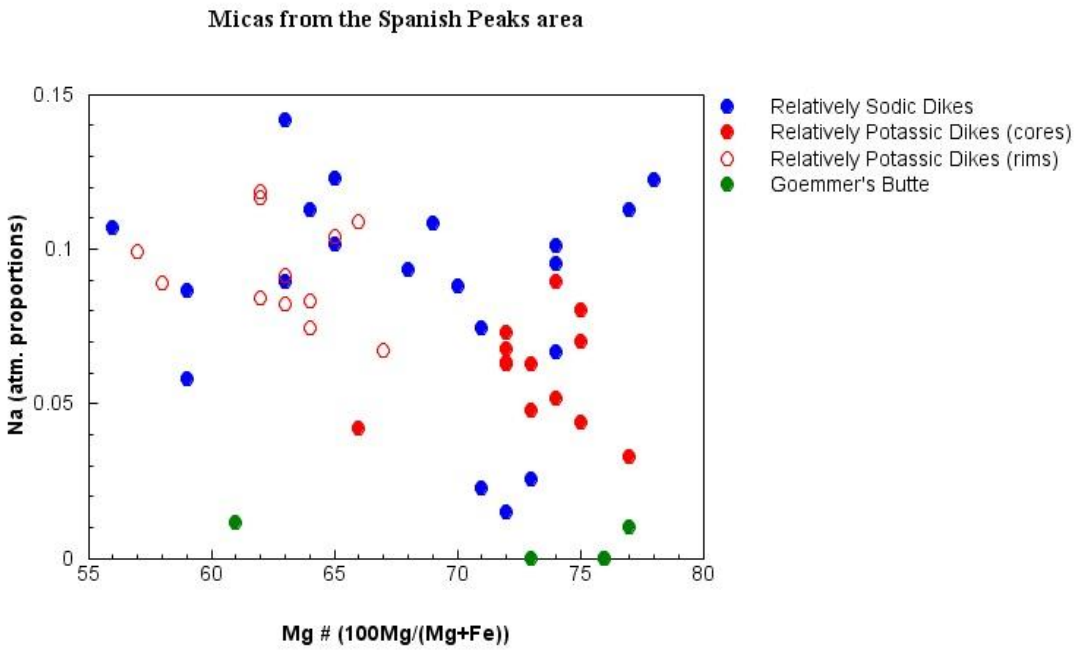

Figure 3.44: Relative atomic proportions of Na are plotted versus Mg # for micas from the Spanish Peaks area. Solid circles are core analyses and open circles are rim analyses. Data from this study were combined with those from McGregor (2010) to produce this figure.

Oxides

Over 50 point analyses were preformed on oxides from relatively sodic and relatively potassic lamprophyres, Goemmer's Butte, and Tres Valles Ranch dike. Representative oxide analyses are shown in tables 3.9 and 3.10, and Fe^{3+} was calculated following Droop (1987). Two relatively sodic lamprophyres (BH-31 and Tercio Ranch dike) contain Cr-spinel (Table 3.9 and Fig. 3.46) occurring as a rare accessory mineral in the groundmass. Tres Valles, Goemmer's Butte, Tercio Ranch, BH-CO10, and BH-SW contain oxides in both the ilmenite and magnetite series, and Goemmer's Butte contains some oxides with a higher Ti proportion (Fig. 3.45).

Table 3.9: Representative spinel analyses						
Type:	sodic	sodic	sodic	sodic	sodic	
Location:	Tercio Ranch	Tercio Ranch	North Lake	Dike 1	Dike 2	MDL:*
SiO_2**	0.08	n.d.****	0.09	0.21	0.32	0.05
TiO_2	5.51	1.73	11.27	9.40	16.57	0.06
Al_2O_3	4.03	13.56	1.04	1.13	0.67	0.04
MgO	1.95	7.68	0.41	0.61	0.82	0.04
FeO***	38.03	24.06	46.26	44.50	46.65	0.16
Fe_2O_3***	35.97	16.72	37.17	39.02	28.62	
CaO	0.20	n.d.	0.11	0.11	0.19	0.04
MnO	1.24	0.45	0.57	1.01	0.85	0.14
Cr_2O_3	11.79	35.29	0.36	n.d.	n.d.	0.17
Total:	98.81	99.49	97.27	95.98	94.69	
	cations normalized to 4 oxygens					
Si	0.004	n.d.	0.004	0.010	0.014	
Ti	0.179	0.046	0.389	0.333	0.557	
Al	0.205	0.566	0.056	0.062	0.036	
Mg	0.126	0.405	0.028	0.043	0.054	
Fe^{2+}***	1.374	0.713	1.773	1.751	1.744	
Fe^{3+}***	1.169	0.446	1.282	1.382	0.963	
Ca	0.009	n.d.	0.005	0.005	0.009	
Mn	0.045	0.013	0.022	0.040	0.032	
Cr	0.403	0.988	0.013	n.d.	n.d.	
Total:	3.514	3.177	3.573	3.626	3.411	

* minimum detection limit; ** oxides in wt. %; *** iron recalculated (Droop, 1987)

**** not detected (below detection limit)

Table 3.9 cont.						
Type:	sodic	sodic	potassic			
Location:	BH-31	BH-31	BH-CO10	Tres Valles	Goemmer's Butte	MDL:
SiO_2**	0.10	0.09	0.06	0.05	0.09	0.05
TiO_2	4.53	1.87	4.75	7.19	2.80	0.06
Al_2O_3	3.07	14.07	0.27	4.72	3.21	0.04
MgO	0.41	8.11	0.49	3.72	1.36	0.04
FeO***	42.06	23.89	45.16	40.25	42.86	0.16
Fe_2O_3***	42.91	19.34	46.34	41.85	46.91	
CaO	0.12	0.15	0.09	n.d.****	0.12	0.04
MnO	1.68	0.35	0.56	0.38	0.25	0.14
Cr_2O_3	2.61	31.50	n.d.	0.44	0.75	0.17
Total:	97.49	99.37	97.72	98.61	98.36	
	cations normalized to 4 oxygens					
Si	0.005	0.003	0.003	0.002	0.004	
Ti	0.160	0.050	0.175	0.238	0.100	
Al	0.170	0.591	0.015	0.245	0.179	
Mg	0.028	0.431	0.036	0.244	0.096	
Fe^{2+}***	1.652	0.712	1.849	1.483	1.697	
Fe^{3+}***	1.517	0.518	1.708	1.387	1.671	
Ca	0.006	0.006	0.005	n.d.	0.006	
Mn	0.067	0.011	0.023	0.014	0.010	
Cr	0.097	0.887	n.d.	0.015	0.028	
Total:	3.702	3.208	3.814	3.629	3.792	

* minimum detection limit; ** oxides in wt. %; *** iron recalculated (Droop, 1987)

**** not detected (below detection limit)

Table 3.10: Representative ilmenite analyses						
Type:	sodic	sodic	potassic			
Location:	BH-SW	Tercio Ranch	BH-CO10	Goemmer's Butte	Tres Valles	MDL:*
TiO_2**	40.15	40.73	41.40	43.71	42.04	0.06
Al_2O_3	0.08	0.07	0.05	0.07	0.05	0.04
MgO	0.74	0.95	1.67	1.03	0.37	0.04
FeO***	27.97	28.52	28.74	31.48	30.07	0.16
Fe_2O_3***	27.70	27.71	25.76	19.68	23.70	
CaO	n.d.****	0.14	0.06	0.12	0.09	0.04
MnO	2.04	1.44	0.88	2.11	2.65	0.14
Total:	98.68	99.57	98.56	98.19	98.97	
	cations normalized to 3 oxygens					
Ti	0.842	0.844	0.856	0.893	0.869	
Al	0.003	0.002	0.002	0.002	0.002	
Mg	0.031	0.039	0.069	0.042	0.015	
Fe^{2+}***	0.652	0.657	0.661	0.715	0.691	
Fe^{3+}***	0.581	0.575	0.533	0.402	0.490	
Ca	n.d.	0.004	0.002	0.004	0.003	
Mn	0.048	0.034	0.020	0.048	0.062	
Total:	2.157	2.155	2.143	2.106	2.130	

* minimum detection limit; ** oxides in wt. %; *** iron recalculated (Droop, 1987)

**** not detected (below detection limit)

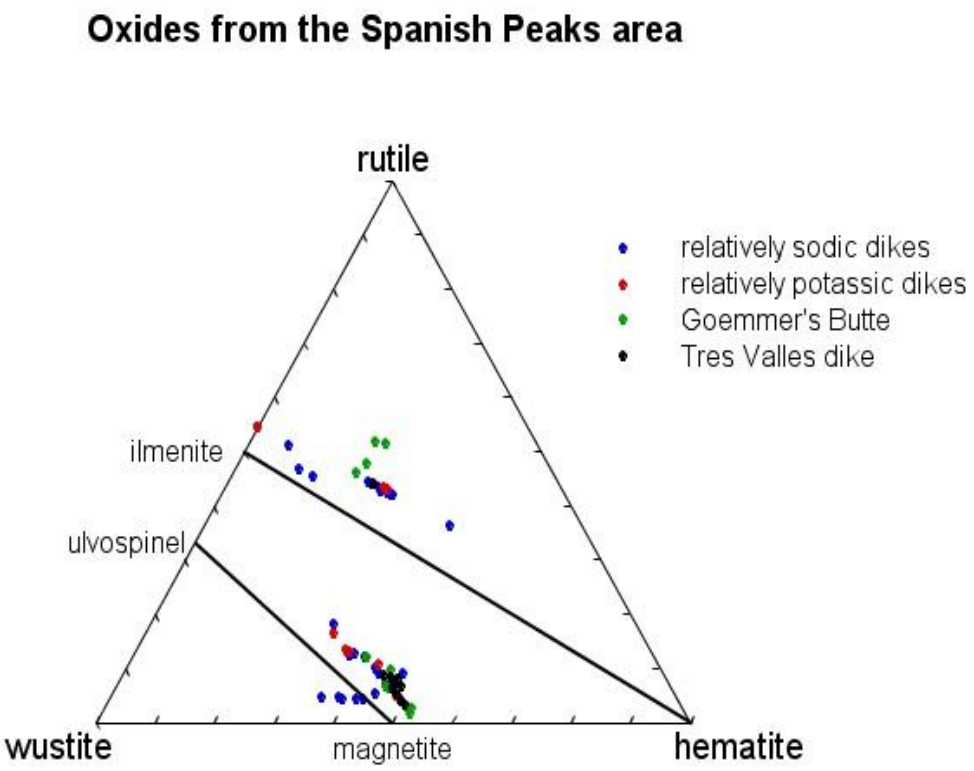

Figure 3.45: Oxide analyses from the Spanish Peaks area (figure modified from Haggerty, 1976). Rutile, wustite, and hematite corners are TiO_2, FeO, and Fe_2O_3 (wt. %), respectively. Data from this study are combined with those from McGregor (2010) for this figure.

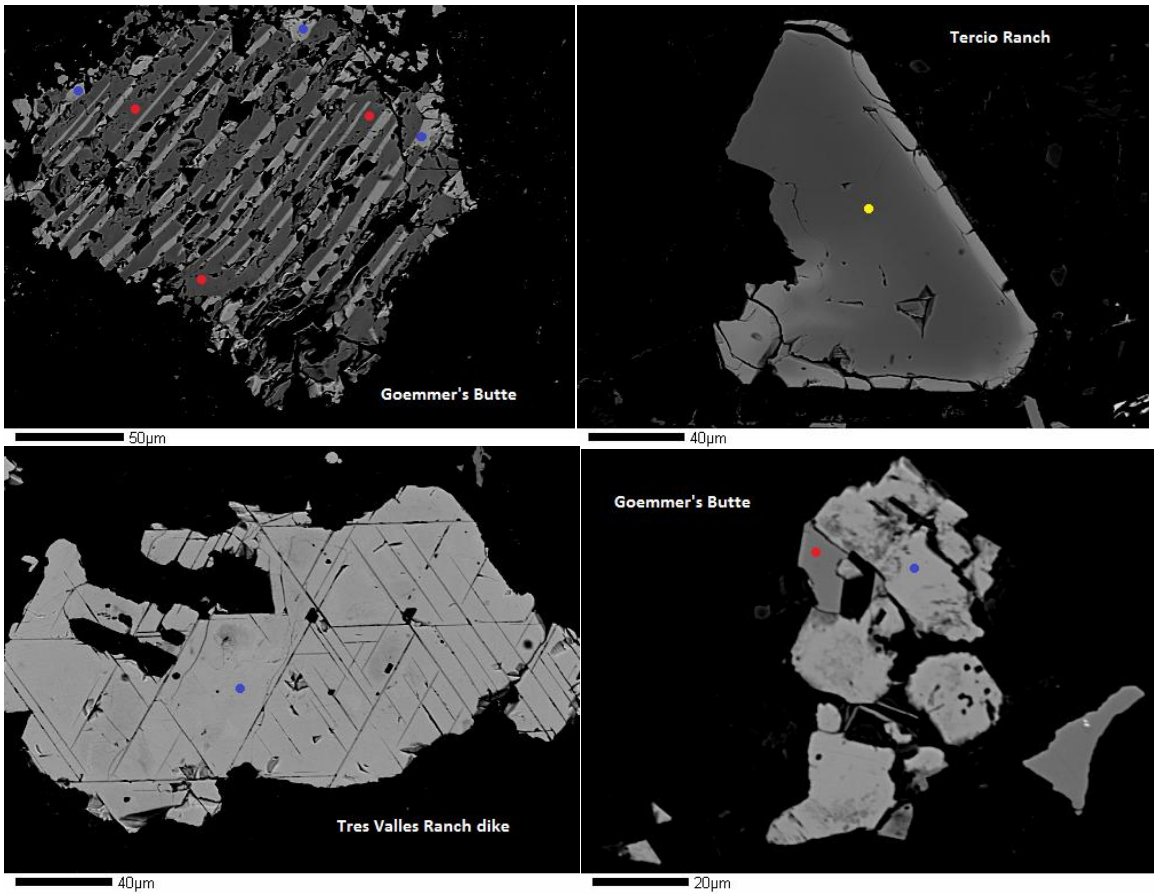

Figure 3.46: BSE images of representative oxides from the Spanish Peaks area. Circles represent locations of electron microprobe analyses. Blue circles (light areas) are magnetite analyses, red circles are ilmenite analyses, and the yellow circle is a Cr-spinel analysis.

Apatite

Over 80 point analyses were preformed on apatites from relatively potassic lamprophyres, relatively sodic lamprophyres, Goemmer's Butte trachyandesite, and Tres Valles Ranch dike. Out of these, about 40 were considered acceptable analyses. Criteria for an acceptable apatite analysis include: total between 98.5 and 100.5 (as low as 96.5 if OH apatite), Ca site occupancy (Ca+Sr+Mg+Ce+Y) between 4.85 and 5.05, P site occupancy (P+Si) between 2.90 and 3.05 (when calculating to 12.5 O equivalents), and halogen site (F + Cl) must not be overfilled (criteria from Patiño Douce et al., 2011). Table 3.11 displays representative and acceptable (following Patiño Douce et al., 2011) apatite analyses from this study. Sarafian (2009) also probed apatite in samples from the Spanish Peaks area, and those analyses were added to my data set.

The relative atomic proportions of OH, F, and Cl for each analysis are plotted in Figure 3.48. All apatites plot on the right side of this diagram, indicating a low proportion of Cl, but the potassic lamprophyres as a group have less Cl than the sodic lamprophyres. Apatites from potassic lamprophyres also tend to have more F than those from sodic lamprophyres, though there is overlap. Goemmer's Butte contains xenoliths of amphibole and apatite, and also smaller apatites in the groundmass. Apatites from the xenolith have lower F/OH ratios than apatites from the groundmass. Only one apatite from Tres Valles was deemed acceptable, and this analysis plots at an intermediate position between the groundmass and xenolith apatite analyses from Goemmer's Butte. Figure 3.47 shows BSE images of typical apatites from relatively sodic lamprophyres.

Sarafian (2009) compared elements that commonly substitute in apatite between the relatively sodic and relatively potassic lamprophyres from the Spanish Peaks area. Si

commonly substitutes for P in apatite and the relatively potassic and relatively sodic lamprophyres have similar amounts of Si in their structure (Fig. 3.49). The groundmass of Goemmer's Butte contains apatites that have more Si and F than the apatites from xenoliths in Goemmer's Butte. S can substitute for Ca and P, and figure 3.50 illustrates that the groundmass apatites from Goemmer's Butte have higher S than the xenolith apatites. Apatites from the relatively sodic and the relatively potassic lamprophyres have similar amounts of S (~ 0.20-0.90 %). Sarafian (2009) noted a negative correlation between Sr and Ca, and this is also seen in apatites from this study (Fig. 3.51). Sr content ranges from ~0.15-0.35 % and apatites from relatively potassic lamprophyres and the groundmass and xenolith of Goemmer's Butte have lower Ca and higher Sr contents than those from relatively sodic lamprophyres. A weak negative correlation is also noted between Sr and Cl (Fig. 3.52).

Table 3.11: Representative Apatite Analyses						
Type:	sodic	sodic	sodic	sodic	sodic	
Location:	BH-SW	Tercio Ranch	North Lake	Dike 1	Dike 2	MDL:*
P_2O_5**	40.88	41.29	41.72	40.78	41.07	0.16
CaO	54.25	54.09	52.79	53.76	54.57	0.09
SrO	0.34	0.36	0.11	0.21	0.24	0.09
Na_2O	0.21	0.24	0.26	0.32	0.19	0.13
FeO	0.58	0.46	0.59	0.48	0.22	0.19
MgO	n.d.***	n.d.	0.20	0.29	0.00	0.09
SO_3	0.69	0.63	0.35	0.49	0.18	0.12
Y_2O_3	n.d.	n.d.	0.20	n.d.	n.d.	0.15
SiO_2	0.53	0.34	0.27	0.28	0.46	0.05
F	2.71	1.94	2.38	3.26	2.18	0.18
Cl	0.35	0.44	0.72	0.59	0.23	0.05
Subtotal:	100.52	99.79	99.58	100.45	99.35	
F + Cl	-1.22	-0.92	-1.17	-1.51	-0.97	
Total:	99.30	98.88	98.42	98.95	98.37	
	cations normalized to 12.5 oxygens					
P	2.827	2.855	2.885	2.820	2.840	
Ca	4.748	4.734	4.620	4.705	4.776	
Sr	0.016	0.017	0.005	0.010	0.012	
Na	0.033	0.038	0.042	0.050	0.030	
Fe^{2+}	0.039	0.031	0.040	0.033	0.015	
Mg	n.d.	n.d.	0.024	0.036	n.d.	
S	0.042	0.038	0.021	0.030	0.011	
Y	n.d.	n.d.	0.009	n.d.	n.d.	
Si	0.043	0.028	0.022	0.023	0.037	
F	0.699	0.502	0.616	0.842	0.056	
Cl	0.049	0.062	0.099	0.082	0.032	
Ion Total:	7.748	7.742	7.668	7.706	7.721	
OH****	0.253	0.437	0.285	0.076	0.404	

* minimum detection limit; ** oxides in wt. %;

*** not detected (below detection limit), ****OH by difference

Table 3.11: Representative Apatite Analyses (cont.)						
Type:	sodic	potassic		groundmass	xenolith	
Location:	BH-31	BH-CO10	Tres Valles	Goemmer's Butte	Goemmer's Butte	MDL:*
P_2O_5**	38.77	40.95	40.66	40.25	40.87	0.16
CaO	52.82	53.81	53.58	53.96	54.91	0.09
SrO	0.31	0.67	0.17	0.22	0.36	0.09
Na_2O	0.35	0.41	0.23	0.32	0.20	0.13
FeO	0.70	0.21	0.37	0.62	0.29	0.19
MgO	0.49	0.21	n.d.***	n.d.	n.d.	0.09
SO_3	0.94	0.81	0.60	0.94	0.19	0.12
Y_2O_3	n.d.	n.d.	n.d.	n.d.	n.d.	0.15
SiO_2	2.14	0.30	0.36	0.41	0.09	0.05
F	2.38	2.30	2.15	2.93	1.33	0.18
Cl	0.18	0.19	0.71	0.35	0.65	0.05
Subtotal:	99.08	99.85	98.84	100.01	98.90	
F + Cl	-1.04	-1.01	-1.07	-1.31	-0.71	
Total:	98.04	98.84	97.77	98.70	98.19	
	cations normalized to 12.5 oxygens					
P	2.681	2.832	2.812	2.783	2.826	
Ca	4.623	4.709	4.689	4.722	4.805	
Sr	0.015	0.032	0.008	0.011	0.017	
Na	0.055	0.065	0.036	0.051	0.031	
Fe^{2+}	0.048	0.014	0.025	0.043	0.020	
Mg	0.060	0.026	n.d.	n.d.	n.d.	
S	0.058	0.050	0.037	0.058	0.012	
Y	n.d.	n.d.	n.d.	n.d.	n.d.	
Si	0.175	0.024	0.030	0.033	0.008	
F	0.615	0.593	0.556	0.756	0.343	
Cl	0.025	0.026	0.098	0.049	0.090	
Ion Total:	7.713	7.752	7.637	7.701	7.720	
OH****	0.360	0.381	0.346	0.194	0.566	

* minimum detection limit; ** oxides in wt. %;

*** not detected (below detection limit), ****OH by difference

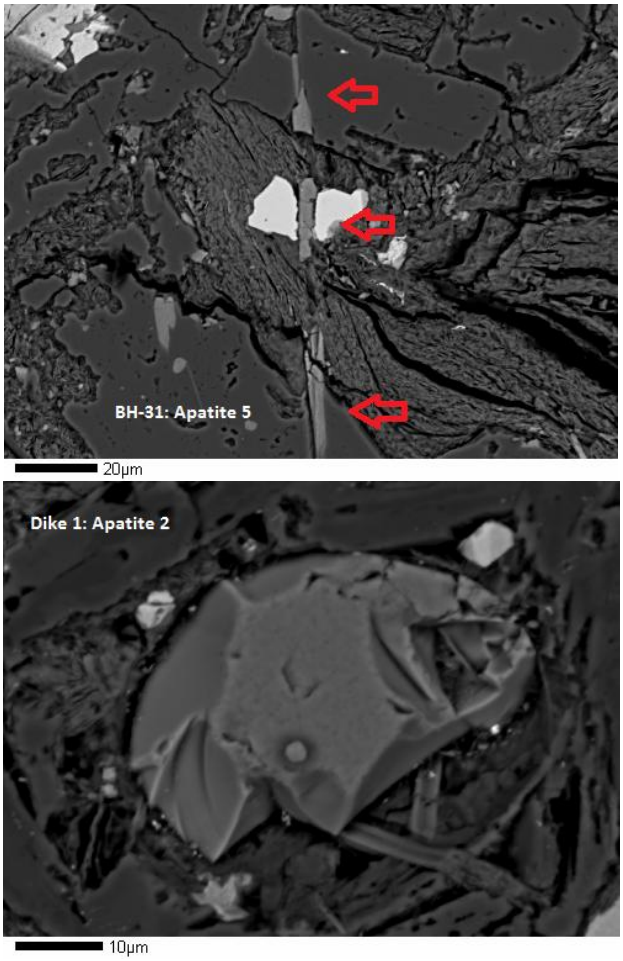

Figure 3.47: Back scatter electron images of apatites from BH-31 and Dike 1.

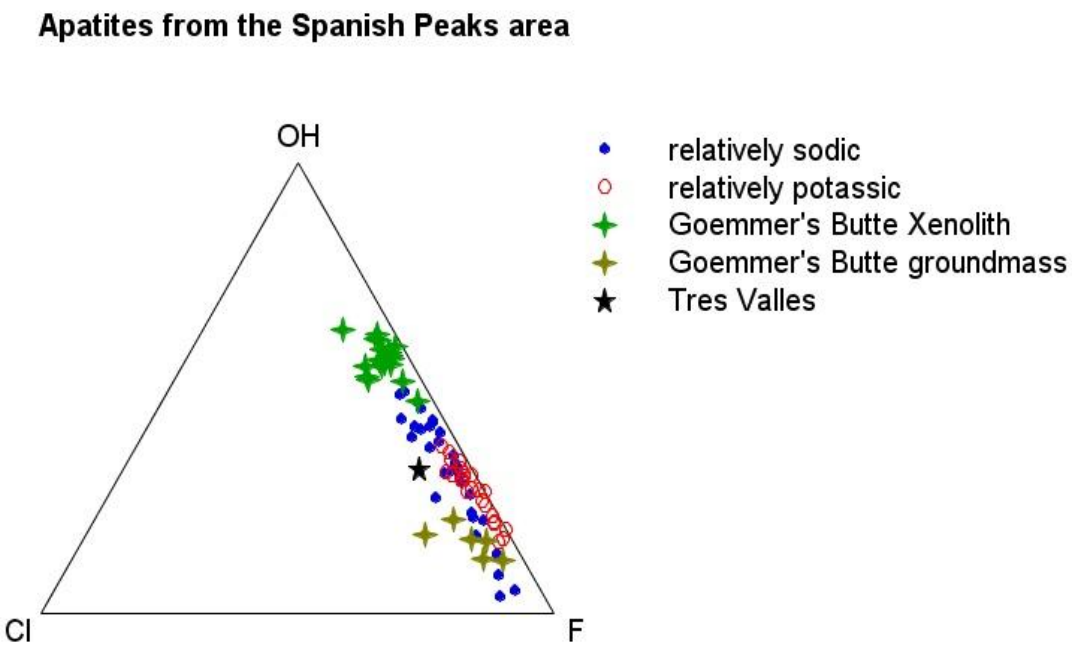

Figure 3.48: Apatite analyses from rocks of the Spanish Peaks area showing relative atomic proportions of OH, Cl, and F. Data from this study were combined with those from Sarafian (2009) to produce this figure.

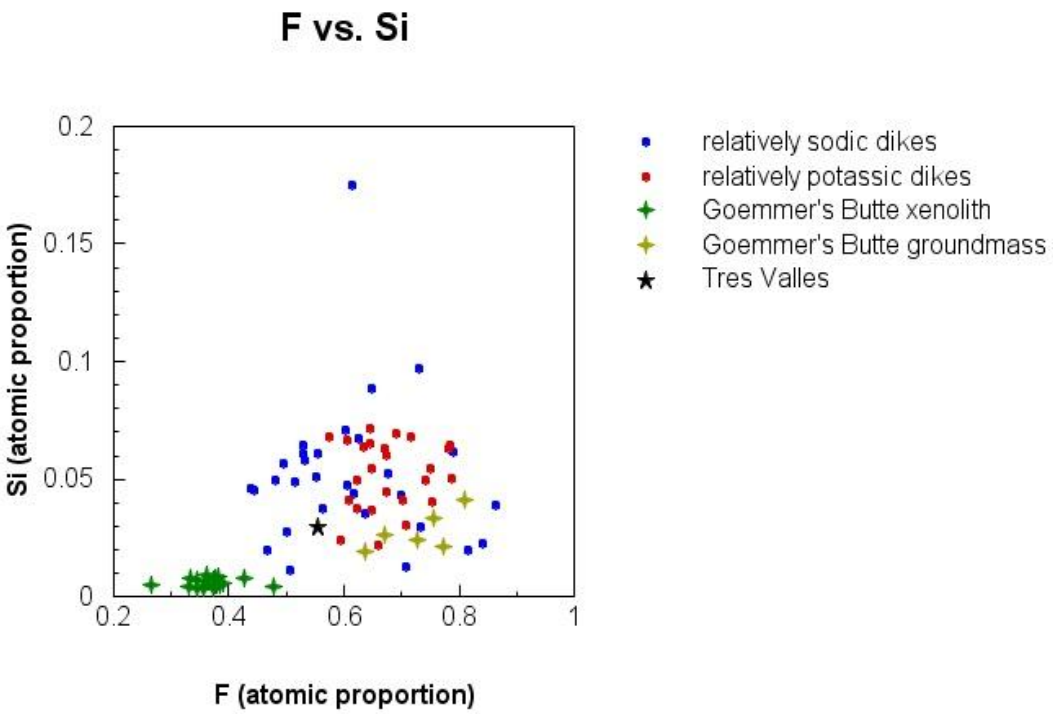

Figure 3.49: Atomic proportion of F is plotted versus Si for samples from the Spanish Peaks area.

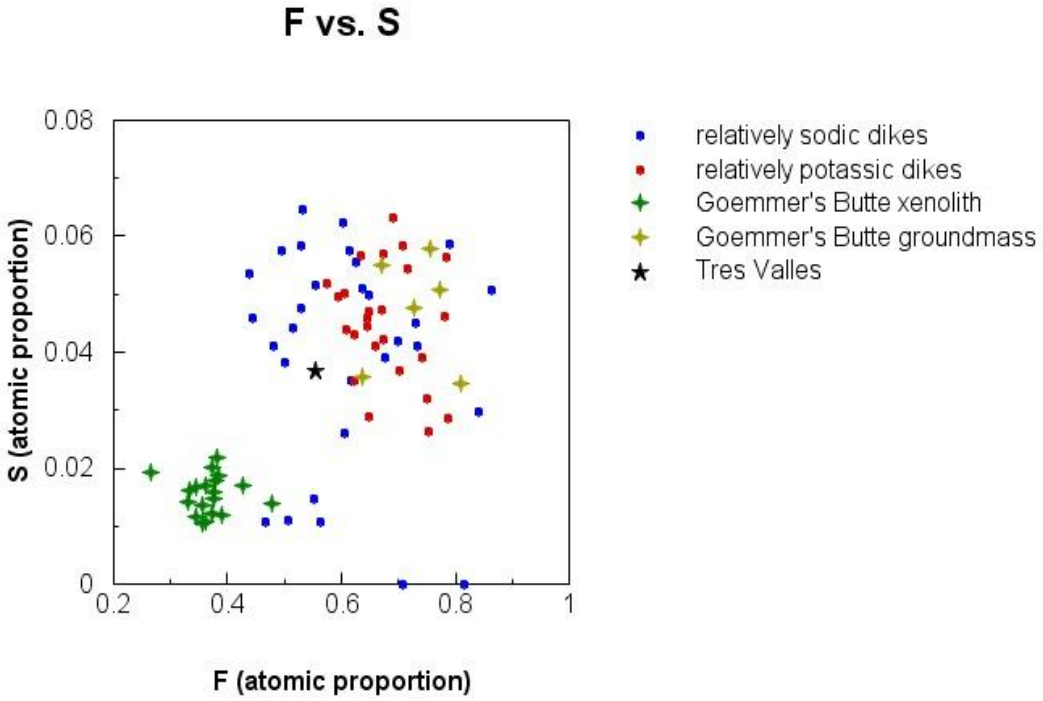

Figure 3.50: Atomic proportion of F is plotted versus S for samples from the Spanish Peaks area.

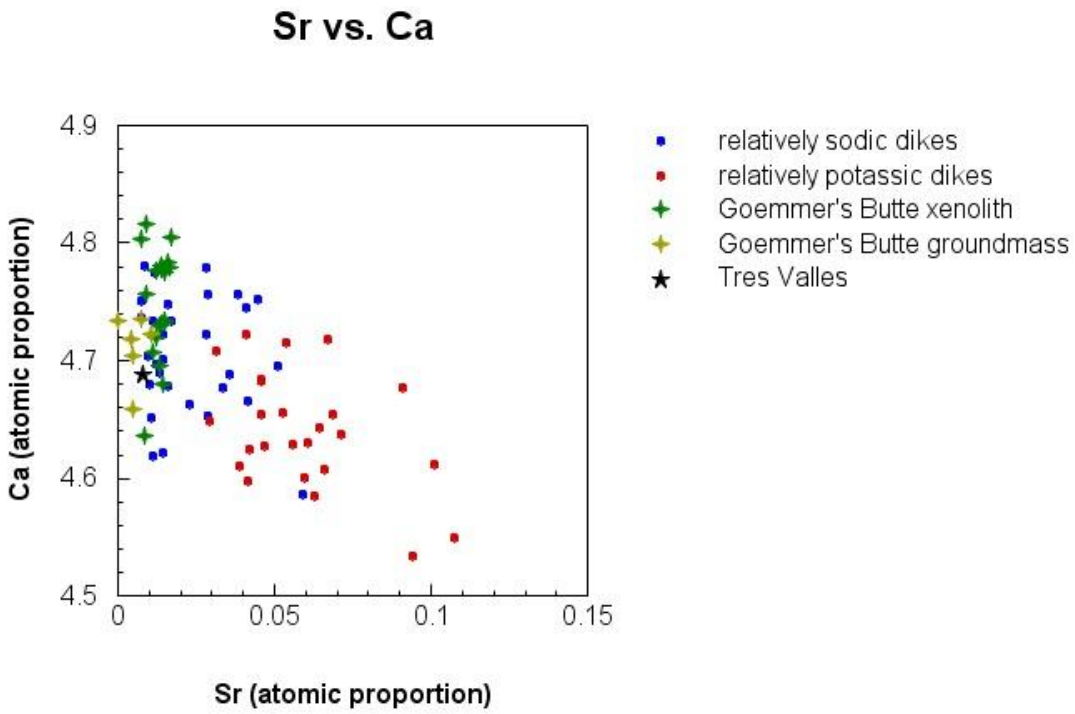

Figure 3.51: Atomic proportion of Sr is plotted versus Ca for samples from the Spanish Peaks area.

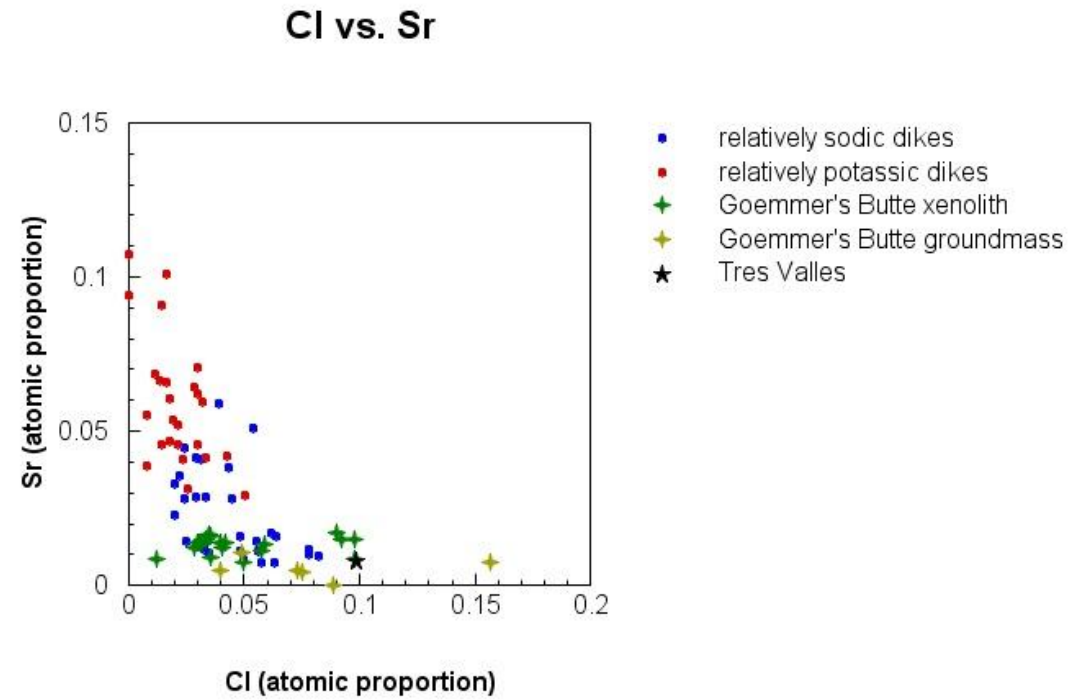

Figure 3.52: Atomic proportion of Cl is plotted versus Sr for samples from the Spanish Peaks area.

STRONTIUM ISOTOPE RESULTS

High precision Rb and Sr concentrations were obtained using ICP-MS and the standard addition method with the exception of BH-CO10. Rb and Sr in this latter sample were measured using the ICP-MS, but the standard addition method was not used.

Samples from this study were taken from localities previously dated by Miggins (2002) and Penn and Lindsey (2009), and their dates were used in the calculations for initial Sr ratios (Table 3.12). However, Goemmer's Butte and its associated amphibole megacryst have not been dated but the intrusive rocks of the butte are thought to be contemporaneous with the subparallel dikes and sills in the Spanish Peaks area. Therefore, the age used for Goemmer's Butte and megacryst is 22 Ma, an average of the ages of dated dikes that were sampled in this study. Initial Sr ratios were calculated after Dicken (1995), using a decay constant for ^{87}Rb of $1.42*10^{-11}$ yr^{-1} and the equation (Fig. 3.53) below.

In figure (3.54), the relatively potassic lamprophyres have the lowest initial $^{87}Sr/^{86}Sr$ ratios. The relatively sodic lamprophyres have higher initial $^{87}Sr/^{86}Sr$ ratios than the relatively potassic lamprophyres and Tres Valles dike. Goemmer's Butte trachyandesite has the highest initial $^{87}Sr/^{86}Sr$ than any of the other samples, and much higher initial $^{87}Sr/^{86}Sr$ than the amphibole megacryst that it contained.

Table 3.12: Sr isotope results				
Sample	**type**	**Age (Ma)**	**$^{87}Rb/^{86}Sr$ (present)**	**$^{87}Sr/^{86}Sr$ (initial)**
BH-SW	sodic	27.3	0.071181	0.705075
BH-D2	sodic	21.1	0.124277	0.706137
BH-CUCH	sodic	24.4	0.011395	0.706817
BH-CO10	potassic	14.3	0.137128	0.704652
HM-28	potassic	22.7	0.086468	0.704344
HM-4	potassic	21.3	0.117604	0.704288
HM-18	potassic	22.7	0.108615	0.704859
GB-gray*	Goemmer trachyandesite	22	0.177345	0.707349
GB-M2*	Goemmer amphibole	22	0.059462	0.704872
BH-TV	Tres Valles dike	33.1	0.118765	0.705168
*age used for Goemmer's Butte is average age of sampled dikes				

$$\left(\frac{^{87}Sr}{^{86}Sr}\right)_{present} = \left(\frac{^{87}Sr}{^{86}Sr}\right)_{initial} + \left(\frac{^{87}Rb}{^{86}Sr}\right)(e^{\gamma t} - 1)$$

Figure 3.53: γ is the decay constant for Sr ($1.42 * 10^{-11}$ $years^{-1}$); t is the age of the sample in years.

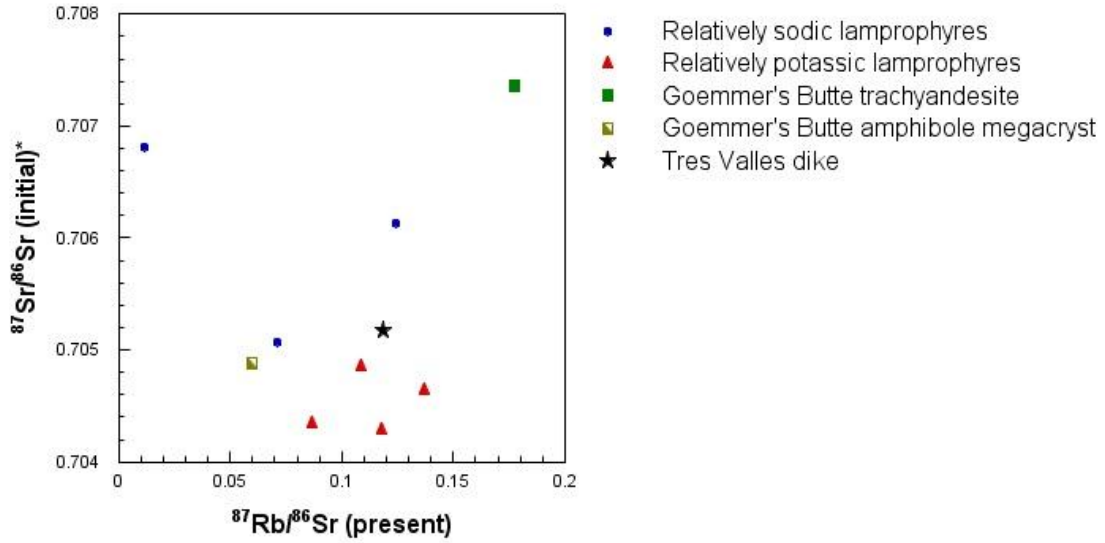

Figure 3.54: Graph of Sr isotope results. The relatively sodic lamprophyres have higher $^{87}Sr/^{86}Sr$ than the relatively potassic lamprophyres.

STABLE ISOTOPES

Amphibole megacrysts from four locations in the Spanish Peaks area were analyzed for $\delta^{18}O$ at the Stable Isotope Lab of the University of Georgia. Amphibole megacrysts were processed with laser fluorination and analyzed with a duel inlet MAT 252 mass spectrometer (Table 3.13). Figure 3.55 shows histograms of $\delta^{18}O$ analyses for UWG-2 garnet and Gore Mountain Hornblende (GMH) standards. $\delta^{18}O$ analyses of the standards cluster around the accepted values but are skewed to the right. One possible outlier is identified in the UWG histogram. Due to the range of the standard values (UWG garnet: 5.2–7.3, accepted value: 5.8; GMH hornblende: 5.8–6.6, accepted value: 6.3) the precision is less than optimum with an error around ± 0.5 ‰. Histograms for $\delta^{18}O$ of the amphibole megacrysts from Spanish Peaks rocks are presented in figure 3.56. All analyses lie between 5.2 and 6.4 ‰. Goemmer's Butte megacrysts have the most analyses (12) and the largest range (5.6 to 6.4 ‰). Big Dike has only three analyses but

they have a restricted range of 5.6 to 5.9 ‰. The mean of analyses for each sample is presented at the bottom of table 3.13. In view of the small number of replicates and the degree of error, there does not appear to be a significant difference between any of the megacrysts.

Table 3.13: $\delta^{18}O$ results of amphibole megacrysts from the Spanish Peaks area

UWG garnet	GMH hornblende	Goemmer's Butte	North Lake	Tres Valles	Big Dike
5.79	6.64	6.15	5.56	5.60	5.68
7.33	6.44	6.07	5.28	5.40	5.90
5.28	6.37	5.75	5.40	5.43	5.61
5.23	6.03	5.74	5.85	5.63	
5.89	6.58	5.62	5.45	5.70	
5.82	6.37	5.98	5.31	6.27	
6.08	5.79	5.88	5.88	5.98	
5.46		5.66	6.21	6.05	
5.75		6.14	6.26		
5.93		6.38			
5.84		5.86			
6.21		6.09			
6.28					
6.17					
6.22					
6.20					
6.49					
6.37					
Mean					
6.02	6.32	5.94	5.69	5.76	5.73

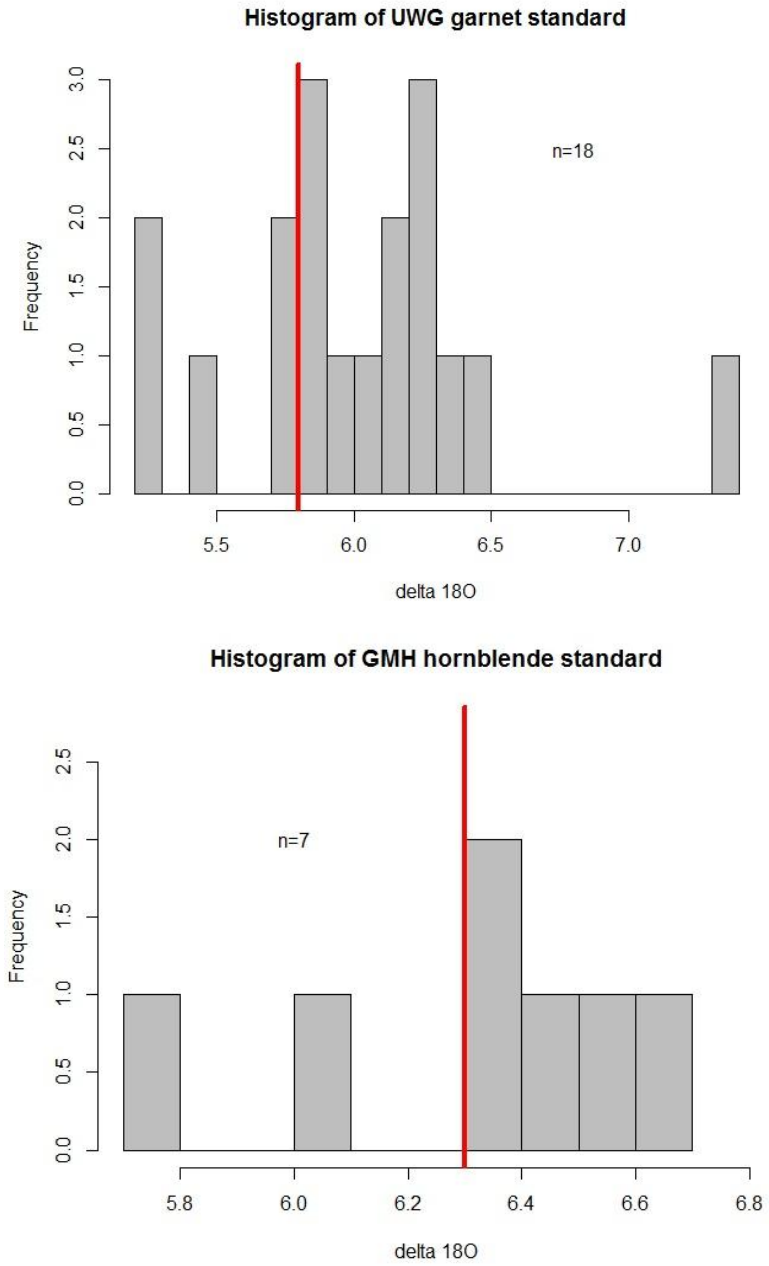

Figure 3.55: Histograms of $\delta^{18}O$ values for UWG garnet and GMH hornblende standards. Red lines are accepted values (UWG = 5.8; GMH = 6.3).

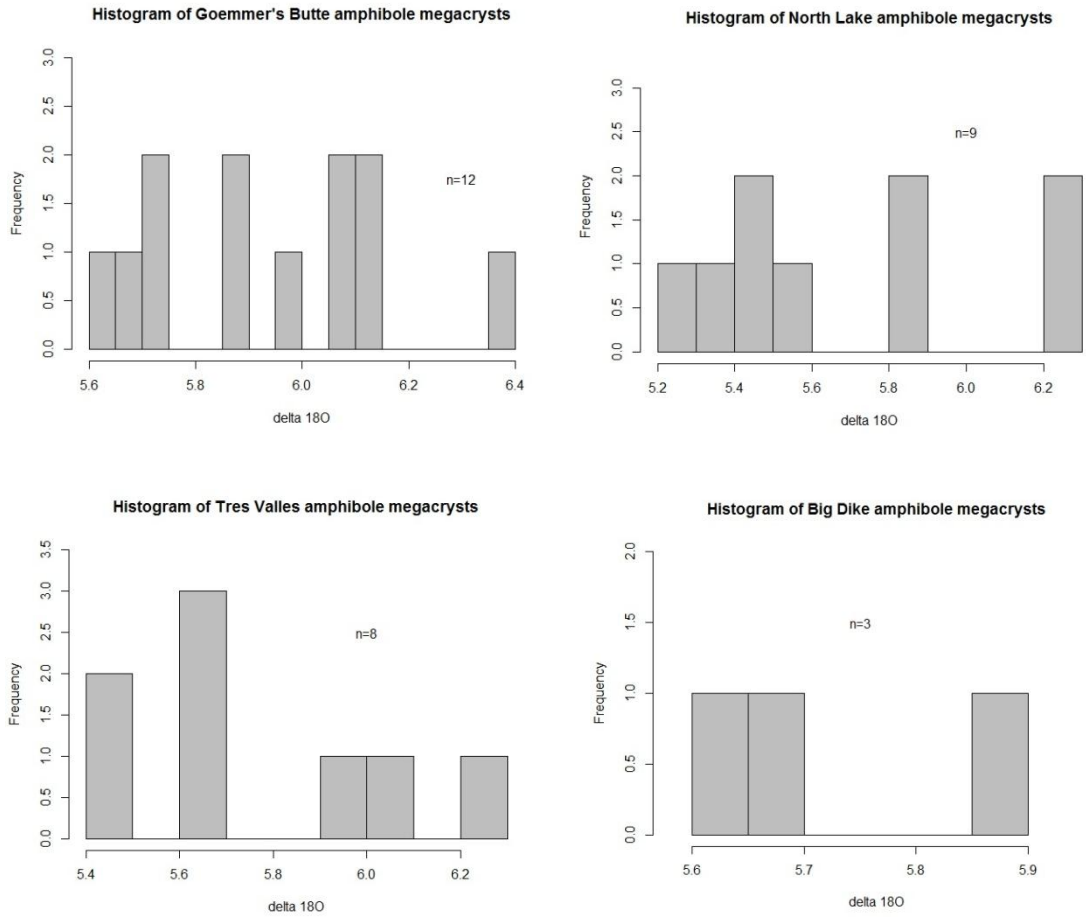

Figure 3.56: Histograms of $\delta^{18}O$ values of amphibole megacrysts from the Spanish Peaks area.

PRESSURE AND TEMPERATURE ESTIMATES

Clinopyroxene (CPX) has been studied as a thermobarometer by Putirka (1996, 2003, 2008) and equations from these works have been used to estimate the pressure and temperature of magma evolution at Spanish Peaks (Table 3.14). Putirka has used the activities of Jd-Di-Hd components in the CPX and liquid to estimate pressure and temperature. Whole rock compositions determined from XRF analysis were used as liquid compositions and electron microprobe analyses of the cores of clinopyroxenes were used for the mineral compositions. Chemical equilibrium is assessed by comparing the activity of Fe-Mg between the CPX and liquid compositions. All pyroxenes were shown to be in approximate chemical equilibrium with the whole rock compositions. Samples are plotted with calculated geothermal gradients in figure 3.57.

Pyroxenes from BH-CO10 (relatively potassic lamprophyre) formed at a wide range of pressures (1.6 to 13.0 kbar). Because some of the cores formed at higher pressures than others, some of the cores may be early formed crystals that record changing pressures and track the magma ascent, or some of the cores could be xenocrystic. These xenocrystic cores would have been subsequently incorporated into the magma during transport to lower pressures, where the rest of the pyroxene crystallized. The temperature range for pyroxenes from BH-CO10 is 1120 to 1220 º Celsius. The pyroxene core that recorded the highest temperature also records the highest pressure, also indicating this pyroxene could be xenocrystic. The sodic lamprophyres that contained clinopyroxene (Dike 2 and Cuchara) recorded pressures in the range of 6.8 to 11.7 kbar and temperatures between 1120 and 1250 º Celsius. Cuchara pyroxene cores all recorded temperatures of 1200 º C or higher. Tres Valles pyroxene cores recorded

pressures ranging from 3.3 to 8.9 kbar and temperatures ranging from 1110 to 1150 º C. Goemmer's Butte pyroxenes recorded pressures ranging from 3.9 to 5.3 kbar and temperatures between 1010 and 1030 º C.

These results suggest that the cores of CPX from the sodic lamprophyres may have formed at higher temperatures and pressures than the cores of CPX of the potassic lamprophyres, that the CPX from Goemmer's Butte formed at the lowest temperatures and pressures, and that Tres Valles CPX formed at temperatures and pressures intermediate between the CPX from the lamprophyres and Goemmer's Butte. Because the cores of CPX from the potassic lamprophyres formed at a range of temperatures and pressures, it may indicate that the magma that formed them was staged at multiple pressures for enough time to grow some crystals during transport.

Table 3.14: P and T estimates			
Sample	**pyx #**	**P(kbar)***	**T(C)***
CO-10	pyx1	1.6	1120
potassic	pyx2	5.9	1160
	pyx3	7.8	1180
	pyx4	13	1220
	pyx5	10.1	1190
Dike 2	pyx1	9.5	1130
sodic	pyx2	7.5	1120
	pyx3	11.7	1160
	pyx4	10.8	1140
	pyx5	10.5	1140
	pyx6	10.1	1140
Cuchara	pyx1	6.8	1200
sodic	pyx2	8.1	1200
	pyx3	11.3	1240
	pyx4	7.8	1200
	pyx5	8.3	1210
	pyx6	10.5	1230
	pyx7	10.1	1230
	pyx8	8.1	1200
	pyx9	9.7	1220
	pyx10	10.2	1230
	pyx11	10.2	1230
	pyx12	11.5	1240
	pyx13	11.4	1250
Tres	pyx1	6	1120
Valles	pyx2	7.6	1140
	pyx3	8.9	1150
	pyx4	8.4	1150
	pyx5	5.6	1120
	pyx6	3.3	1110
	pyx7	5.6	1130
Goemmer's	pyx1	4.6	1020
Butte	pyx2	2.7	1010
	pyx3	3.9	1010
	pyx4	4.4	1020
	pyx5	5.3	1030
* P and T values calculated after Putirka (2003)			

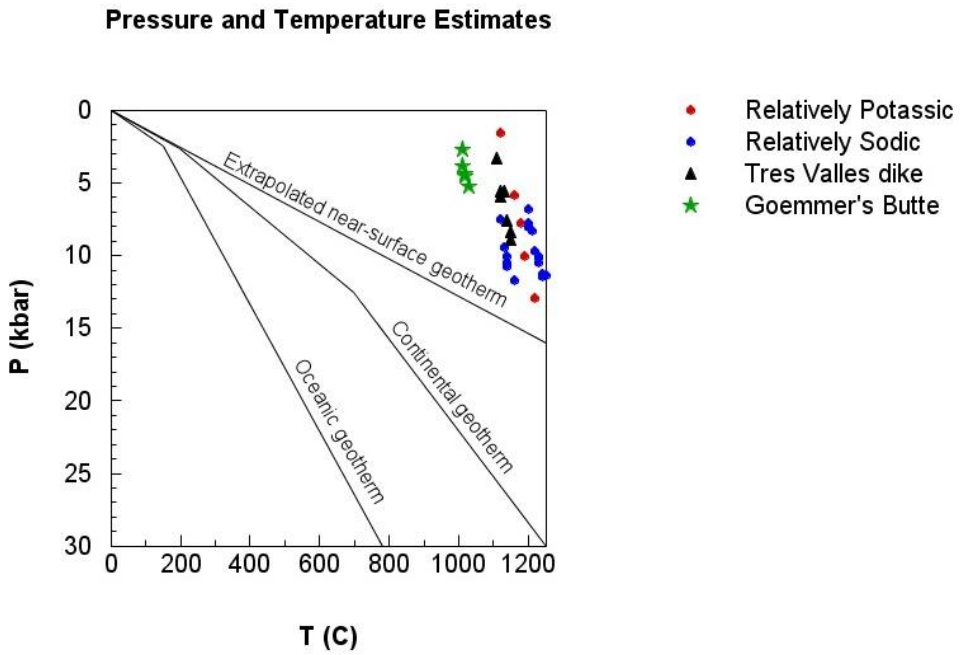

Figure 3.57: Pressures and temperatures calculated after Putirka (2003) and plotted with calculated geothermal gradients (after Winter, 2001).

CHAPTER 4

DISCUSSION

This chapter discusses the results from the field and laboratory analysis completed in this study.

ORIGIN OF GOEMMER'S BUTTE AND THE AMPHIBOLE MEGACRYSTS

Goemmer's Butte contains megacrysts of amphibole that range from < 1 cm up to 10 cm in diameter. One of the fundamental questions about the megacrysts that occur in Goemmer's Butte trachyandesite is whether they formed from the host magma or were incorporated as xenocrysts from a deeper source. This question can be explored with a combination of field and petrographic observations, microprobe analysis, and trace element modeling.

Goemmer's Butte trachyandesite is a gray, aphanitic igneous rock that shows little evidence of alteration. Amphibole megacrysts have a sharp interface between the mineral and surrounding groundmass, with no obvious secondary minerals along the interface. The crystals are euhedral to subhedral and a trachytic groundmass texture is present, with small grains aligned around the megacryst due to flow. Overall, the megacrysts appear to be in textural equilibrium with the groundmass, with no visible textures due to resorption or reaction rims. Microprobe results from the amphibole megacrysts at Goemmer's Butte show that they are not zoned and are all very similar in composition (Fig. 3.38).

Amphibole partitions certain elements more strongly into its crystal structure than others, and the strength of this partitioning is represented by the magnitude of a partition

coefficient (or K_d) which can be estimated by dividing the concentration of trace elements in the megacryst by the melt concentrations, which are approximated by the host concentrations (GB-gray). The host rock includes both groundmass and phenocrysts, but in this case the Goemmer's Butte trachyandesite abundances can be approximated as melt concentrations because the rock contains virtually no phenocrysts except for the amphibole megacrysts. In figure 4.2, the calculated partition coefficients are compared to published partition coefficients for amphibole in similar rock types. The patterns correspond very closely, and this observation along with the field, petrographic, and microprobe observations support the hypothesis that the amphibole megacrysts at Goemmer's Butte precipitated from the host magma, and are not foreign xenocrysts. Stable isotope results suggest that Goemmer's Butte is magmatic in origin, and was not influenced by meteoric water or seawater. Results from Sr isotopes complicate the picture of the origin of amphibole megacrysts at Goemmer's Butte, because the initial Sr ratio of the amphibole megacryst is significantly different than the host trachyandesite (0.70487 and 0.70735, respectively). One explanation is that the megacrysts are xenocrystic in nature, but more likely sedimentary material with elevated $^{87}Sr/^{86}Sr$ ratios from the surrounding Cuchara formation was incorporated into the Goemmer's Butte magma during emplacement. Evidence of highly explosive emplacement is the sedimentary clast-rich breccia adhered to the sides of Goemmer's Butte and radiating dikes, and it is likely that enough sedimentary rock was incorporated into the host magma to affect the initial Sr ratio.

The origin of Gommer's Butte itself is an interesting puzzle. The presence of breccia adhering to the surfaces of the butte and the associated radiating dikes indicates

an explosive event that may have vented to the surface. The top of Goemmer's Butte is ~5500 ft below the stock of West Spanish Peak, an intrusive rock that would have cooled below the surface. The age of Goemmer's Butte is thought to be similar to the other magmatism in the area and thus erosion is not the answer. The vent facies present at Goemmer's Butte indicates a very deep explosive eruption similar to those that form kimberlites.

Amphibole megacrysts from four locations in the Spanish Peaks area were chosen for stable isotope analysis. All of the samples had $\delta^{18}O$ values that indicated that structural water was magmatic in origin and was not influenced by meteoric water or seawater. Petrographic analysis indicates that the megacrysts are in equilibrium with their hosts because none of them show any zoning or resorption textures. This indicates that megacrysts occurring in Spanish Peaks rocks are magmatic in origin and are not xenocrysts. Figure 4.1 shows that the Mg #'s of amphibole megacrysts are consistently higher than their host rock. This may indicate that the amphibole megacrysts are in chemical equilibrium because Fe-Mg silicates typically have higher Mg # than their hosts. In the case of Goemmer's Butte, Sr isotopes are significantly different between the megacryst and the host, but this most likely is the result of crustal contamination, which would also have decreased the Mg # of the host rock.

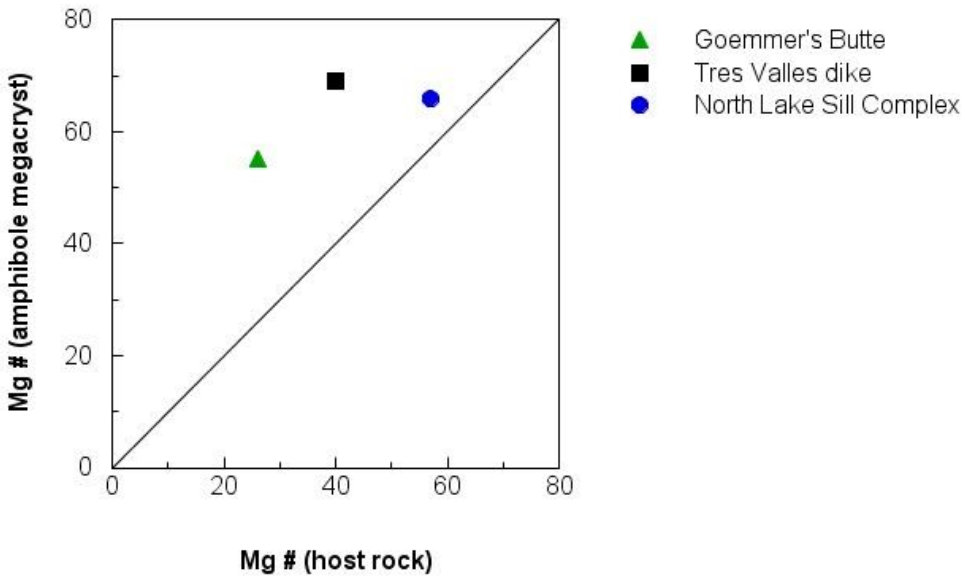

Figure 4.1: The average Mg # of the amphibole megacrysts are plotted versus the Mg # of the host rock. The line is a 1 to 1 ratio. The megacrysts consistently have higher Mg #'s than their hosts.

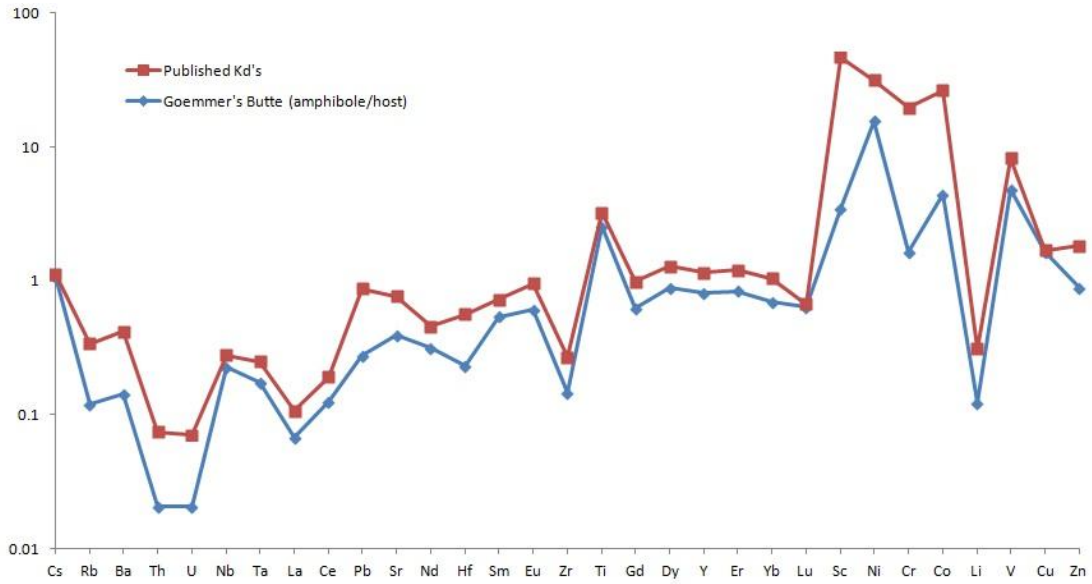

Figure 4.2: Plot comparing published partition coefficients (amphibole/melt) and calculated amphibole/host ratios of megacrysts from Goemmer's Butte. Curve for Goemmer's Butte was created by dividing the trace element concentration of the amphibole megacryst by the trace element concentration in the whole rock. Published partition coefficients are from Luhr (1984), Villemant et al. (1981), Dalpe and Baker (1994), Matsui et al. (1977), and Dostal et al. (1983) and were obtained from http://www.earthref.org.

TRES VALLES

Tres Valles is a dike that is located in the northern part of the Raton Basin and is thought to be related to Mt. Mestas and has been dated as older than the alkaline lamprophyres of the Spanish Peaks area (~33 Ma; Miggins, 2002). Because this dike contained large megacrysts of amphibole, it was sampled to compare to megacrysts from other Spanish Peaks localities and to evaluate whether it is related in any way to the alkaline lamprophyres or Goemmer's Butte. Measurement of $\delta^{18}O$ on the amphibole megacrysts revealed that they are similar to other amphibole megacrysts from Spanish Peaks rocks and trace element patterns are very similar, indicating a relationship between

Tres Valles and the other types of rocks from this study. However, pressure and temperature estimates place the crystallization of clinopyroxene in Tres Valles at an intermediate range between the CPX at Goemmer's Butte and the lamprophyres, and microprobe analysis indicates different chemical makeup of the amphibole (lower Ti). Whole rock analysis shows that the Tres Valles magma was less primitive and more silicic than any of the other rocks in this study.

While it is possible that Tres Valles had a source similar to those of the other Spanish Peaks rocks, it is older, more evolved and possibly contaminated as evidenced from the wide array of crustal xenoliths it contains.

MODELS FOR MAGMA GENESIS

McGregor (2010) favored a model of sequential melting of a metasomatized vein to produce the two types of lamprophyres (relatively sodic and relatively potassic) that occur as dikes and sills in the Spanish Peaks area. In this case, the source of the lamprophyres is a group of metasomatic veins in the upper mantle in which minerals are preferentially melted to produce an evolving phase assemblage through time. He showed that the sodic and potassic lamprophyres are not related through fractional crystallization on the basis of major and trace element abundances and ratios, thus must be produced from distinct phase assemblages, though there were similarities in trace element abundances and mineral compositions that indicated they may have a similar parent source.

In this study, more of the sodic and potassic lamprophyres were sampled to add to the data set of McGregor (2010) and analyzed for major elements and subjected to microprobe analysis for mineral compositions. Major element results are consistent with

those of McGregor (2010) and the two groups show distinct trends and no observable liquid line of descent when various oxides are plotted versus Mg # (Fig. 3.28).The relatively potassic lamprophyres have higher Mg #s indicating they are more primitive than the relatively sodic lamprophyres. Compatible and incompatible trace elements plotted versus Mg # will decrease or increase smoothly if a liquid line of descent is present indicating a genetic relationship between the two types. This is not evident thus the relatively sodic and relatively potassic lamprophyres are not related through fractional crystallization (Fig. 4.3).

Both the relatively potassic and relatively sodic lamprophyres have very similar REE and multi-element spidergram patterns indicating the strong similarity in the two types, and suggesting a similarity in the sources of the magmas. Potassic lamprophyres are slightly more enriched in the LREEs than the sodic lamprophyres.

While the major and trace element results support the sequential melting hypothesis, Sr isotope results tell a different story. The relatively potassic lamprophyres have significantly lower initial $^{87}Sr/^{86}Sr$ ratios (0.70423-0.70486) than the sodic lamprophyres (0.70508-0.70682), indicating that the sources for the two types of lamprophyres were distinct and must have been separated for a long enough time to develop distinct Sr isotope ratios. This observation rules out the model of sequential melting of one type of metasomatic vein to produce the two chemically distinct types of lamprophyres.

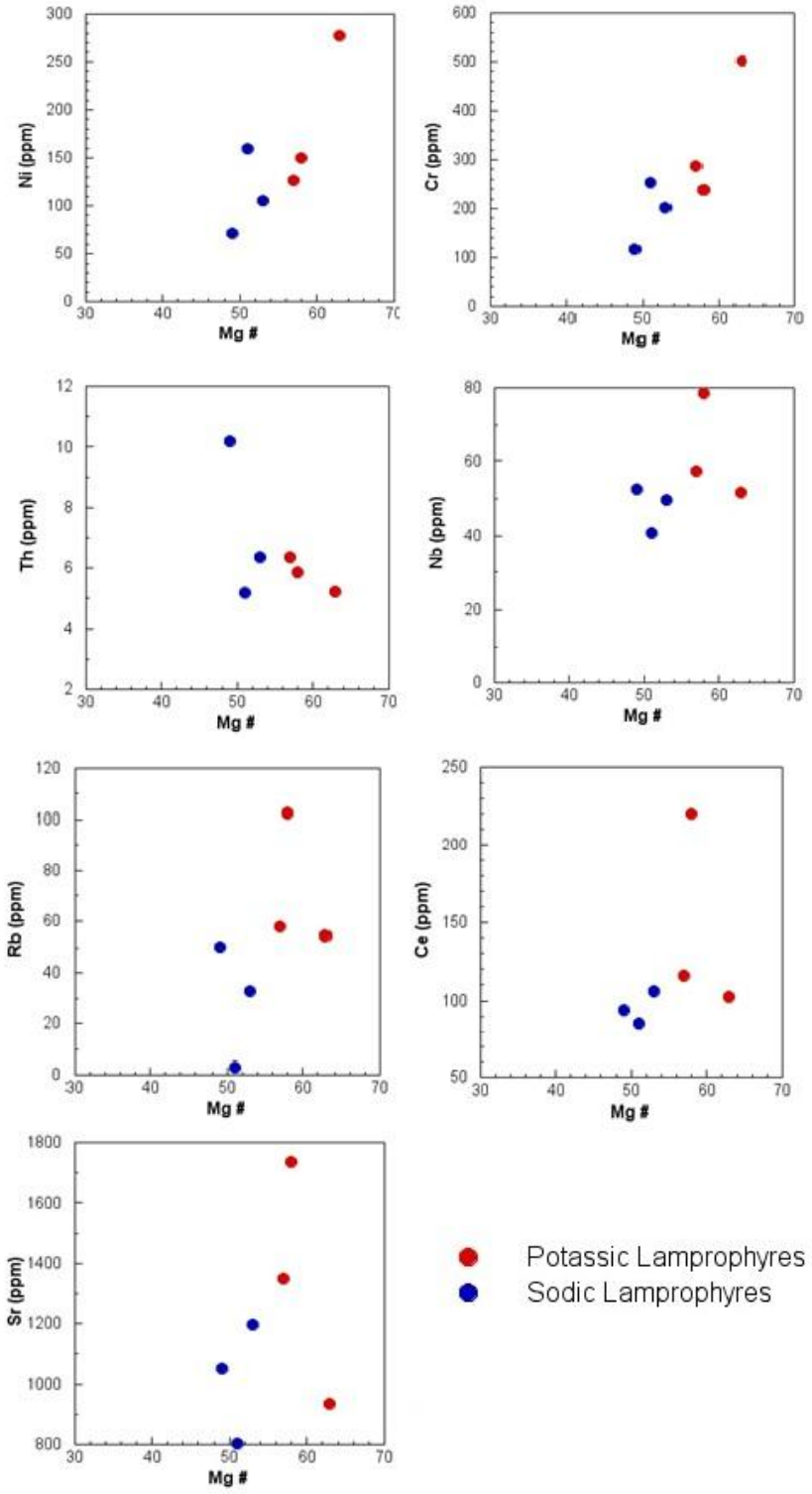

Figure 4.3: Various trace elements plotted versus Mg # for relatively potassic and relatively sodic lamprophyres in the Spanish Peaks area.

The relatively sodic and relatively potassic lamprophyres of the Spanish Peaks area have fundamentally distinct phase assemblages and chemical makeup that are not related by fractional crystallization and have distinct sources that have been separated for a long time. However, they intruded very close to each other (sometimes a matter of feet) at about the same time and have very similar trace element patterns. One possible explanation is that one pervasive metasomatic event occurred introducing fluids and forming hydrous minerals. If this fluid affected mantle rocks at different pressures, then distinct phase assemblages could form. The metasomatic event that formed these distinct sources must have occurred long enough before subsequent melting to result in a difference in initial Sr ratios. Foley (1992) showed that when a metasomatic vein is present in the upper mantle, certain minerals in the vein will melt preferentially to the wall rock. As melting was induced these metasomatic veins melted preferentially to the surrounding rock and produced the alkaline lamprophyres of the Spanish Peaks area. The deeper veins would melt first and then the shallower veins with a different phase assemblage and different initial Sr ratio. Pressure and temperature estimates of the sodic and potassic lamprophyres from clinopyroxene and whole rock analysis indicate that the clinopyroxene crystals in the sodic lamprophyres were formed at depths >7 kbars and at temperatures between 1100 and 1200 º Celsius, and that the clinopyroxene crystals from the potassic lamprophyres recorded both higher (13 kbar) and lower (1.6 kbar) pressures and about the same temperature. This range in pressures of cpx formation most likely represent magmatic pauses or staging where the magma was stalled during ascent for a period of time, allowing some cpx to crystallize. Because the relatively potassic

lamprophyres record the highest pressure in their CPX cores, it could indicate a deeper origin for than the relatively sodic lamprophyres.

Experiments by Foley (1991) have shown that a high ratio of F/OH in minerals such as phlogopite allows them to be stable at higher temperatures and pressures. Phlogopite contains a large amount of potassium, and the potassic dikes have a higher concentration of F in mica and apatite than the sodic lamprophyres. This supports the hypothesis that phlogopite was in the source of the potassic lamprophyres and not the sodic lamprophyres, and that the phlogopite could have been stable at higher pressures indicating that the source for the potassic lamprophyres may be deeper than the source for the sodic lamprophyres. The source of heat that induced melting in the veins would have come from below and thus it makes sense that the deeper veins would melt first to produce the potassic lamprophyres before the sodic lamprophyres. The source of this heat could be a thermal pulse related to convection currents in the mantle above the subducted Farallon plate as it delaminated from the lower lithosphere and/or related to the Rio Grande Rift.

One of the possible sources of the fluids that produced the metasomatized veins is the subducted Farallon plate. A negative Nb-Ta anomaly is considered a signature of fluids from the subducting Farallon plate (Gibson et al., 1993; Carlson and Nowell, 2001) and the presence of Cl in hydrous mineral phases and apatite could also be a signature of fluids derived from subducted lithosphere. None of the samples from this study show a negative Nb-Ta anomaly, and none of the mineral analyses of hydrous minerals and apatite show an unusually high amount of Cl. These observations indicate that subduction-related fluids from the Farallon plate were probably not involved in the

petrogenesis of the relatively potassic and relatively sodic lamprophyres from the Spanish Peaks area, or at least did not impart a distinct subduction related signature to the lamprophyres.

CHAPTER 5

CONCLUSIONS

This study was conducted in order to investigate the sources of the contemporaneous relatively potassic and relatively sodic lamprophyric dikes that occur in the Spanish Peaks area of south-central Colorado. This work builds upon the work of Heath McGregor (2010) by expanding the sample set and adding stable isotope, high precision trace element, and radiogenic isotope analyses to his data.

The results of this study suggest that the trace elemental abundances measured by XRF compare well to the ICP-MS data although many more elements were measureable on ICP-MS. Goemmer's Butte amphibole megacrysts precipitated from the gray trachyandesite host magma, and do not record meteoric or seawater interaction as shown by stable isotope, trace element, and mineral compositions. Other amphibole megacrysts in the area also are magmatic, appear to be in equilibrium with the groundmass of their host rocks, and do not record meteoric or seawater interaction. Tres Valles dike is different in major elements and has different phenocryst compositions than the lamprophyres and rocks of Goemmer's Butte and was affected by crustal contamination; however, the trace element pattern was similar to other rocks from this study. The sequential melting hypothesis of McGregor (2010) was ruled out due to a pronounced difference in initial Sr ratio, though trace element patterns of both types of lamprophyre are similar and suggest a relationship between the source rocks. No evidence of subduction-related fluids from the Farallon plate was found in any of the rocks from this

study. The model proposed to explain the petrogenesis of the relatively sodic and potassic lamprophyres consists of a pervasive ancient metasomatic event that veined the upper mantle with hydrous minerals and produced different phase assemblages at different pressures. When melting was induced, these veins melted preferentially and produced two different magmas in a relatively short time period that exploited the same weaknesses in the lithosphere during ascent.

REFERENCES

Carlson, R., and Nowell, G., 2001, Olivine-poor sources for mantle-derived magmas: Os and Hf isotopic evidence from potassic magmas of the Colorado Plateau, Geochemistry, Geophysics, Geosystems, 2; 6.

Dalpe, C., and Baker, D., 1994, Partition coefficients for rare-earth elements between calcic amphibole and Ti-rich basanitic glass at 1.5 Gpa, 1100 degrees C, *Mineralogical Magazine,* 58; 207-208.

Dicken, A., 1995, Radiogenic Isotope Geology, Cambridge University Press, New York; 452 p.

Dostal, J., Dupuy, C., Carron, J., Dekerneizon, M., and Maury, R., 1983, Partition-Coefficients of Trace-Elements - Application to Volcanic-Rocks of St-Vincent, West-Indies, *Geochimica et Cosmochimica Acta,* 47, 3; 525-533.

Droop, G., 1987, A general equation for estimating Fe^{3+} concentrations in ferromagnesian silicates and oxides from microprobe analyses, using stoichiometric criteria, *Mineralogical Magazine,* 51; 431-435.

Foley, S., 1991, High-pressure stability of the fluor- and hydroxy- end-members of pargasite and K-richterite, *Geochimica et Cosmochimica Acta*, 55; 2689-2694.

Foley, S., 1992, Vein-plus-wall-rock melting mechanism in the lithosphere and the origin of potassic alkaline magmas, *Lithos,* 28; 435-453.

Gibson, S., Thompson, R., Leat, P., Morrison, M., Hendry, G., Dickin, A., and Mitchell, J., 1993, Ultrapotassic magmas along the flanks of the Oligo-Miocene Rio Grande Rift, USA; monitors of the zone of lithospheric mantle extension and thinning beneath a continental rift, *Journal of Petrology,* 34; 187-228.

Haggerty, S., 1976, Opaque mineral oxides in terrestrial igneous rocks, in *Oxide Minerals, Mineralogical Society of America Short Course Notes*, 3; Hg101-Hg300.

Hills, R., 1889, Additional notes on the eruptions of the Spanish Peaks region, *Proceedings of the Colorado Scientific Society*, 3; 224-227.

Irvine, T., and Baragar, W., 1971, A Guide to the chemical classification of the common volcanic rocks, *Canadian Journal of Earth Sciences*, 8; 523-548.

Jahn, B., Sun, S., and Nesbitt, R., 1979, REE distribution and petrogenesis of the Spanish Peaks igneous complex, Colorado, Contributions *to Mineralogy and Petrology*, 70; 281-298.

Johnson, R., 1968, Geology of the igneous rocks of the Spanish Peaks region, *in U.S. Geological Survey Professional Paper*, Report P 0594-G; 47 p.

Knopf, A., 1936, Igneous geology of the Spanish Peaks region, Colorado, *Geological Society of America Bulletin*, 47; 1727-1784.

Leake, B., 1978, Nomenclature of amphiboles, *Canadian Mineralogist*, 16; 501-520.

Leake, B., Woolley, A., Arps, C., Birch, W., Gilbert, M., Grice, J., Hawthorne, F., Kato, A., Kisch, H., Krivovichev, V., Linthout, K., Laird, J., Mandarino, J., Maresch, W., Nickel, E., Rock, N., Schumacher, J., Smith, D., Stephenson, N., Ungaretti, L., Whittaker, E., and Youzhi, G., 1997, Nomenclature of the amphiboles: Report of the subcommittee on amphiboles of the International Mineralogical Association, Commission on New Minerals and Mineral Names, *The Canadian Mineralogist*, 35; 219-246.

Le Bas, M., Le Maitre, R., Streckeisen, A., and Zanettin, B., 1986, Chemical classification of volcanic rocks based on the total alkali-silica diagram, *Journal of Petrology*, 27; 745-750.

Lehnert, K., Su, Y., Langmuir, C., Sarbas, B. and Nohl, U., 2000,. A global geochemical database structure for rocks, *Geochemistry, Geophysics, Geosystems* 1; 5.

Lindsey, D., 1995, Geologic map of the Cuchara Quadrangle, Huerfano County, Colorado, *Miscellaneous Field Studies Map - U. S. Geological Survey*

Lindsey, D., 1996, Laramide structure of the central Sangre de Cristo Mountains and adjacent Raton Basin, southern Colorado, *Mountain Geologist*, 35; 55-70.

Lipman, P., and Mehnert, H., 1975, Late Cenozoic basaltic volcanism and development of the Rio Grande depression in the southern Rocky Mountains, *Mem. of the Geological Society of America*, 144; 119-154.

Luhr, J., Carmichael, I., and Varekamp, J., 1984, The 1982 eruptions of El Chichon volcano, Chiapas, Mexico: mineralogy and petrology of the anhydrite-bearing pumices. *Journal of Volcanology and Geothermal Research*, 23; 69-108.

Lyubetskaya, T., and Korenaga, J., 2007, Chemical composition of Earth's mantle and its variance: 1. Method and results, *Journal of Geophysical Research*, 112; B3.

Matsui, Y., Onuma, N., Nagasawa, H., Higuchi, H., and Banno, S., 1977, Crystal structure control in trace element partition between crystal and magma, *Tectonics*, 100; 315-324.

McGregor, H., 2010, Petrogenetic relationships between relatively potassic and relatively sodic alkaline rocks from the Spanish Peaks area near Walsenburg, Colorado, unpublished M.S. thesis, University of Georgia, 155 p.

Miggins, D., 2002, Chronologic, geochemical, and isotopic framework of igneous rocks within the Raton Basin and adjacent Rio Grande Rift, south-central Colorado and northern New Mexico, unpublished M.S. thesis, University of Colorado at Boulder, 379 p.

Morimoto, N., 1989, Nomenclature of pyroxenes, *Canadian Mineralogist*, 27; 143-156.

Patiño Douce, A., Roden, M., Chaumba, J., Fleisher, C., and Yogodzinski, G., 2011, Compositional variability of terrestrial mantle apatites, thermodynamic modeling of apatite volatile contents, and the halogen and water budgets of planetary mantles, *Chemical Geology*, 288; 14-31.

Penn, B., 1994, An investigation of the temporal and geochemical characteristics and the petrogenetic origins of the Spanish Peaks intrusive rocks of south-central Colorado, unpublished Ph.D. dissertation, University of Colorado School of Mines.

Penn, B., and Lindsey, D., 1996, Tertiary igneous rocks and Laramide structure and stratigraphy of the Spanish Peaks region, south-central Colorado; road log and descriptions from Walsenberg to La Veta (first day) and La Veta to Aguilar (second day), *Colorado Geological Survey Open-File Report*, 21 p.

Penn, B., and Lindsey, D., 2009, $^{40}Ar/^{39}Ar$ dates for the Spanish Peaks intrusions in south-central Colorado, *Rocky Mountain Geology*, 44; 17-32.

Putirka, K., Johnson, M., Kinzler, R., Longhi, R., and Walker, D., 1996, Thermobarometry of mafic igneous rocks based on clinopyroxene-liquid equilibria, 0-30 kbar, *Contributions To Mineralogy And Petrology*. 123, 1; 92-108.

Putirka, K., Mikaelian, H., Ryerson, F., and Shaw, H., 2003, New clinopyroxene-liquid thermobarometers for mafic, evolved, and volatile-bearing lava composition, with applications to lavas from Tibet and the Snake River plain, Idaho, *American Mineralogist*, 88, 10; 1542-1554.

Putirka, K., 2008, Thermometers and barometers for volcanic systems, Reviews in Mineralogy and Geochemistry, 69; 61-120.

Sarafian, A., 2009, Apatite in sodic and potassic lamprophyres from Spanish Peaks, Colorado, unpublished senior thesis, University of Georgia, 28 p.

Shaw, C., and Penczak, R., 1996, Barium- and titanium-rich biotite and phlogopite from the western and eastern gabbro, Coldwell alkaline complex, northwestern Ontario, *Canadian Mineralogist*, 34; 967-975.

Smith, R., 1975, Structure and petrology of Spanish Peaks dikes, south-central Colorado, unpublished Ph.D. dissertation, University of Colorado at Boulder, 270 p.

Tschegg, C., Bizimis, M., Schneider, D., Akinin, V., and Ntaflos, T., 2011, Magmatism at the Eurasian-North American modern plate boundary; constraints from alkaline volcanism in the Chersky Belt (Yakutia), *Lithos*, 125, 1-2; 825-835.

Villemant, B., Jaffrezic, H., Joron, J., and Treuil, M., 1981, Distribution Coefficients of Major and Trace-Elements - Fractional Crystallization in the Alkali Basalt Series of Chaine-Des-Puys (Massif Central, France), *Geochimica et Cosmochimica Acta*, 45, 11; 1,997-2,016.

Winter, J., 2001, *An introduction to igneous and metamorphic petrology*, Prentice Hall, Upper Saddle River, New Jersey, 697 p.

APPENDIX

This appendix reports the results from radiogenic isotopic analysis for Sr, Nd, Hf, and Pb, which were analyzed at the National High Magnetic Field Laboratory of Florida State University using the TIMS and ICP-MS.

Sample	$^{87}Sr/^{86}Sr$	$^{143}Nd/^{144}Nd$	$^{176}Hf/^{177}Hf$	$^{206}Pb/^{204}Pb$	$^{207}Pb/^{204}Pb$	$^{208}Pb/^{204}Pb$
BH-SW	0.70510	0.51240	0.28274	17.907	15.497	37.532
BH-D2	0.70617	0.51262	0.28288	18.082	15.510	37.695
BH-CUCH	0.70680	0.51257	0.28286	20.819	15.764	39.094
BH-CO10	0.70468	0.51237	0.28272	17.602	15.459	37.213
HM-28	0.70437	0.51238	0.28276	17.928	15.496	37.547
HM-4	0.70432	0.51238	0.28279	17.677	15.465	37.326
HM-18	0.70489	0.51237	0.28275	17.977	15.503	37.592
GB-gray	0.70740	0.51223	0.28262	18.248	15.533	37.308
GB-M2	0.70489	0.51227	0.28261	18.269	15.553	37.930
BH-TV	0.70522	0.51236	0.28276	17.806	15.486	37.330